5-1 Survey Method

The flow chart of gravity survey is shown in Figure 5-1.

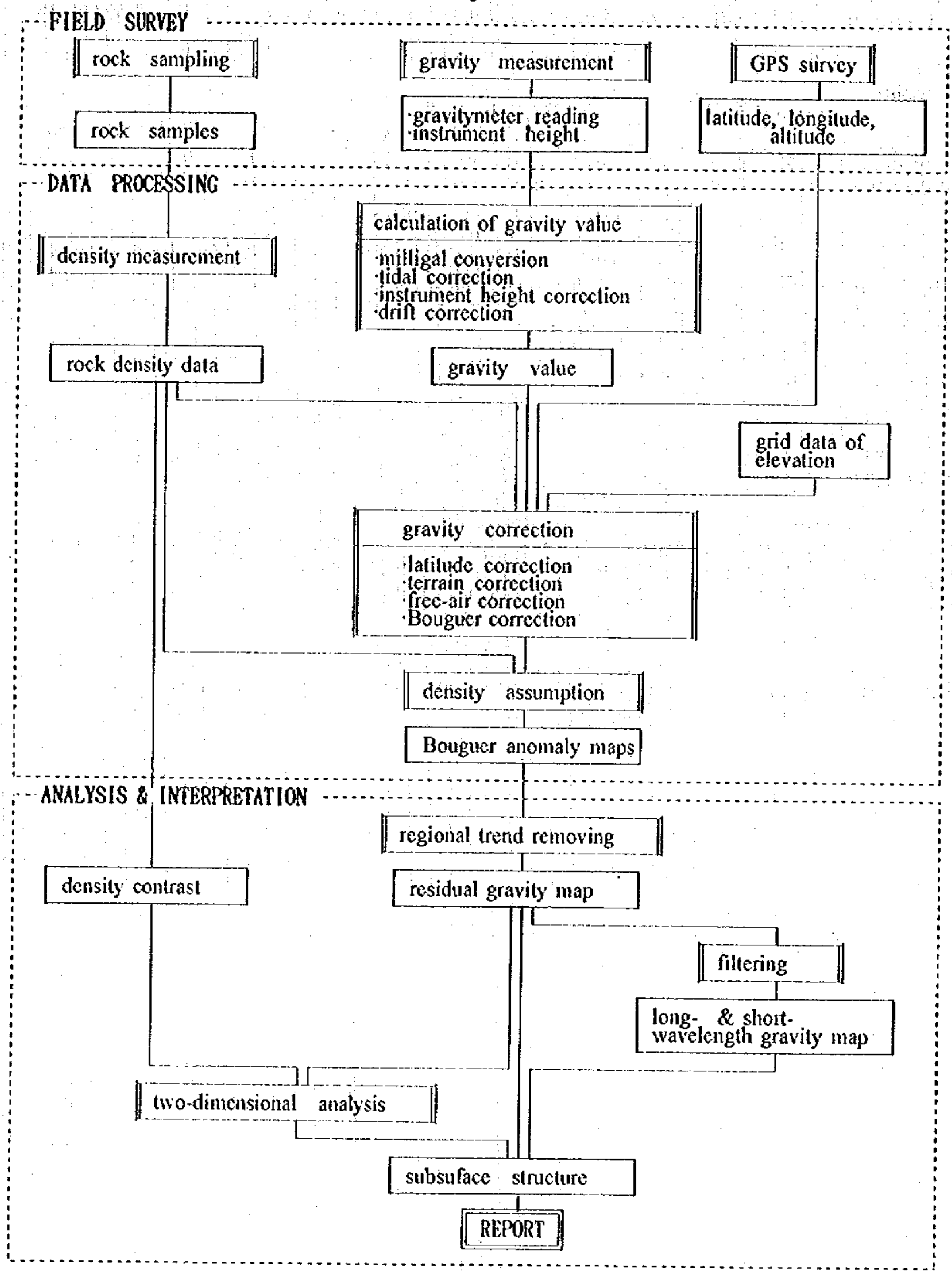

Fig. 5-1 Flow Chart of Gravity Survey

5-1-1 Field Survey

1. Gravity measurements

Gravity measurement was carried out at 265 stations in an area of about 170 km ^{2}. The locations of the stations are shown in Figure 5-2.

Two sets of LaCoste G gravity meters were used for field measurements. The specifications of the LaCoste gravimeters used are as follows.

Gravity meter No.	G-178	G-365
Year of manufacture	Feb. 1968	Mar. 1974
Operating range	0 ~ 7,344.88 mgal	0 ~ 7,447.81 mgal
Accuracy	0.02 mgal	
Size	14 × 15 × 20 cm	
Weight	8.6 kg	
Power source	12 V battery	
Manufacturer	LaCoste & Romberg (USA)	

A gravity base station(No.1000) was established in the central part of Espiye, where the survey base was layed. The detailed location of the base stations are shown together with a photograph in the Annex.

The gravity value of the base station was determined by measuring the gravity differences between the base station and two MTA gravity stations(No.187 and No.193) located near Espiye. The results of measurements are shown below.

```
Y  M  D: 1995 / 10 / 11   LACOSTE G- 365
 NO   TIME  READING INST. * FACT. ETCOR  INST. + COR  DRIFT  GRVTY   GRAVITY
                     H                    COR         COR     DIF.    VALUE
       H  M          CM      MGAL  MGAL  MGAL      MGAL  MGAL    MGAL     MGAL
1000  8 27 3809.021 27.0 4052.774 -.068 0.083 4052.789 0.000  17.106 980272.546
 187 13 15 3792.890 25.0 4035.601 -.007 0.077 4035.671 0.012   0.000 980255.440
1000 16 33 3809.004 27.0 4052.756 -.071 0.083 4052.768 0.021  17.106 980272.546

Y  M  D: 1995 / 10 / 12   LACOSTE G- 365
 NO   TIME  READING INST. * FACT. ETCOR  INST. + COR  DRIFT  GRVTY   GRAVITY
                     H                    COR         COR     DIF.    VALUE
       H  M          CM      MGAL  MGAL  MGAL      MGAL  MGAL    MGAL     MGAL
1000  8  9 3808.982 27.0 4052.732 -.066 0.083 4052.749 0.000  96.043 980272.423
 193 12 23 3718.714 26.0 3956.633 -.017 0.080 3956.696 0.010   0.000 980176.380
1000 15 59 3808.952 27.0 4052.700 -.052 0.083 4052.731 0.018  96.043 980272.423
                             MTA-187:  980 272.546 mgal
                             MTA-193:  980 272.423 mgal
                             --------------------------
Gravity value of No.1000 :  <average>  980 272.485 mgal
```

2. Leveling

The elevation of the stations was determined by GPS (Global Positioning System) static survey which uses the signals from artificial satellites. There are two methods, single and referencial positionings, with

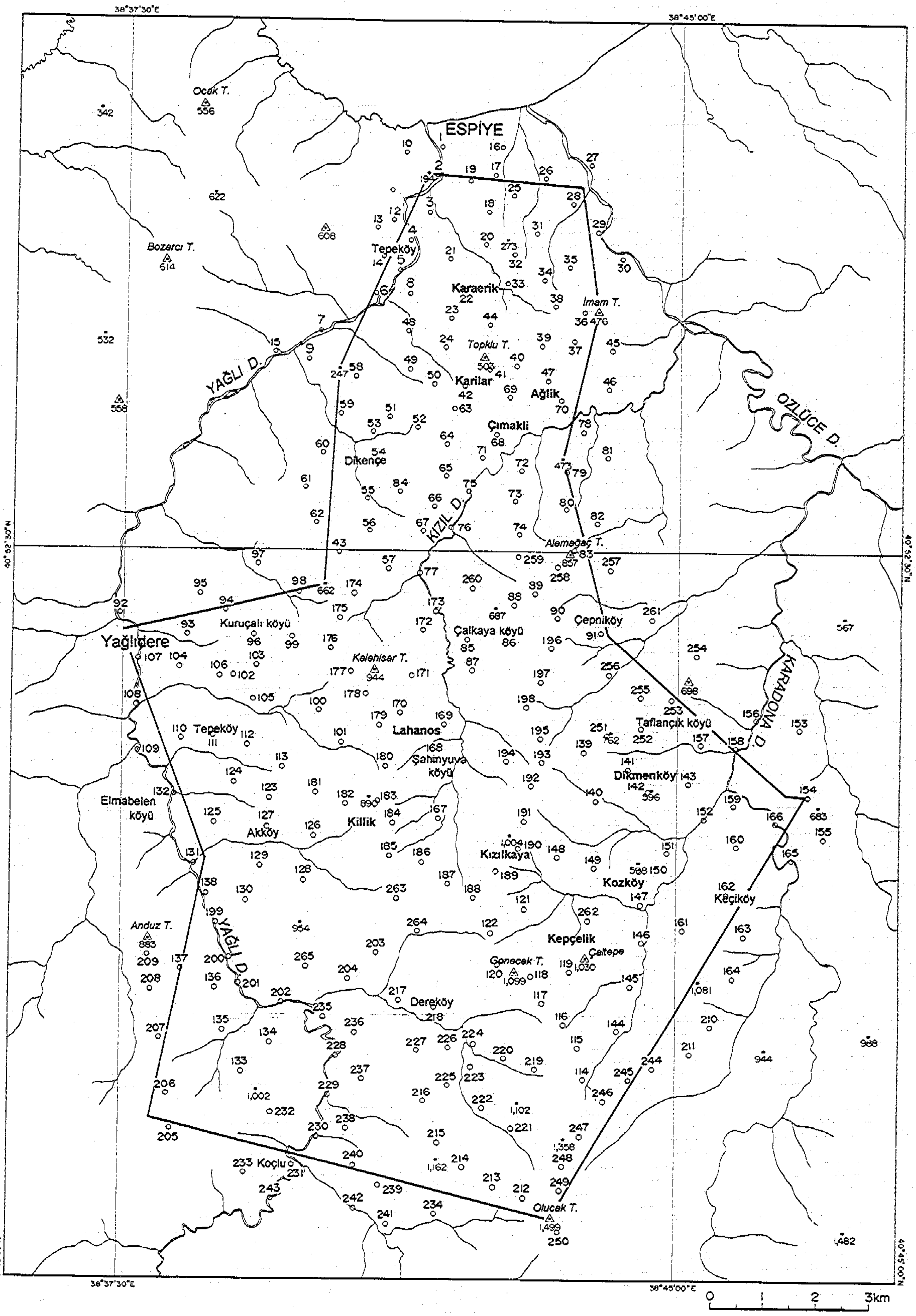

Fig. 5-2 Gravity Stations

GPS survey and the referencial positioning ,which is more precise than the former, was employed in this survey. This method determines the relative positions, dx, dy and dz, between the measuring point and the base station by receiving the satellite signals simultaneously. By this relative positioning, accuracy of several centimeters can be obtained by one hour observation and of less than several tens centimeters by 20 to 30 minutes observation. Three sets of 4000ST GPS surveyers (Trimble Navigation Ltd.) were used for the observations.

The GPS base station was established on the roof of a five-storied building in the central part of Espiye. The elevation of the GPS base stations was determined by a relative positioning with Imam Tepe Triangulation point, whose elevation is 476 meters above sea level.

3. Rock sampling

Rock samples for density measurements were collected throughout the survey area with due consideration to the stratigraphy, lithology and other relevant factors. The number of collected samples amounted to 112 and the number of the nearest gravity station was given to each sample.

5-1-2 Data Processing

1. Calculation of gravity values

In order to calculate the gravity values from the gravity meter readings, "milligal conversion", "tidal correction", "instrument height correction" and "drift correction" were carried out.

a. Milligal conversion

This process converts the dial readings to milligal value. In the case of LaCoste gravimeters, the scale constant slightly changes with the stretching of the spring. Therefore, this conversion is carried out using the milligal constant(K) and scale constant(κ) designated for every 100 units of the reading value. The basic equation for the conversion is as follows.

$$Vr = K + (R - R_0) \times \kappa \qquad (5\text{-}1)$$

Vr : Measured value in milligal

R : Gravity meter reading

R_0 : Under 100 omitted from R

b.Tidal correction

The observed gravity values vary periodically within the range of 0.2 mgal because of the following two factors. The correction for these variations is the tidal correction.

1) Periodic variation by tidal force.

2) Deformation of the earth by the tidal force(earth tide).

Tidal force is expressed by equation(5-2).

$$U = \frac{3}{2} \cdot G \cdot M \frac{a}{r^3} \{ 3 (\sin^2 \delta - \frac{1}{3}) \cdot (\sin^2 \phi - \frac{1}{3}) + \sin 2\delta \cdot \sin 2\phi \cdot \cos \theta + \cos^2 \delta \cdot \cos^2 \phi \cdot \cos 2\theta \} \qquad (5\text{-}2)$$

U : Tidal force of celestial body

G : Gravitational constant
M : Mass of celestial body (sun,moon etc.)
a : Distance from the center of the earth to the station (earth's radius)
ϕ : Latitude of the station
r : Distance between the earth and the celestial body
δ : Declination of the celestial body (angle from the equator)
θ : Hour angle of the celestial body (angle between terrestial and celestial meridian plane)

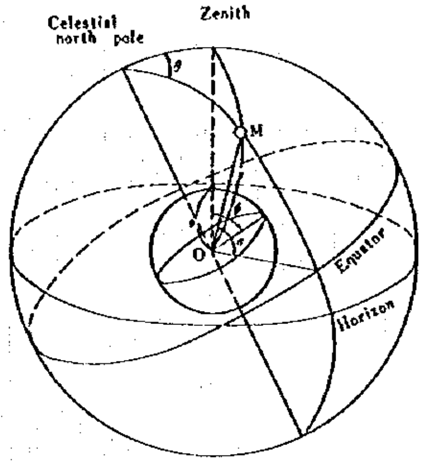

Tidal correction parameters

The tidal force of the sun and moon is overwhelmingly greater than that of other celestial bodies. Therefore, the correction for these two bodies will suffice for gravity prospecting.

The gravity variation caused by earth tide has the same sense as that by the tidal force and the rate of change differs somewhat by the elasticity of the rocks of the area, but it is in the order of 20 % of that caused by tidal force. Therefore, in normal tidal correction, the tidal force by the sun and moon is multiplied by 1.20 which is called the tidal constant.

c. Instrument height correction

This correction is made in order to compensate for the difference of the height for leveling and gravity measurements. The correction is done by using the vertical normal gravity gradient on the surface of the ellipsoid of revolution(=0.3086 mgal/m) on equation(5-3).

$$V\,hi \fallingdotseq \frac{2\,\gamma_0}{R}\,hi \fallingdotseq 0.3086\ hi \quad (5\text{-}3)$$

V hi: Instrument height correction value
γ_0 : Normal gravity
R : Distance from the earth's center to the station
hi : Hight from the leveled point on the earth's surface to the top of the gravity meter

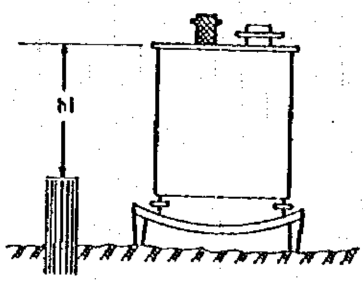

Instrument height

d. Drift correction

The drift is the variation of reading values of the gravimeter caused by the stretching of the spring. The value of the drift is roughly proportional to time. The correction for this drift is done by time-proportional allotment of the closed error for each station. The variation of readings are caused not only by drift, but also by the changes of temperature, atmospheric pressure and mechanical shock during transportation. In practice, these changes are also corrected by this process.

c. Calculation of gravity values

All corrections for measured gravity values are expressed by equation(5-4).

$$Vc = Vr + Vt + Vhi + Vd \tag{5-4}$$

V c: Corrected gravity value

V t: Tidal correction value

V d: Drift correction value

The corrected gravity value Vc shows the relative value of gravity and not the absolute value of gravity. The gravity value of each station is calculated by obtaining the difference of the corrected gravity values between the station and the base station and then adding the gravity value of the base station to this difference. The gravity value of the base station is obtained by separate measurement between the base station and the reference station where the gravity value is known.

3. Gravity reduction

The process of calculating the Bouguer anomaly values is called the gravity reduction and it consists of "latitude correction", "terrain correction", "atmospheric correction", "free air correction" and "Bouguer correction".

a. Latitude correction

This correction is done by subtracting the standard gravity of the earth from the gravity value. The standard gravity is given as a function of the latitude and normal gravity of equation(5-5) is presently used as the standard gravity.

$$\gamma_0 = \frac{a\gamma_E \cos^2\phi + b\gamma_P \sin^2\phi}{\sqrt{a^2\cos^2\phi + b^2\sin^2\phi}} \tag{5-5}$$

a : Equatorial radius of the ellipsoid of revolution(6,378.160km)

b : Polar radius of the ellipsoid of revolution(6,356.775km)

γ_E : Equatorial normal gravity of the ellipsoid of revolution (978.031 85 gal)

γ_P : Polar normal gravity of the ellipsoid of revolution(983.217 73 gal)

However, for practical gravity prospecting, the following approximation is used.

$$\gamma_0 = 978031.85(1 + 0.005278895 \sin^2\phi + 0.000023462 \sin^4\phi) \text{ (mgal)} \tag{5-6}$$

b. Terrain correction

For the present survey, the range of terrain correction was set for a radius of 60 km and the area was divided into seven correction zones as follows.

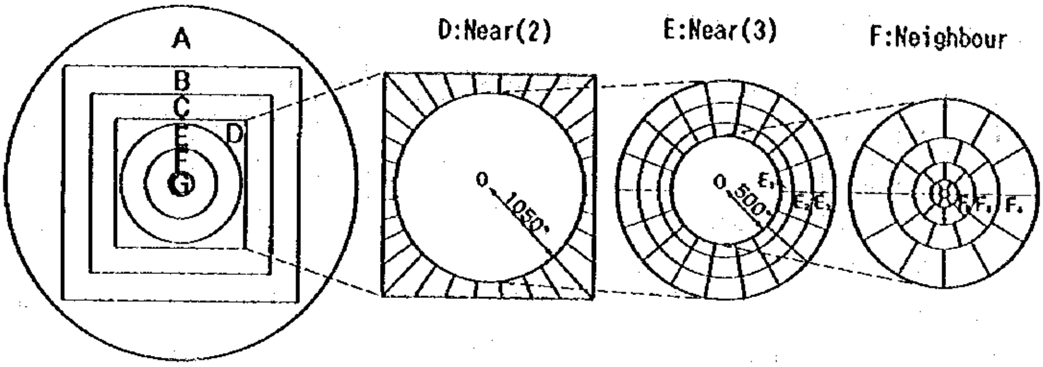

Terrain Correction Concept

The topographic elevation mesh data were prepared by reading elevation in the 1/500,000 air navigation map for the Zones A and B and in the 1/25,000 topographic maps for the Zones C-E. Hammer's chart was applied for the Zone F and a sketched topographic profile of 20 m radius from the station was used for the correction of Zone G.

Items of Terrain Correction

Zone	Range of correction	Mesh interval and etc.	correction type
A	60km radius - Zone B	3'(E-W) × 2'(N-S)	Far
B	21'(E-W) × 16'(N-S)	45"(E-W) × 30"(N-S)	Medium
C	5'15"(E-W) × 4'(N-S)	11.25"(E-W) × 7.5"(N-S)	Near(1)
D	Between Zone C and E	Pentahedron	Near(2)
E	500 - 1,050m radius	Cylindrical sector	Near(3)
F	20m - 500m radius	Hammer's chart	Neighbour
G	20m radius from station	Sketched profile	Close

c. Atmospheric correction

This is done in order to correct the effect of the atmosphere to gravity measurement. The atmospheric pressure will be integrated to a height of 50 km above the station using the atmospheric density distribution based on standard atmospheric model. The correction value decreases exponentially with altitude. The variation of the correction values, however, can be approximated by a linear function for altitude below 3 km. And equation(5-7) is usually used for this correction.

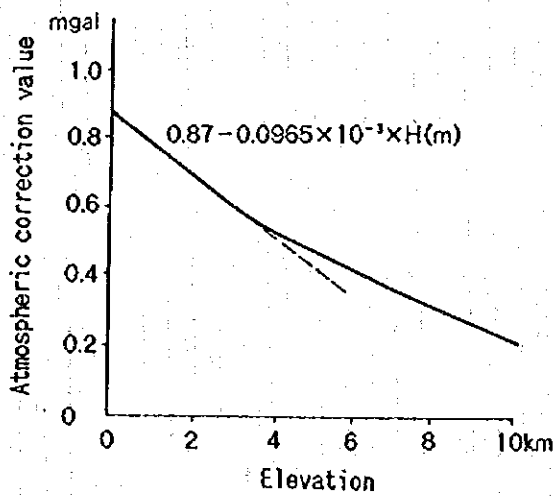

$$\delta g_A = 0.87 - 0.0965 \times 10^{-3} H \qquad (5\text{-}7)$$

δg_A : Atmospheric correction(mgal)

H : Elevation of the station(m)

d. Free air correction

The vertical gravity gradient near the earth's surface is -0.3086 mgal/m, and thus the gravity decreases with height. The free air correction corrects the effect of elevation for each station.

$$\delta g_F \fallingdotseq \frac{2\,\gamma_0 H}{R} \fallingdotseq 0.3086\ H \qquad (5\text{-}8)$$

δg_F : Free air correction value

γ_0 : Normal gravity

R : Distance from the earth's center to the station

H : Elevation from the geoid

The value defined by equation(5-9) is called the free air anomaly.

$$\triangle g_F = g - \gamma_0 + \Sigma\,\delta g_T + 0.3086\ H \qquad (5\text{-}9)$$

$\triangle g_F$: Free air anomaly

g : Gravity value

$\Sigma\,\delta g_T$: Terrain correction value

e. Bouguer correction

The difference of the gravity values measured at different elevations corresponds to the attraction of the material(rocks) which exists between the elevations of the stations. Bouguer correction eliminates this difference by setting a datum plane and eliminating material between the datum and a parallel plane passing through each station. Usually geoid is used as the datum. A homogeneous circular slab is assumed to exist between the geoid and a parallel plane including the station for the correction equation(5-10). The radius of this slab is set at 60 km, the same as the range of terrain correction.

$$\delta g_B = -2\,\pi\,G\,\rho\,(\,A + H - \sqrt{A^2 + H^2}\,)$$
$$\fallingdotseq -0.0419\,\rho\,(\,A + H - \sqrt{A^2 + H^2}\,) \qquad (5\text{-}10)$$

δg_B : Bouguer correction value

G : Gravitational constant

ρ : Density(avarage rock density between the geoid and earth's surface)

A : Circular slab radius(60 km)(60km)

H : Station elevation

f. Bouguer anomaly values

The values obtained by correcting the gravity values for latitude,terrain, atmosphere, free air and Bouguer are called the Bouguer anomalies and are expressed by equation(5-11).

$$\varDelta g_B = g - \gamma_0 + \Sigma\,\delta g_T + 0.87 - 0.0965 \times 10^{-3} H + 0.3086\ H$$
$$- 0.0419\,\rho\,(\,A + H - \sqrt{A^2 + H^2}\,) \qquad (5\text{-}11)$$

$\varDelta g_B$: Bouguer anomaly value

The Bouguer anomaly is defined at the earth's surface and the value varies by the density used for the Bouguer and terrain corrections. Thus the Bouguer anomaly contains infonnation not only on the density structure below the geoid but also the difference of the real and the assumed density used in correction for the rocks between the geoid and the surface.

Tables of relevant data regarding this gravity survey are attached in the Appendices. These data include; location (coordinates and elevation) of stations, gravity values, various correction values, normal gravity values and Bouguer anomalies, and Bouguer anomalies for eight different assumed density.

g. Calculation of surface density and Bouguer anomaly with variable density

In a Bouguer gravity map with a single assumed density, there remains frequently anomalies affected by topographic relief. For such case, a variable density correction, in which assumed density changes with the stations, is useful. Surface density at each station is obtained at first to carry out the variable density correction and then Bouguer anomaly value is calculated by using the surface density for the density of terrain and Bouguer corrections. Surface density in this survey is computed based on Moribayashi's method(1990) as follows.

$$\Delta g_B(x,y) = a_1 x^3 + a_2 y^3 + a_3 x^2 y + a_4 xy^2 + a_5 x^2 + a_6 y^2 + a_7 xy + a_8 x + a_9 y + a_{10} + \Delta\rho\,(0.04191H - T) \qquad (5\text{-}12)$$

Δg_B : Bouguer anomaly with a certain assumed density at the station with the co-ordinate (x,y)

H : Station elevation

T : Total terrain correction value(ρ =1.00 g/cm ^{3})

The first ten terms of the right side of the equation(5-12) are ones for the third order polynomial approximation to Bouguer anomalies caused by the subsurface density structure. The last term stands for the uncorrected value which remains due to the difference between the assumed and actual densities. The calculation to determine all coefficients of the right side of the formula(5-12) is made by the least square method using the station data in the window with a station to be calculated as the center and a radius of several km. The surface density is obtained by adding the coefficient of the last term to the assumed density employed in the calculation..

5-1-3 Analytical Methods

1. Density measurement of rock samples

The density of the collected samples was calculated by the following formula.

$$\text{Natural dry density} = \frac{W_1}{W_2 - W_3} \qquad (5\text{-}13)$$

$$\text{Wet density} = \frac{W_2}{W_2 - W_3} \qquad (5\text{-}14)$$

W_1 : Weight in air of the sample left in a normal room condition for several days.

W_2 : Weight in air of the sample immersed in water for more than 24 hours under natural atmospheric pressure and wiped on the cloth.

W_3 : Weight in water after immersion under natural atmospheric pressure for more than 24 hours.

2. Gravity analysis

a. Trend-surface analysis

The purpose of a trend-surface analysis is to isolate local anomalies from Bouguer gravity features. The first step of this analysis is determining regional gravity trend by polynomial fitting . Polynomials are expressed as follows:

- a first-order surface

$$\Delta g_1(x,y) = a_0 + a_1 x + a_2 y \tag{5-15}$$

- a second-order surface

$$\Delta g_2(x,y) = a_0 + a_1 x + a_2 y + a_3 x^2 + a_4 xy + a_5 y^2 \tag{5-16}$$

- a n-th-order surface

$$\Delta g_n(x,y) = a_0 + a_1 x + a_2 y + a_3 x^2 + \cdots \cdots + a_{m-1} xy^{n-1} + a_m y^n \tag{5-17}$$

where $m=n(n+3)/2$

Two kinds of data, gridded values of gravity field and random values at the stations located at the outcrops of a special geology, are used to compute the coefficients of polynomial expression by least square method. In this survey, the first-order surface was computed for the regional gravity trend using the gridded data.

In the second step of this analysis, the residual gravity is obtained by removing the first-order surface from Bouguer gravity field. The residual gravity shows local anomalies which reflect the subsurface density structures of the survey area.

b. Frequency analysis (separation of anomalies)

Frequency analysis is used with the objective of separating the longer wavelength anomalies caused by deep-seated structures and the shorter wavelength anomalies caused by shallow structures.

The gravity anomalies $\Delta g(x,y)$ over a rectangular area with two sides of $L_1 \times L_2$ can be expanded in Fourier series as follows:

$$\Delta g(x,y) = \sum_{m=0}^{\infty}\sum_{n=0}^{\infty}\{A_{mn}\cos(m\omega_1 x)\cos(n\omega_2 y) + B_{mn}\cos(m\omega_1 x)\sin(n\omega_2 y) + C_{mn}\sin(m\omega_1 x)\cos(n\omega_2 y) + D_{mn}\sin(m\omega_1 x)\sin(n\omega_2 y)\} \tag{5-18}$$

where $0 \leqq x \leqq L_1$, $0 \leqq y \leqq L_2$

$\omega_1 = 2\pi/L_1$, $\omega_2 = 2\pi/L_2$

m, n: wave number in x- and y-direction respectively

Fourier coefficient A_{mn} can be calculated as

$$A_{mn} = \frac{4}{\varepsilon_{mn} L_1 L_2} \int\int_{-\infty}^{\infty} \Delta g(x,y)\cos(m\,\omega_1 x)\cos(n\,\omega_2 y)dxdy \qquad (5\text{-}19)$$

$$\varepsilon_{mn} = \begin{cases} 2 : m=n=0 \\ 1 : m,n=1,2,3,4,\cdots\cdots \end{cases}$$

B_{mn}, C_{mn} and D_{mn} are given in the same way.

There are three kinds of filters of frequncy analysis; high-cut, low-cut and band-pass filter. Long wavelength anomalies can be obtained by using high-cut filter which removes the terms with larger wave number of equation(5-18), since they consist of the terms with smaller wave number. Short wavelegth anomalies, conversely, can be obtained by low-cut filter.

FFT(Fast Fourier Transform) was used in this survey for computation of filtering to produce the long and short wavelength gravity maps .

c. Two-dimensional analysis

The purpose of two-dimensional gravity analysis is to construct a two-dimensional model of the subsurface structure which would result in gravity anomalies approximating most closely those measured in the area. The gravity anomalies of the model are calculated by the following Talwani et al.(1959) equation.

$$g = 2G\Delta\rho\Sigma Z_i \qquad (5\text{-}20)$$

$$Z_i = A_i\sin\phi_i - \cos\phi_i \left(\theta_i - \theta_{i+1} + \tan\phi_i \log \frac{\cos\theta_i(\tan\theta_i - \tan\phi_i)}{\cos\theta_{i+1}(\tan\theta_{i+1} - \tan\phi_i)}\right) \qquad (5\text{-}21)$$

g : Calculated gravity anomaly

G : Gravitational constant

$\Delta\rho$: Density contrast($\rho_2 - \rho_1$)

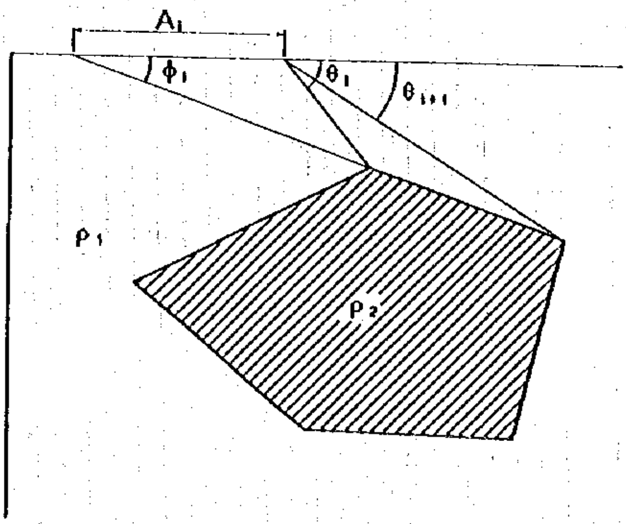

Schematic two-dimensional analysis by Talwani's method

When the geologic structure can be approximated by two-layered dendity model, unique solution can be obtained by inversion method; designating a density contrast and a control depth, and then gradually altering the shape of the density boundary thus approximating the calculated values closer to the measured values. But, when the geologic structure is complicated, much time is nessesary to find the most suitable model because it must be approximated by multi-layered density model and inversion method is not applicable to the multi-layered model.

5 - 2 Results of the Survey

5 - 2 - 1 Density Measurement

The results of density measurement of 112 rock samples collected at the survey area are listed in Table 5-1. Also the average densities (wet condition) of the rocks of each formation are shown in Table 5-2. In the calculation of average densities, Sample Nos. 202, 204, 236, 240 were excluded because of their abnormaly high values.

The following characteristics are noted from Table 5-2.

(1) Average density is generally higher for stratigraphically lower formations.

(2) The density difference between Kızılkaya and Çatak formations is large while that of Çağlayan and Kızılkaya formations is small.

(3) Within the Çatak formation, andesite lava and andesitic tuff breccia has high density while sandstone has relatively low value.

(4) The density of intrusive rocks vary considerably, and granitic rocks and biotite dacite show high values.

5 - 2 - 2 Gravity Features

1. Bouguer aomaly maps

Three types of Bouguer anomaly maps, namely those with correction density of ρ=2.20, 2.40, and 2.60 g/cm^3 are shown in Figures 5-3 to -5. The Bouguer anomaly value is high in the northern part of the area and low in the south in all three maps. Thus there is a regional trend of southward decreasing Bouguer anomaly values in this area.

In the Bouguer anomaly map with ρ=2.20 g/cm^3, there are two notable gravity lows related to topography at the Yağlı River basin in the southwest and at the Karadona River basin in the southeast. The two gravity lows are considerably attenuated in the ρ=2.40 g/cm^3 map and is hardly noticable in the ρ=2.60 g/cm^3 map. This indicates that relatively high assumed density of around 2.60 g/cm^3 is appropriate from the southeast to southwestern part of the survey area.

On the other hand, in the ρ=2.60 g/cm^3 map, a high gravity anomaly related to topography appears at the Kızıl River basin in the northern part of the area. This gravity high does not appear in the ρ=2.20 g/cm^3 map and this indicates that a relatively low assumed density of around ρ=2.20 g/cm^3 is appropriate in the northern part of the area.

It is seen from the above that the density of the rocks near the surface differs considerably between the northern and southern parts of the survey area. In these cases, it is necessary to apply variable density correction using different densities in accordance with the geologic conditions.

2. Surface density and Bouguer anomaly with variable density

Table 5-1 Rock Density (1/3)

Staratigraphic units	Sample NO.	Rock name	Density (g/cm^3) Natural dry	Wet
Çağlayan Formation	123	Acidic Lapilli Tuff	2.22	2.26
	262	Acidic Tuff	2.43	2.45
	148	Hematic Dacite	2.46	2.49
	180	Dacite Lava	2.38	2.41
	186	Dacite Lava	2.38	2.42
	187	Dacite Lava	2.27	2.37
	189	Dacite Lava	2.42	2.45
Kızılkaya Formation	68	Dacite Lava	2.22	2.32
	69	Dacite Lava	2.37	2.44
	76	Dacite Lava	2.35	2.42
	77	Dacite Lava	2.55	2.56
	86	Dacite Lava	2.44	2.48
	87	Dacite Lava	2.33	2.39
	114	Dacite Lava	2.59	2.61
	116	Dacite Lava	2.29	2.39
	140	Dacite Lava	2.34	2.39
	167	Dacite Lava	2.34	2.42
	190	Dacite Lava	2.37	2.41
	216	Dacite Lava	2.47	2.50
	226	Dacite Lava	2.55	2.58
	236	Dacite Lava	(2.92)	(2.94)
	261	Dacite Lava	2.34	2.41
	263	Dacite Lava	2.50	2.54
	152	Hematic Dacite	2.47	2.49
	153	Hematic Dacite	2.42	2.46
	154	Hematic Dacite	2.52	2.55
	156	Hematic Dacite	2.51	2.54
	158	Hematic Dacite	2.54	2.59
	160	Hematic Dacite	2.24	2.32
	223	Dacitic Tuff Breccia	2.45	2.49
Çatak Formation	93	Andesite Lava	2.35	2.40
	102	Andesite Lava	2.59	2.61
	104	Andesite Lava	2.52	2.54
	106	Andesite Lava	2.55	2.57
	108	Andesite Lava	2.42	2.47
	109	Andesite Lava	2.60	2.63
	110	Andesite Lava	2.59	2.60
	115	Andesite Lava	2.54	2.59
	127	Andesite Lava	2.54	2.55
	130	Andesite Lava	2.62	2.63
	132	Andesite Lava	2.67	2.69
	138	Andesite Lava	2.52	2.55

Table 5-1 Rock Density (2/3)

Staratigraphic units	Sample NO.	Rock name	Density (g/cm³)	
			Natural dry	Wet
Çatak Formation	163	Andesite Lava	2.66	2.70
	164	Andesite Lava	2.63	2.64
	166	Andesite Lava	2.70	2.70
	202	Andesite Lava	(2.92)	(2.93)
	204	Andesite Lava	(2.96)	(3.00)
	206	Andesite Lava	2.62	2.63
	220	Andesite Lava	2.70	2.70
	240	Andesite Lava	(2.83)	(2.83)
	243	Andesite Lava	2.67	2.68
	246	Andesite Lava	2.59	2.62
	247	Andesite Lava	2.51	2.54
	248	Andesite Lava	2.61	2.62
	264	Andesite Lava	2.74	2.75
	144	Sandostone	2.50	2.53
	201	Andesitic Tuff Breccia	2.64	2.66
	209	Andesitic Tuff Breccia	2.68	2.71
	212	Fine Tuff Breccia	2.58	2.62
	249	Andesitic Tuff Breccia	2.48	2.54
Intrusive Rocks	2	Nevaditic Dacite	2.38	2.42
	5	Nevaditic Dacite	2.41	2.46
	12	Nevaditic Dacite	2.07	2.12
	29	Nevaditic Dacite	2.40	2.43
	73	Nevaditic Dacite	1.74	2.00
	80	Nevaditic Dacite	2.31	2.35
	84	Nevaditic Dacite	2.43	2.46
	100	Nevaditic Dacite	2.44	2.48
	113	Nevaditic Dacite	2.50	2.53
	126	Nevaditic Dacite	2.47	2.51
	161	Nevaditic Dacite	2.58	2.59
	228	Nevaditic Dacite	2.56	2.57
	229	Nevaditic Dacite	2.65	2.66
	237	Nevaditic Dacite	2.58	2.60
	11	Hematic Dacite	2.16	2.21
	33	Hematic Dacite	1.94	2.17
	35	Hematic Dacite	1.77	1.90
	37	Hematic Dacite	2.07	2.17
	38	Hematic Dacite	2.27	2.34
	44	Hematic Dacite	1.93	1.97
	52	Hematic Dacite	2.31	2.35
	64	Hematic Dacite	2.18	2.26
	66	Hematic Dacite	2.35	2.39
	70	Hematic Dacite	1.97	2.05

Table 5-1 Rock Density (3/3)

Staratigraphic units	Sample NO.	Rock name	Density (g/cm³)	
			Natural dry	Wet
Intrusive Rocks	71	Hematic Dacite	2.20	2.28
	90	Hematic Dacite	2.32	2.39
	146	Hematic Dacite	2.44	2.49
	168	Hematic Dacite	2.36	2.45
	179	Hematic Dacite	2.35	2.41
	197	Hematic Dacite	2.42	2.43
	199	Hematic Dacite	2.51	2.53
	255	Hematic Dacite	2.43	2.45
	256	Hematic Dacite	2.32	2.42
	62	Dacite	2.43	2.46
	81	Dacite	2.28	2.34
	131	Dacite	2.61	2.64
	134	Dacite	2.47	2.49
	135	Dacite	2.45	2.50
	136	Dacite	2.47	2.50
	174	Dacite	2.57	2.58
	194	Dacite	2.49	2.50
	200	Dacite	2.55	2.56
	219	Dacite	2.65	2.70
	221	Dacite	2.58	2.59
	232	Dacite	2.71	2.73
	234	Dacite	2.48	2.52
	238	Dacite	2.55	2.57
	265	Dacite	2.41	2.46
	137	Granodiorite	2.68	2.70
	165	Granitic Rock	2.57	2.59
	231	Granitic Rock	2.62	2.63
	242	Granodiorite	2.69	2.70

Table 5-2 Average of Rock Density (wet)

Age	Startigraphic units	Rock name	Number	Average density (g/cm³)	
MESOZOIC	Çağlayan Formation	Acidic Lapilli Tuff	2	2.35	2.41
		Hematic Dacite	1	2.49	
		Dacite Lava	4	2.41	
	Kızılkaya Formation	Dacite Lava	15	2.46	2.47
		Hematic Dacite	6	2.49	
		Dacitic Tuff Breccia	1	2.49	
	Çatak Formation	Andesite Lava	22	2.61	2.61
		Sandstone	1	2.53	
		Andesitic Tuff Breccia	4	2.63	
	Intrusive Rocks	Nevaditic Dacite	14	2.44	2.43
		Hematic Dacite	19	2.30	
		Dacite	15	2.54	
		Granitic Rock	4	2.65	
Average			108	2.48	

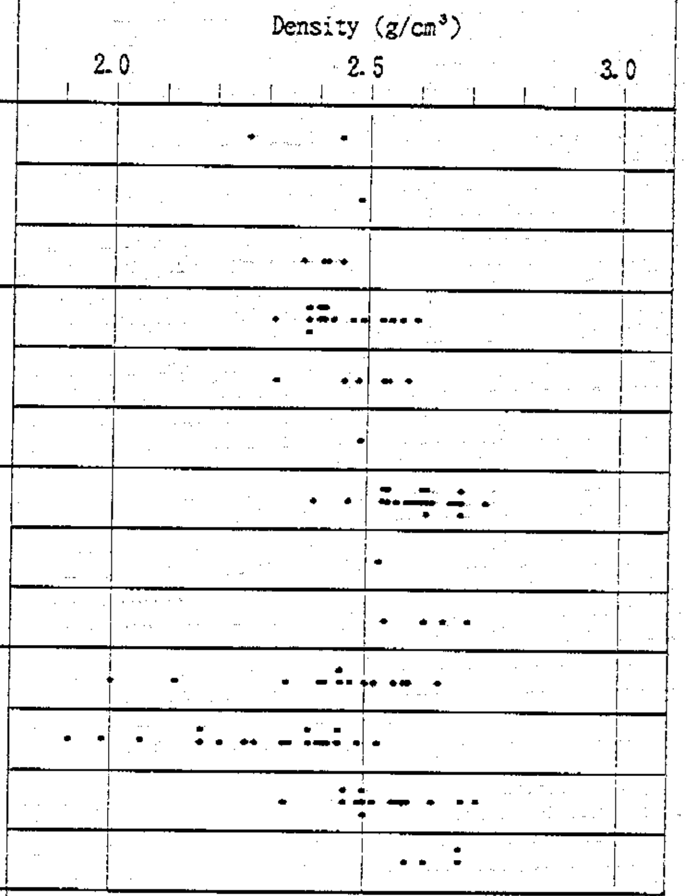

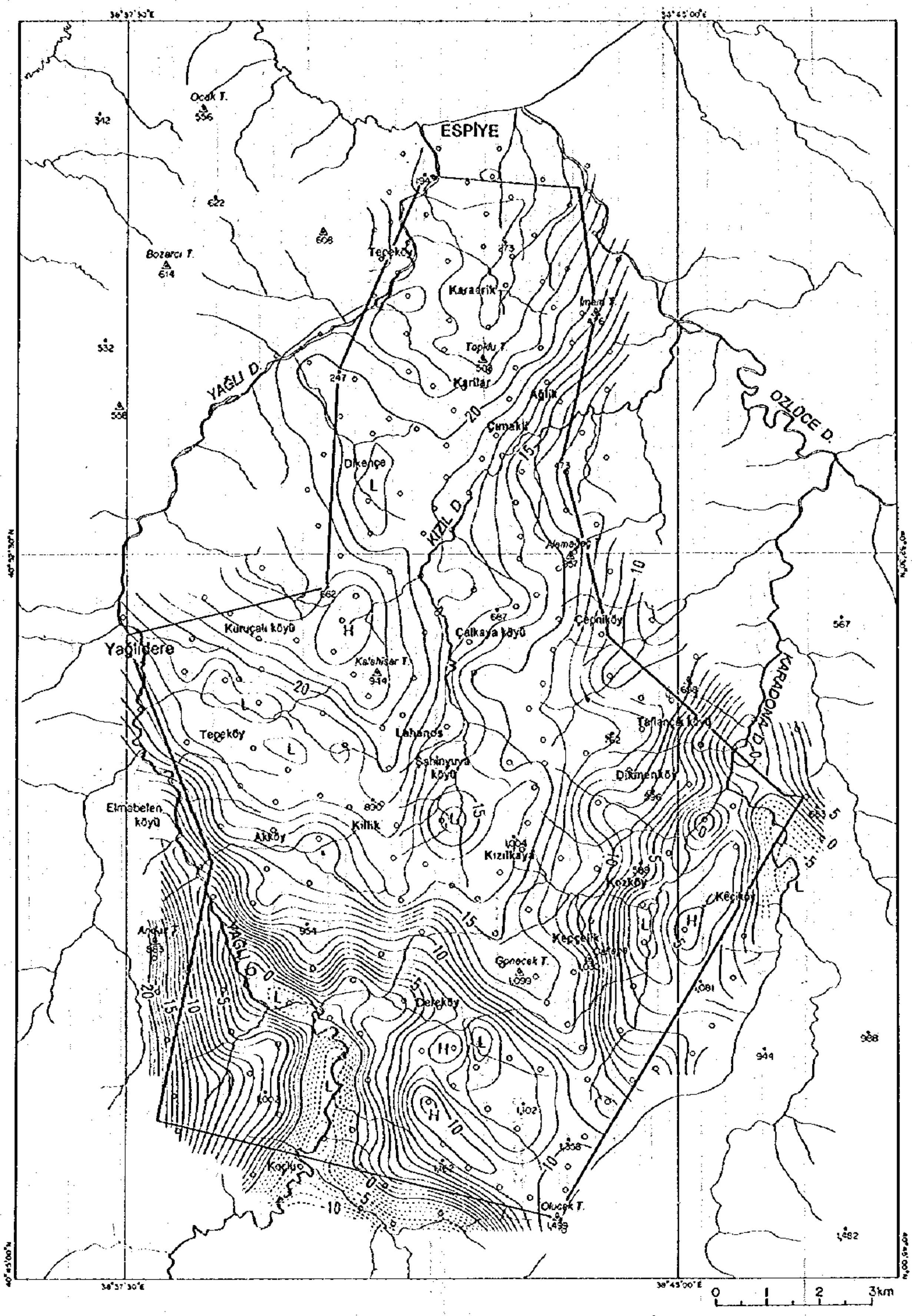

Fig. 5-3 Bouguer Anomaly Map (ρ =2. 20g/cm ^{3})

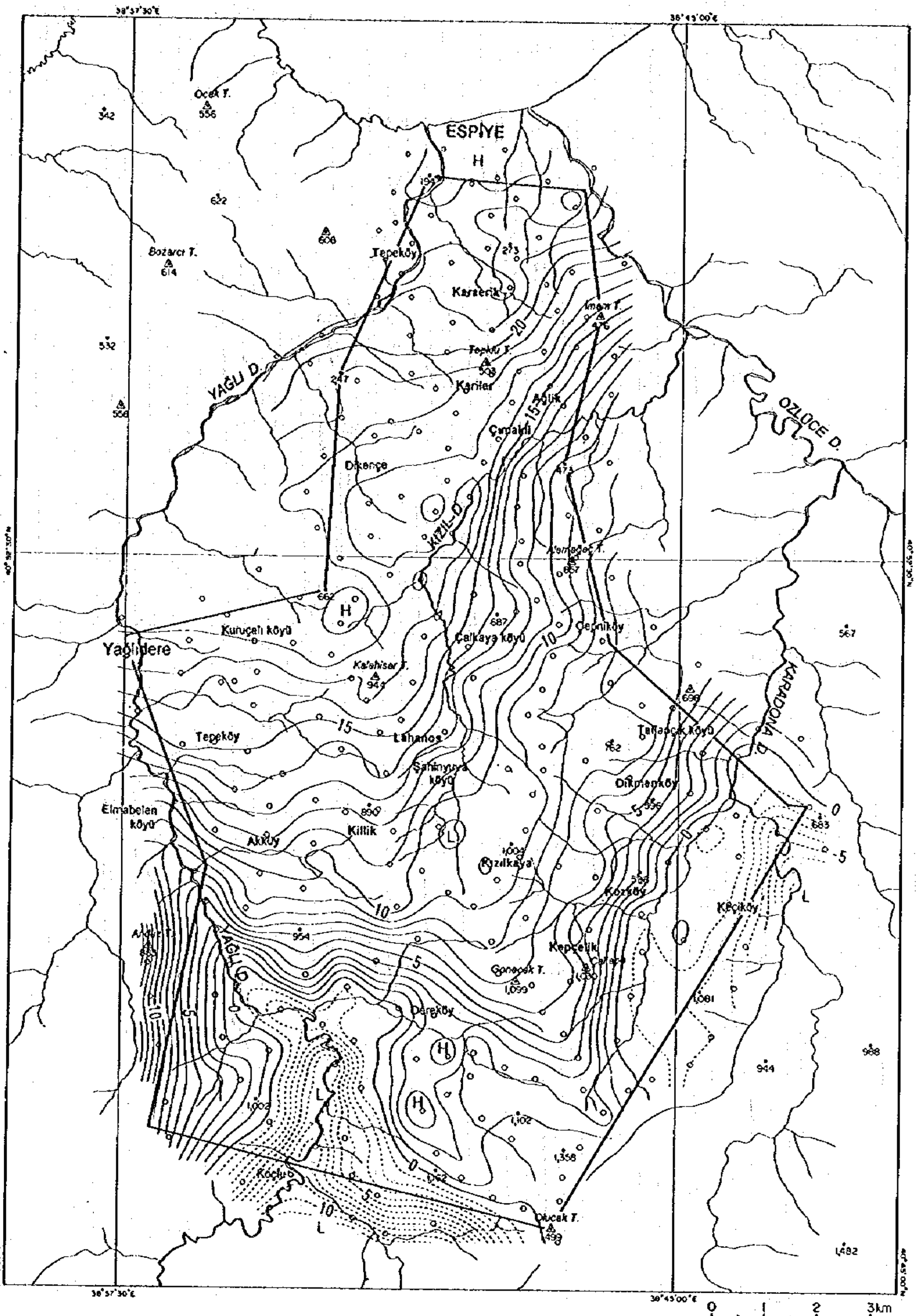

Fig. 5-4 Bouguer Anomaly Map (ρ =2.40g/cm^{3})

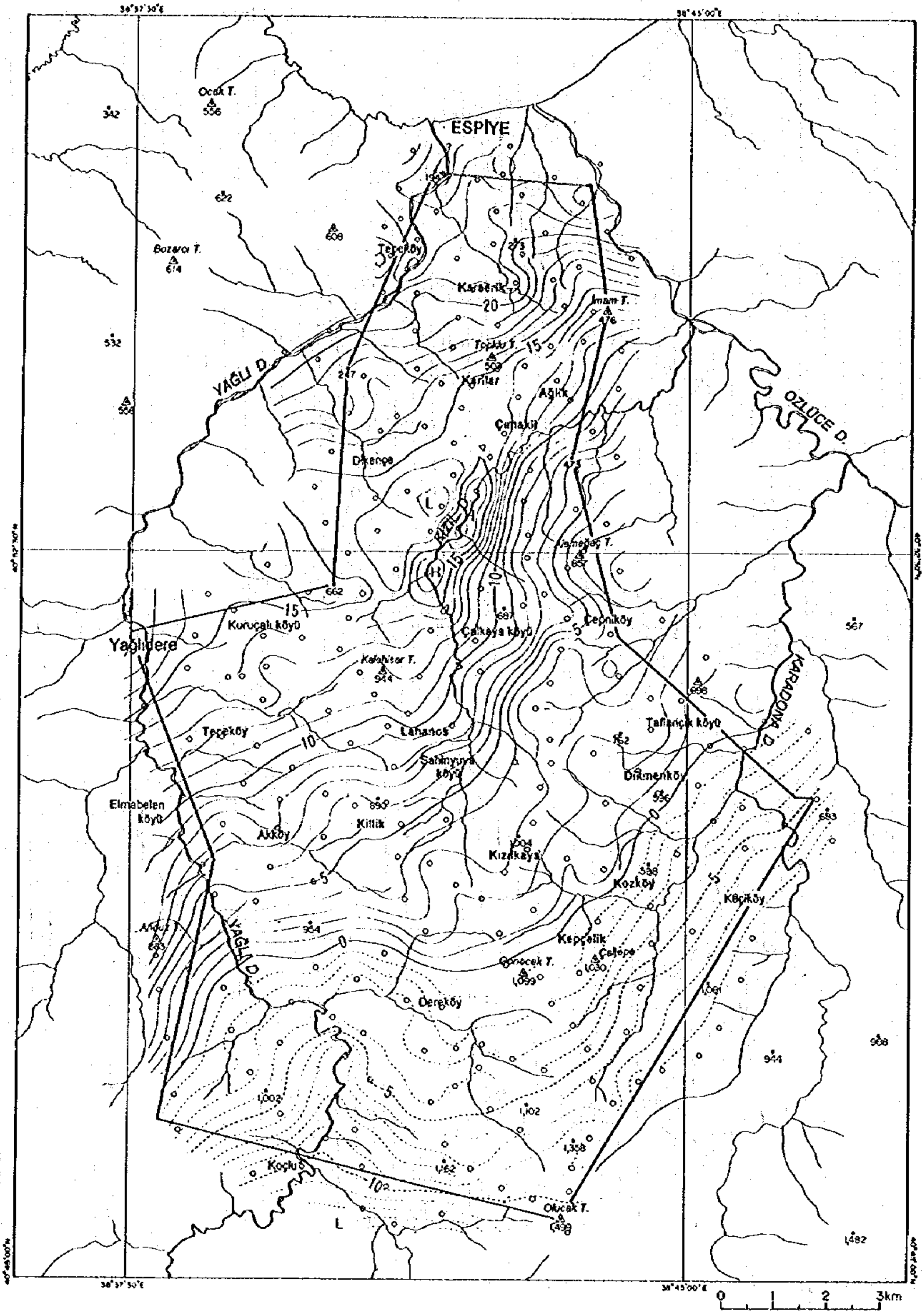

Fig. 5-5 Bouguer Anomaly Map (ρ =2.60g/cm^3)

Surface density map is shown in Figure 5-6, and Bouguer anomaly map with variable density in Figure 5-7. Figure 5-7 is a map prepared by using the surface density of Figure 5-6 as the correction density.

Surface density distribution shows that the northern part of the survey area has low density while in the south the density is high, and the density change is very steep in the central part. In the northernmost part, the density is lower than 2.30g/cm^3 and also in the Kızıl River basin. In the southernmost part, there is a wide area with density higher than 2.70g/cm^3 and the highest exceeds 2.74g/cm^3. It is seen from the geological map (Fig. 2 -1) that the stratigraphically low Çatak formation generally corresponds to the high density zone, while the upper Kızılkaya and Çağlayan formations to the low density zone. This is in general agreement with the average density of the formations laid out in Table 5 -2.

This Bouguer anomaly map with variable density has eliminated the effect of topography and the surface, and it is interpreted as reflecting the density distribution of the subsurface zones. In localities where the actual density differs locally from the surface density of Figure 5-6, however, local gravity anomaly may have been formed by the deficiency and excess of the correction density.

The Bouguer anomaly map with variable density (Fig. 5-7) shows the regional trend of the gravity of this area very clearly, namely the Bouguer anomaly is high in the north and low to the south. As will be mentioned later, regional gravity map indicates that, in the southern coast of the Black Sea where this survey area is located, the Bouguer anomaly decreases southward at a steep gradient. Therefore, the shape of the local gravity anomaly within this steep gradient is distorted and it is difficult to read the characteristics of the anomaly from the straight Bouguer anomaly map. In such cases, it is necessary to eliminate the effect of the regional gravity trend from the Bouguer anomaly and extract only the local anomaly. Thus the regional trend was eliminated from the Figure 5-7.

3. Residual gravity map

Figure 5-8 is the regional Bouguer anomaly map of the Black Sea coastal area prepared by MTA using gravity data measured at 5-10 km intervals. The Bouguer anomalies are 50mgal in the northernmost part of the map and approximately -100 mgal in the southernmost area with average N-S gradient of about -2 mgal/km. The general trend of the contour lines is NE-SW in the survey area, but the regional trend is ENE-WSW.

The regional trend was calculated as the first order surface fitting to the gravity distribution of Figure 5-8. The result is shown in Figure 5-9. In the first order surface, the contours have ENE-SWS trend and the Bouguer anomalies are 22 mgal in the northernmost part of the survey area and -25 mgal in the southern end.

Residual gravity map shown in Figure 5-10 was prepared by subtracting the gravity trend of Figure 5-9 from the variable density map (Fig. 5-7). The residual gravity map shows that the residual gravity is low in the north and increases towards the central and southern parts. A marked gravity high is highlighted in the central part about 1km north of the Lahanos mine. This high anomaly has the highest residual value of 15.5mgal at its center and has a wide peak extending over 1.5 x 2km with a low gravity gradient and northern and eastern slope with steep gravity gradients.

The residual gravity in the northern part ranges from 0 to 10 mgal, and decreases northward. The contour interval is gentle between the Karaerik and Karilar deposits indicating the existence of local gravity high.

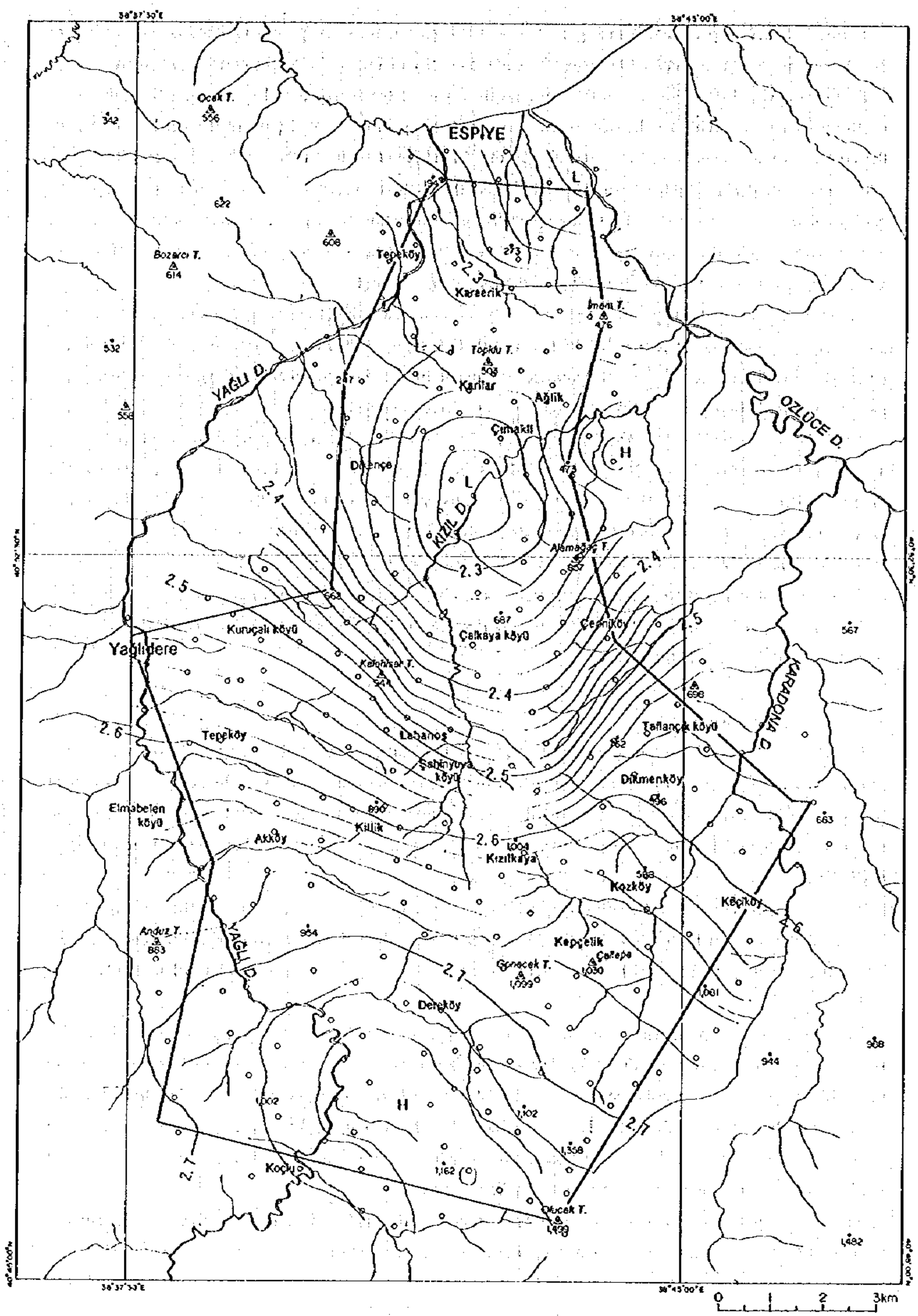

Fig. 5－6 Surface Density Map

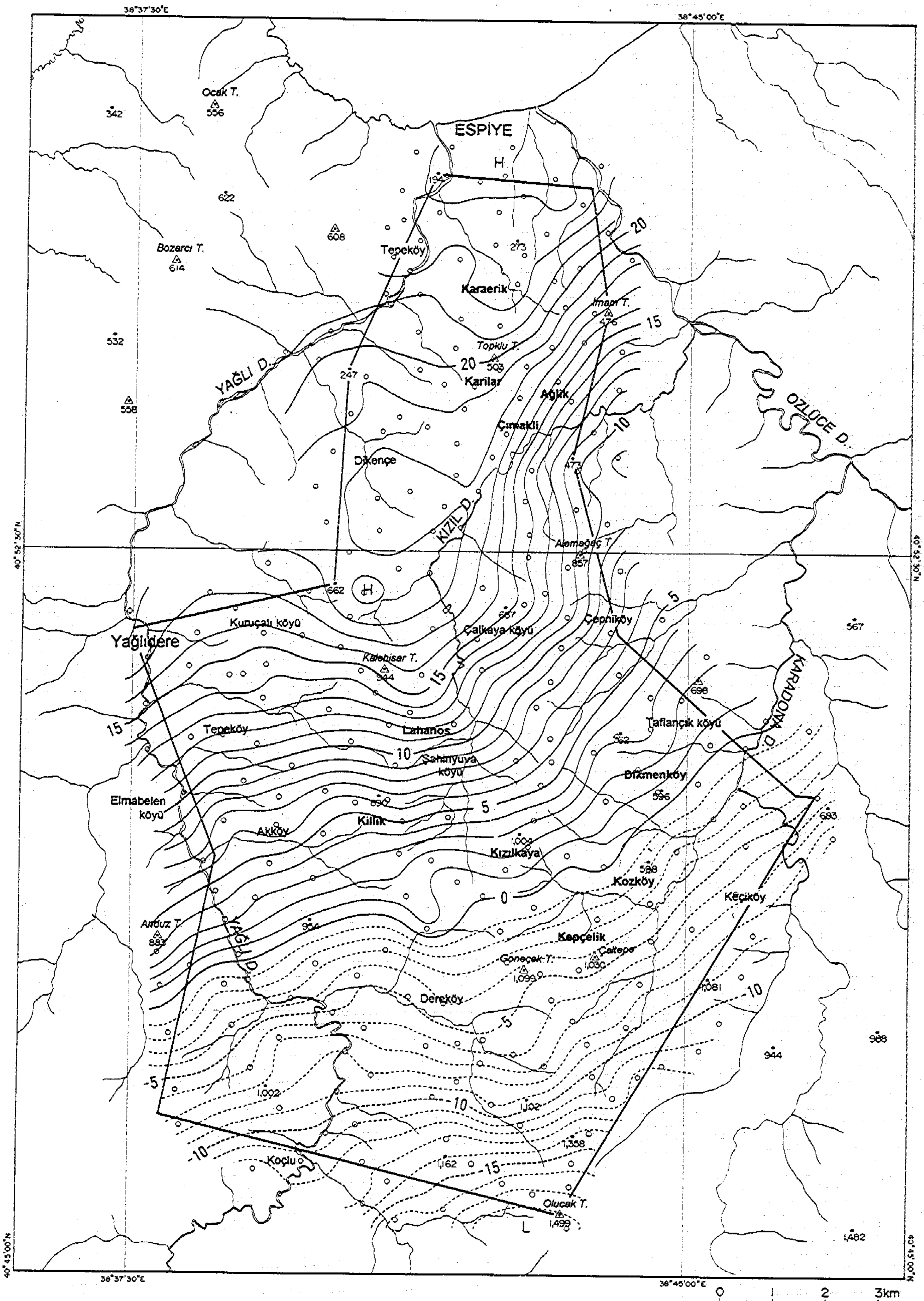

Fig. 5-7 Bouguer Anomaly Map (Variable Density)

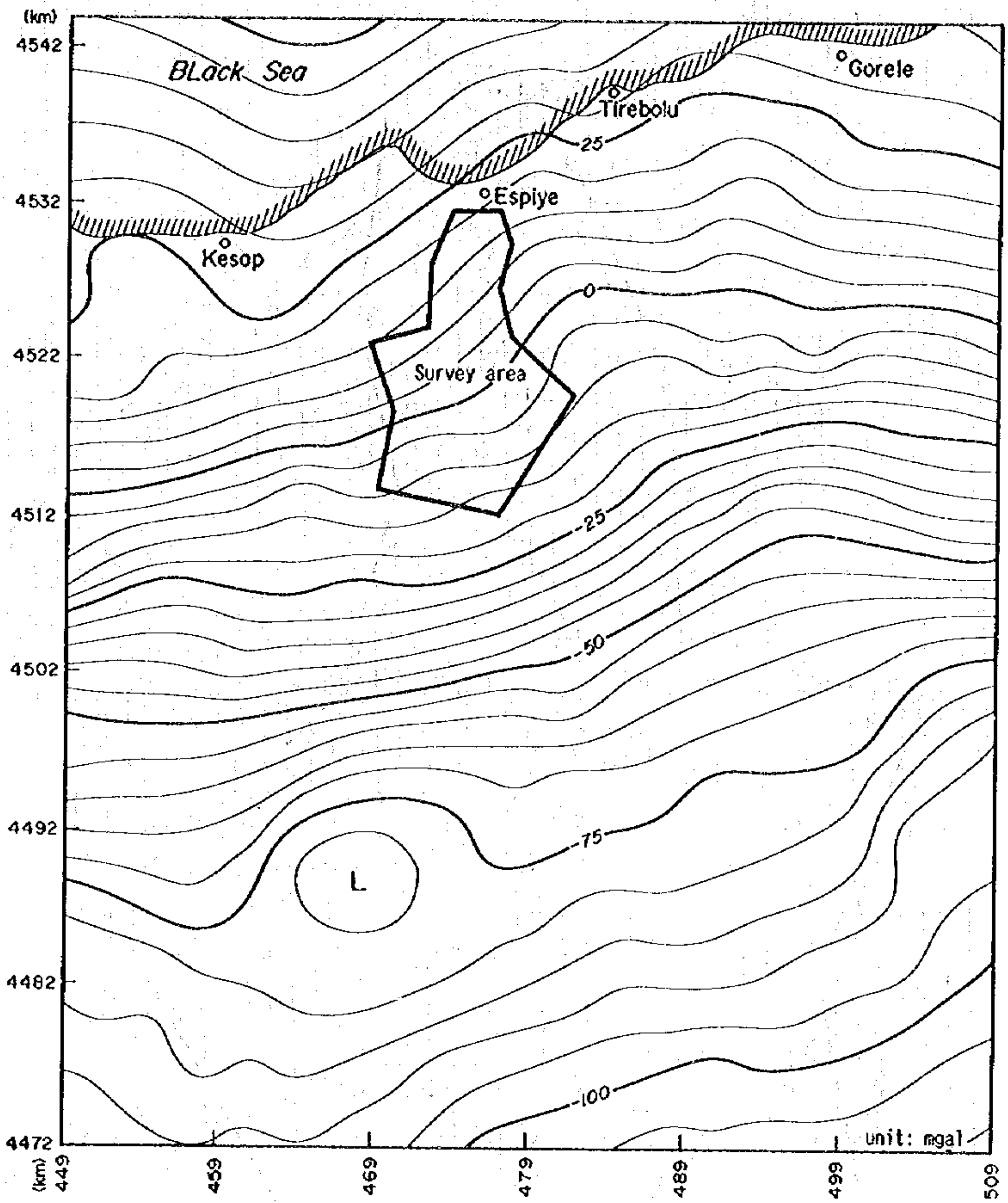

Fig. 5-8 Regional Bouguer Anomaly Map (ρ =2.67g/cm^3)

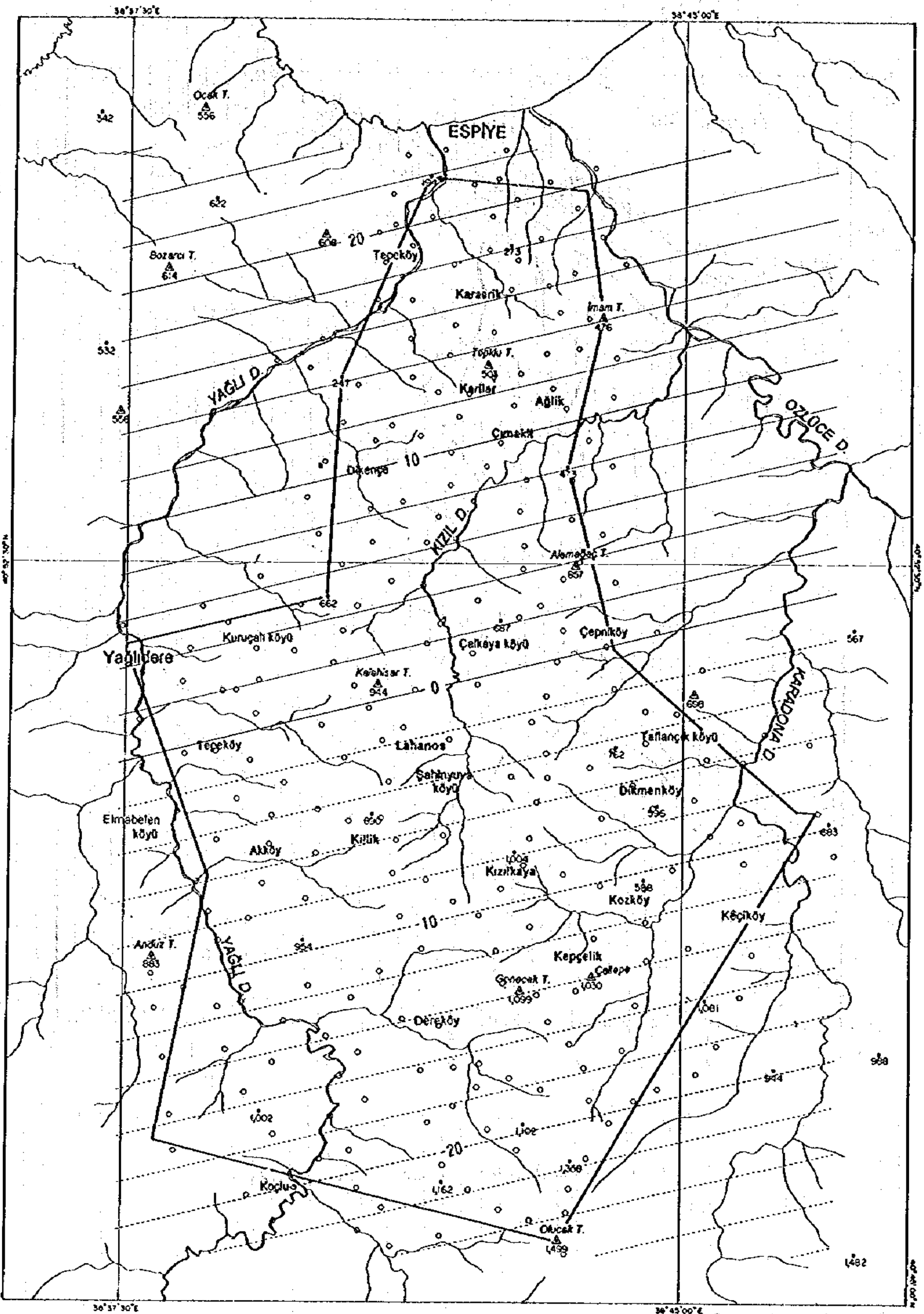

Fig. 5-9 First-order Gravity Trend

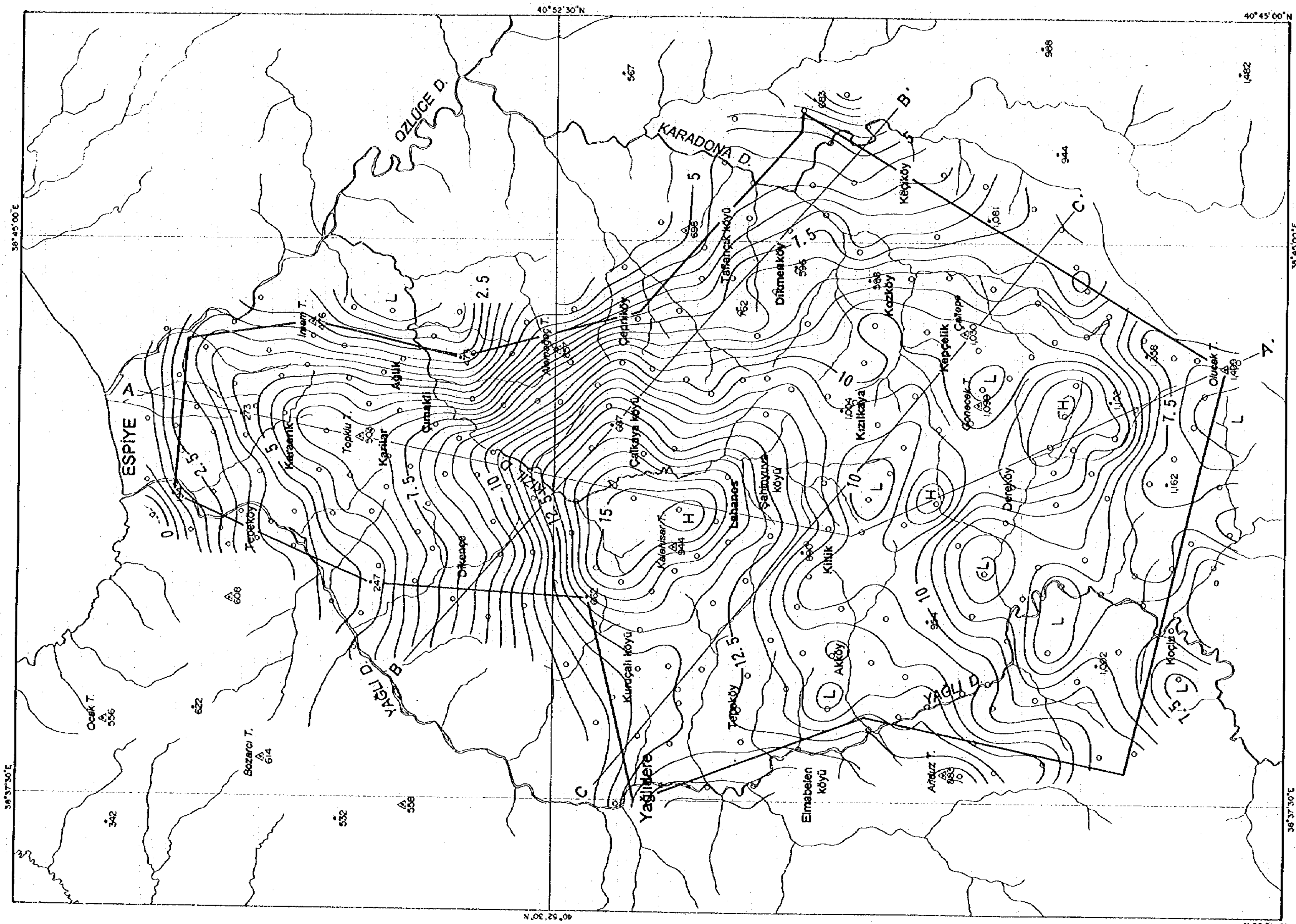

Fig. 5–10 First-order Residual Gravity

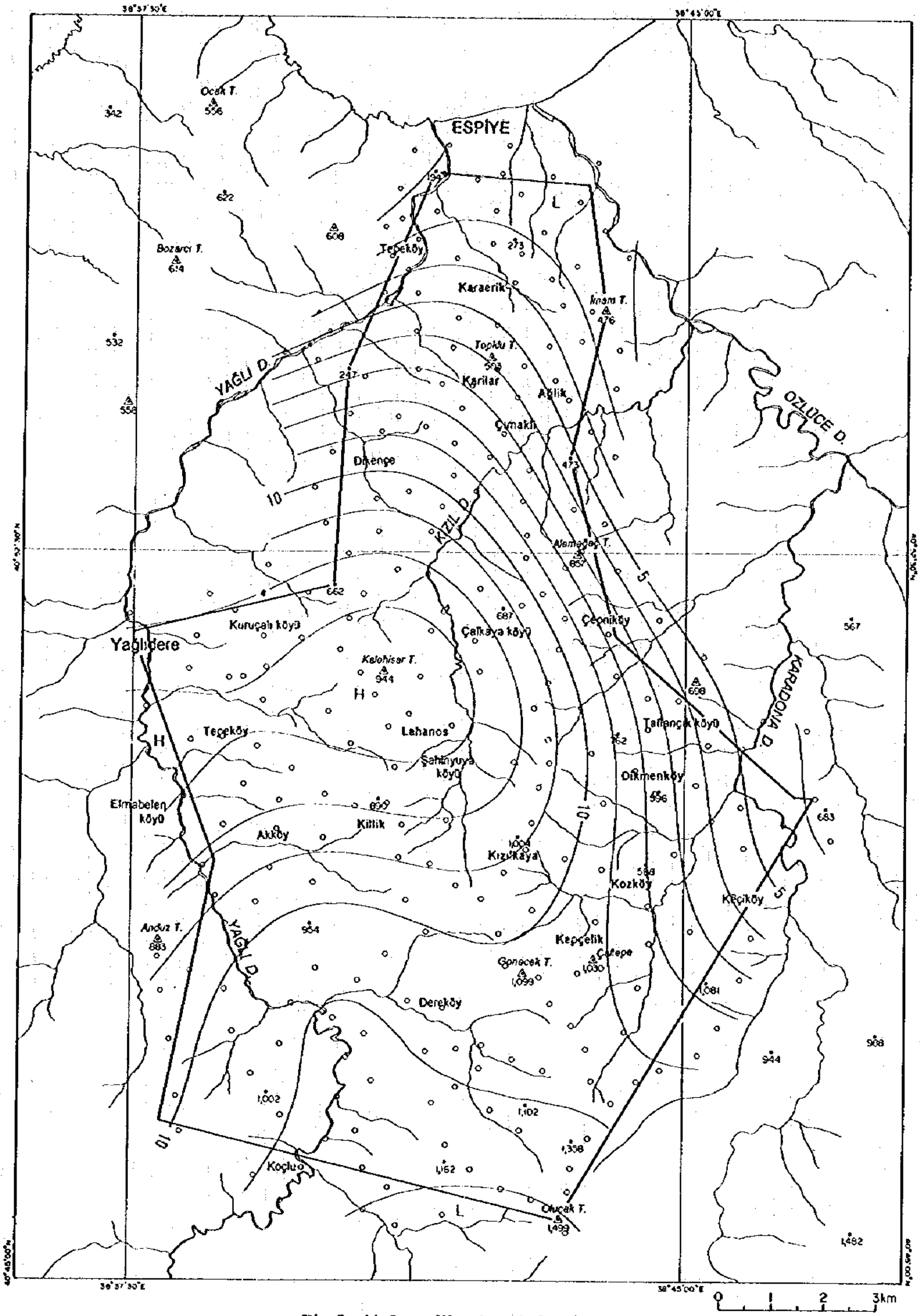

Fig. 5－11 Long Wavelength Gravity

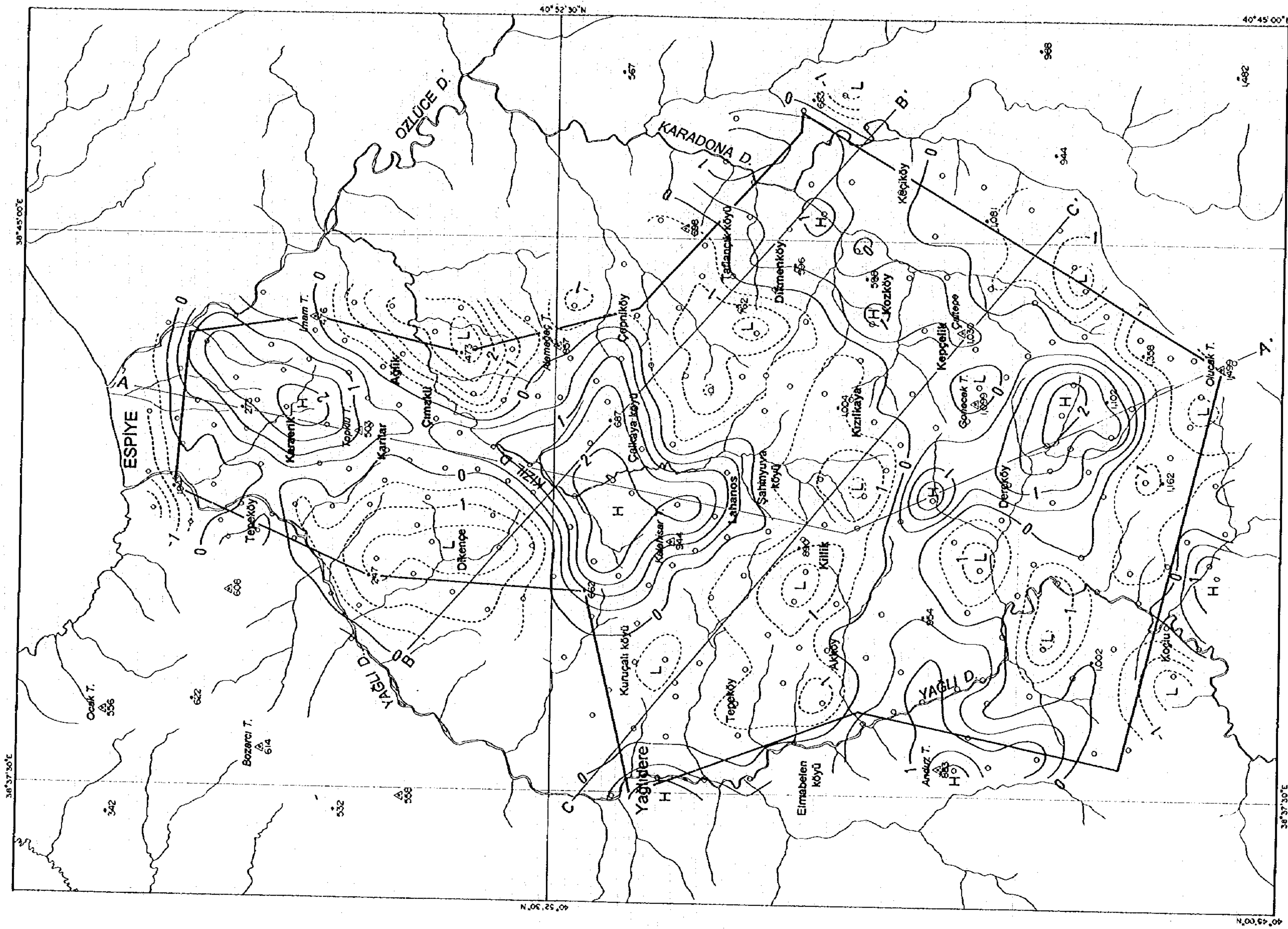

Fig. 5-12 Short Wavelength Gravity

The residual gravity ranges from 5 to 10 mgal in the southeastern to southwestern part of the survey area. Many local high and low anomalies with 1 to 2 km diameter occur in these parts, and the gravity distribution is complex.

The vicinity of Yağlıdere in the western part of the survey area is located in the periphery of a large scale gravity high which is inferred to exist to the west and the residual value is high exceeding 13mgal. This western gravity high and that in the central part is connected by a high residual gravity zone exceeding 12.5 mgal.

4. Long wavelength and Short wavelength gravity maps

The residual gravity map with variable density shown in Figure 5-10 was separated into longer wavelength component with anomaly diameters of 7km or more and shorter wavelength component with anomaly diameters of less than 7km.The longer wavelength gravity anomalies are shown in Figure 5-11 and that of shorter wavelength in Figure 5-12.

It is seen from the long wavelength gravity map that the gravity high in the central part of the survey area is an extension of the high in the western part and extends further southeastward.

From the short wavelength gravity map, clear gravity highs exceeding 2 mgal are seen in four localities, namely west of Çalkaya köyü in the central part of the survey area, vicinity of Karaerik in the north, east of Dereköy in the south, the vicinity of Anduz Tepe in the southwestern border. The low gravity anomalies, on the other hand, are seen to occur surrounding the high in the central part, namely the vicinity of Dikence in the northwest, east of Çımakli in the northeast, between Çalkaya köyü and Dikmenköy in the central part, and from Kızılkaya to Killik. Another gravity low is seen from the Yağlı River basin in the southwest to Olucak Tepe in the south.

5 - 2 - 3 Two-Dimensional Analysis

Two-dimensional anlysis was carried out along the three profiles A-A', B-B', and C-C' of the residual gravity map (Fig. 5-10) and the shorter wavelength gravity map (Fig. 5-12). Long wavelength gravity anomalies and short wavelength anomalies were used for the analysis of the deeper structures and the shallower structures respectively. The results are shown in Figures 5-13 to -15.

For analysis of the deep structure, as data concerning the depth and density of the deep-seated high density layers are non-existant, the depth of the upper surface of this layer was assumed to be -500m below sea-level at the center of the high density anomaly in the central part of the area, and the difference of density from the upper beds was assumed to be 0.20g/cm^3. These assumption, however, do not have solid ground, and thus the results of this analysis should be regarded as only for reference. The calculation was first done on profile A-A' and then on profiles B-B' and C-C' by using the results of the A-A' profile as control points at the intersecting points.

For shallow structure analysis, the formation which is the source of the gravity anomalies was identified from geological cross sections and suitable density was alocated to the unit for calculation. The results of the analysis shows that most of the short wavelength gravity anomalies can be explained by the low density bed on the surface.

1. A-A' profile

The short wavelength gravity lows of this profile correspond well with the distribution of the tuffs of the Çağlayan formation with the exception of those in the vicinity of Olucak Tepe. Although the average density of the tuffs of the Çağlayan formation is listed as 2.35g/cm^3 (2 samples) in Table 5-2, the result of the analysis show a density contrast of -0.20g/cm^3 with the surrounding units and the density of the formation is probably considerably lower. The gravity low near Olucak Tepe is believed to be caused by nevaditic dacite intrusion. The density contrast of -0.20g/cm^3 is to the surrounding Çatak formation.

The calculated values do not agree with the observed values in the short wavelength gravity highs. It is easy to assume the existence of high density rocks near the surface to explain the anomalies, but it is difficult to assume such rocks from the geology of the area and it is considered more reasonable to assume such existence in deeper zones. The first possibility is the existence of high density intrusive rocks which do not appear in the geological secion, and the second possibility is that deep high density layer has risen to shallow zones.

The result of the analysis shows that the deep high density body rises largely in the vicinity of Lahanos mine and it sinks to relatively deeper parts in the northern and southern parts of the cross section. The topography of the surface of such body is not harmonious with the structure of the Çatak formation as seen from the geological section. This fact suggests that the long wavelength gravity reflects the structure of the zones deeper than the Çatak formation.

2. B-B' profile

In this profile, aside from the vicinity of the Karadona River, the short wavelength gravity lows also correspond well with the distribution of the tuffs of the Çağlayan formation. The Çağlayan formation of this profile is not particularly rich in tuff, but the low gravity anomalies are marked where the tuff content is high and there is a clear relation between the two. As mentioned above, the gravity low in the vicinity of the Karadona River is not caused by Çağlayan formation, Çatak formation with relatively low density units such as sandstone and other sedimentary rocks are considered to be the cause of the gravity low.

The gravity high in the area between Çalkaya köyü to the Kızıl River does not agree with the calculated values. The geological cross section of the area show that the Kızılkaya formation forms an anticline and it is probable that the gravity high relects this anticlinal stucture.

The analysis indicates that deep high density body occurs in a relatively shallow zone between Dikence and Çalkaya köyü, and becomes deeper to the northwest and southeast.

3. C-C' profile

In this profile, short wavelength gravity lows are observed in the central part between Killik and Kızılkaya and in the southeastern part (right end of the profile), but both are not notable. The Çağlayan formation does not occur widely in this profile, and the low gravity between Killik and Kızılkaya is considered to be caused by the strongly altered part of the Kızılkaya formation. The Çatak formation is distributed at the right end of the proile, and the low gravity is believed to be caused by extensively occurring sedimentay rocks of relatively low density.

The gravity high from Kızılkaya to Çaltepe does not agree with the calucated values, but the difference

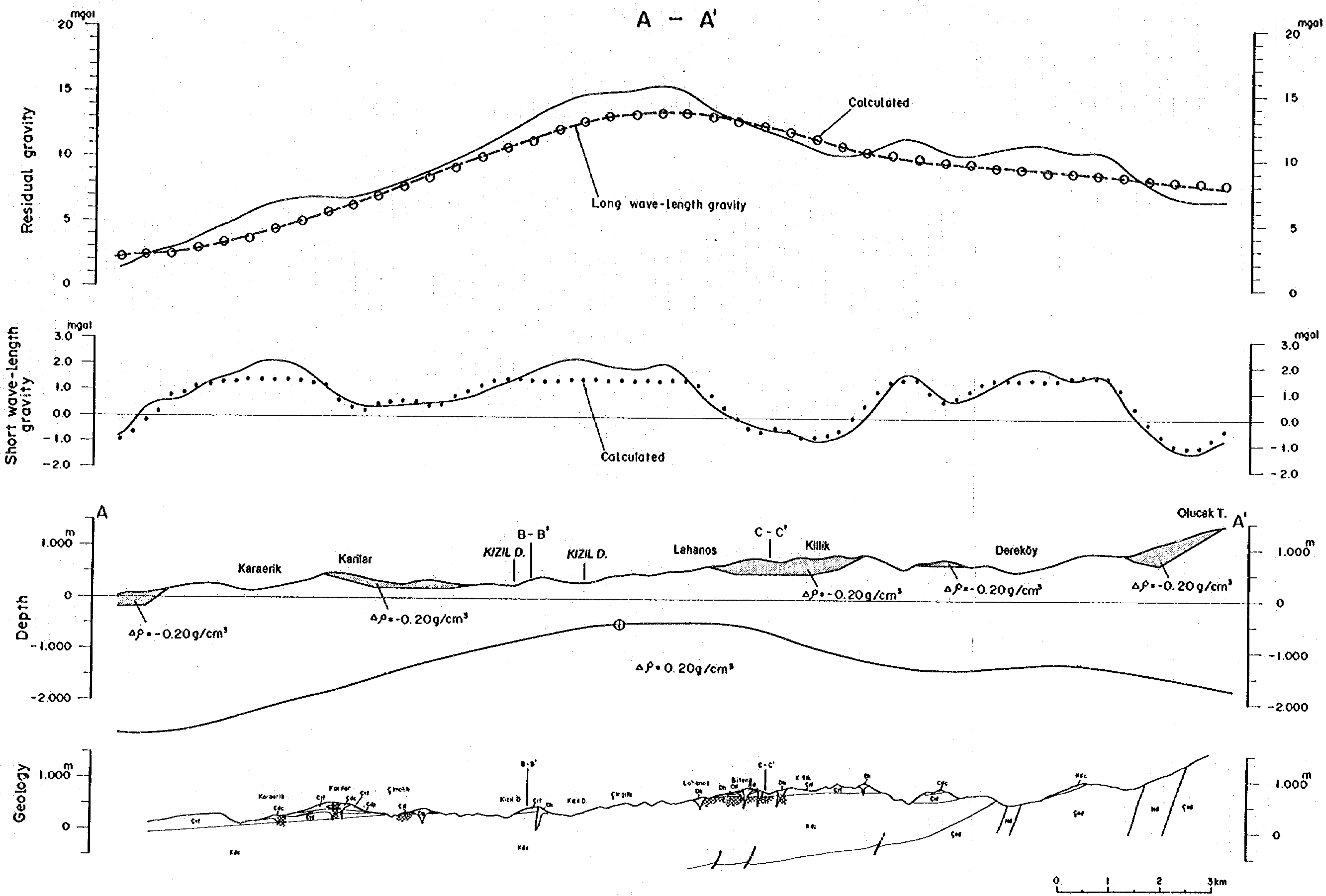

Fig. 5-13 Gravity Analysis Profile A-A'

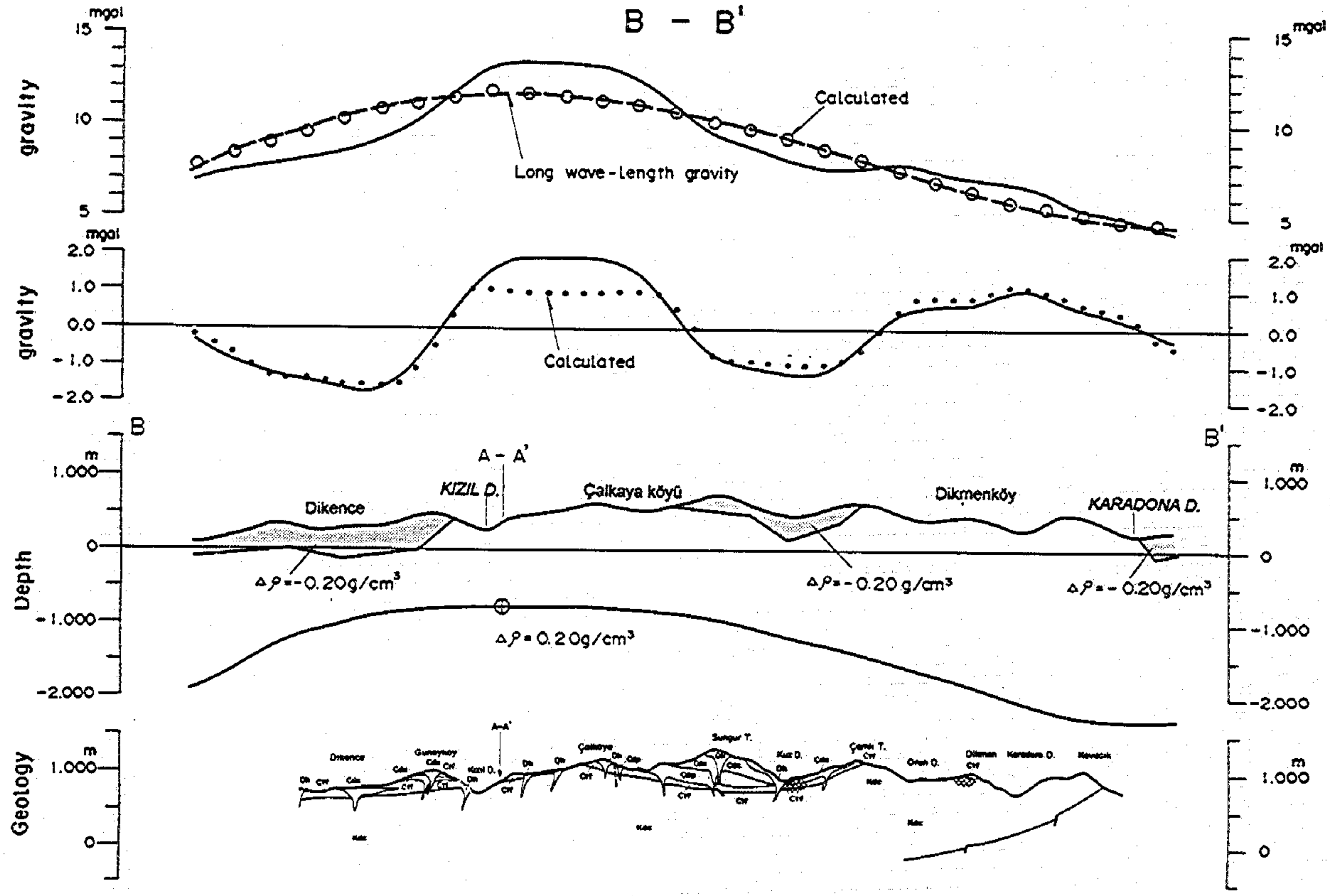

Fig. 5-14 Gravity Analysis Profile B-B'

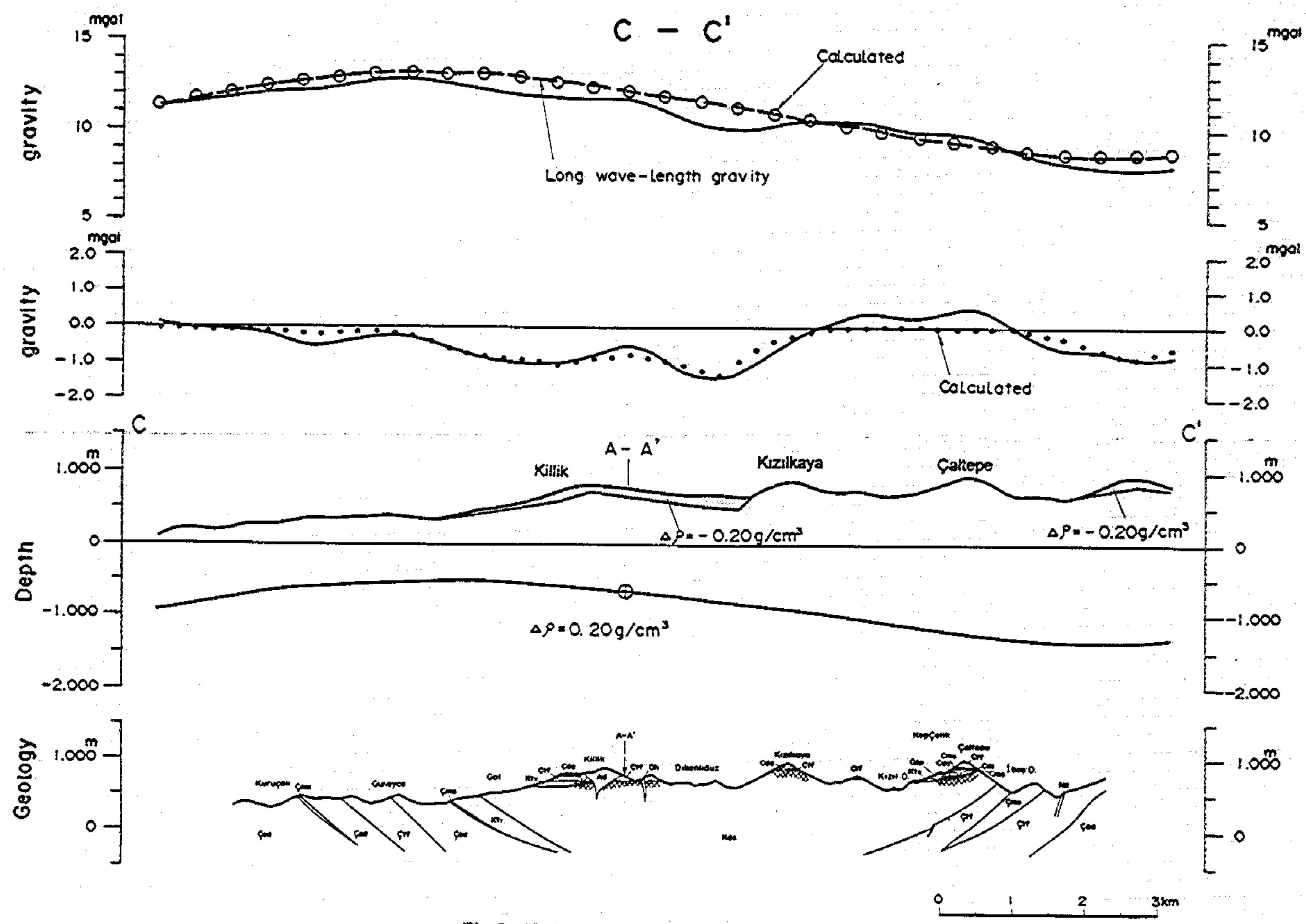

Fig. 5-15 Gravity Analysis Profile C-C'

is small and the gravity high itself is not marked. Thus it is considered not necessary to assume the existence of high density body for this anomaly.

The long wavelength gravity in this profile does not vary very much and thus the relief of the upper surface of the high density body obtained by deep structure analysis is small.

5-3 Consideration

5-3-1 Gravity Features and Geology

1. Short wavelength gravity and geology

The results of the correlation of short wavelength anomalies (Fig. 5-12) and geology (Fig. 2-1) over the survey area are as follows.

1) The distribution of the Çağlayan formation mostly corresponds to that of the low gravity anomalies.
2) The distribution of the Kızılkaya formation more or less corresponds to that of the high gravity anomalies.
3) Half of the Çatak formation occur in the high gravity zones and the other half in the low gravity zones.
4) The intrusive bodies are clearly divided by rock species into those corresponding to high gravity anomalies and those corresponding to low anomalies.

The Çağlayan formation is distributed mostly in low gravity anomaly area with the exception of the vicinity of the Karaerik deposit with high gravity. This is in harmony with the relatively low average density of the rock samples of this formation. The high gravity near Karaerik is considered to be the effect of either the raised stucture of the lower Kızılkaya formation or the intrusion of a relatively high density body.

The Kızılkaya formation is distributed in a well defined two high gravity zones, namely that extending in the N-S direction between the vicinity of the Lahanos mine and Çımakli, and that extending from Dikmenköy through Kozköy to Dereköy. The density of the rock samples of this formation is not high, but aside from the low density tuff zones and strongly altered zones, this formation is often distributed in high gravity areas. The gravity highs in these areas is considered to be not due to the Kızılkaya formation, but to the rise of the basement (deep high density layer) or to the intrusion of high density bodies.

The area from the west of Lahanos mine to Killik and the vicinity of Kızılkaya are low gravity anomaly zones, and this is believed to be caused by the low density tuff of the Kızılkaya formation or to strongly altered parts.

The density of the rock samples of the Çatak and Çağlayan formations is clearly higher than that of the Kızılkaya formation, but their distribution does not correspond to high gravity anomalies. This probably is due to the fact that low density sedimentary units are dominant in the Çatak formation in these areas. But there are high density andesite areas which do not form high gravity anomalies, and the reason for this fact is not clear, but there are possibilities of the existence of low density intrusive bodies, or of strongly altered Çatak formation in these areas. It also is possible that the formation could have significant amounts of voids and fissures lowering the apparent macro density.

Regarding intrusive bodies, the occurrence of nevaditic dacite corresponds well with the low gravity anomaly zones. This is particularly clear with the large nevadite bodies at Çımakli. Since, according to the regional residual gravity map, the areal distribution of the low gravity zone is larger than the rock body, factors other than the navadite may be contributing to this anomaly.

One of the intrusive rocks which can be correlated to high gravity anomalies is biotite dacite. The dacite occurring widely in the vicinity of Kalchisar Tepe in the central part of the survey area is related to the southwestern part of the high gravity anomaly to the west of Çalkaya köyü, and thus it is considered that the dacite plays a strong role in the formation of this gravity high.

2. Long wavelength gravity and geology

The correlation between the long wavelength gravity map (Fig. 5-11) and the geological map (Fig. 2-1) is not good. This fact indicates that the long wavelength gravity reflects deep subsurface structure below the Çatak formation. It is difficult to discuss the relation between the long wavelength gravity and geology because information regarding strata below the Çatak formation is very limited. It is, however, possible to interpret the long wavelength high gravity anomalies as reflecting either rise of the basement or intusion of high density bodies.

5 - 3 - 2 Gravity Features and Occurrence of Ore Deposits

In the northern half of the survey area, there are; Karaerik, Karilar, Ağalik, and Çımakli deposits. And in the southern half, Lahanos, Killik, Kızılkaya, Kepçelik, Kozköy, and Dikmen deposits occur.

According to the long wavelength gravity map, the deposits in the north all occur in the intermediate zone between the high and low gravity anomaly zones, while in the short wavelength gravity map, Karaelik deposit occurs in the cental part of the high gravity anomaly and the others occur in the periphery of the same gravity high.

In the long wavelength gravity map of the southern half; Lahanos deposit occurs at the margin of a gravity high, and Kızılkaya and Kepçelik deposits in the ridge of a gravity high extending southwestward from the center of a high anomaly. The Killik, Kozköy, and Dikmen deposits are located in the transition zone between gravity high and low. With the short wavelength gravity map, the three deposits Lahanos, Kepçelik, and Kozköy occur in the high gravity anomaly zones and the other three namely Killik, Dikmen, and Kızılkaya deposits are located in the transition zone between the high and low anomaly zones.

The above relation between the gravity anomalies and ore deposits are summarized as follows.

1) There is a relatively clear tendency regarding the ore deposits and long wavelength gravity anomalies. The ore deposits occur in the intermediate zone between the high and low anomaly zones or in the margin of high gravity anomaly. None occurs in the low gravity anomaly. Thus the distribution of the ore deposits are closely related to the long wavelength high gravity anomalies. This fact indicates that the ore genesis is controlled by the geologic structure which gives rise to the long wavelength gravity high.

2) With short wavelength gravity anomalies, again the ore deposits do not occur in the center of low gravity anomalies, and the tendency to be located in the transition zone between the high and low gravity anomaly zones is clear.

5 - 3 - 3 Comparison with the Gravity Features over the Japanese "Kuroko" Area

A gravity map of the Hokuroku District is shown in Figure 5-17. This area is a representative "Kuroko" zone in Japan. Seya (1965) showed that almost all of the kuroko deposits in this area occur in the intermediate zone between high and low gravity anomalies or in the high gravity side, and the relationship can be seen from Figure 5-17. This is similar to the long wavelength gravity and ore deposits of the present survey area, and thus is a common feature between the two areas.

Nakajima (1993) wrote that larger kuroko deposits such as Hanaoka, Shakanai, Kosaka are located at the margin of depressions of the basement, while the medium to small deposits such as Furutobe, Ainai, Fukazawa are situated in the small valleys which dissect the ridge-shaped uplift topography. It is seen in Figure 5-17 that the large Hanaoka and Shakanai deposits occur in the boundary between the high and low gravity anomalies where the gravity gradient is steep, and although Kosaka deposit is located where the gravity gradient is not steep, it is in the proximity. Nakajima's "margin of the basement depression" agrees extremely well with the gravity features. The gravity features in the vicinity of the medium and small Furutobe and Fukazawa deposits again is interpreted to relect Nakajima's "ridge-shaped uplift topography".

The deposits of the present survey area are located where the gravity gradient is steep, similar to those of Hokuroku area. Ağalik and Dikmen can be classified as large deposits and others as medium to small. In the present survey area, however, low gravity anomaly corresponding to the "basement depression" is not clearly confirmed, and it is not clear whether the steep gravity gradient of Ağalik and Dikmen deposits indicates basement depression or not. There is a large eastward extending low gravity anomaly in the eastern margin of the survey area and this could be reflecting a "basement depression", but this needs to be confirmed in the future.

The area from Çalkaya köyü to Çepniköy located accross the Kızıl River from Lahanos deposit is considered promising and warrant future exploration from gravity features and geology. The hangingwall Çağlayan formation is widely distributed in this area, and the tuff unit of Kızılkaya formation - the ore horizon - have not been eroded. The gravity features shows this area to be in the ridge-shaped extended part of a short wavelength gravity high, similar to the Lahanos deposit. Regarding the long wavelength gravity, Çepniköy is situated at the steep gravity gradient zone and has the conditions for the occurrence of large deposits.

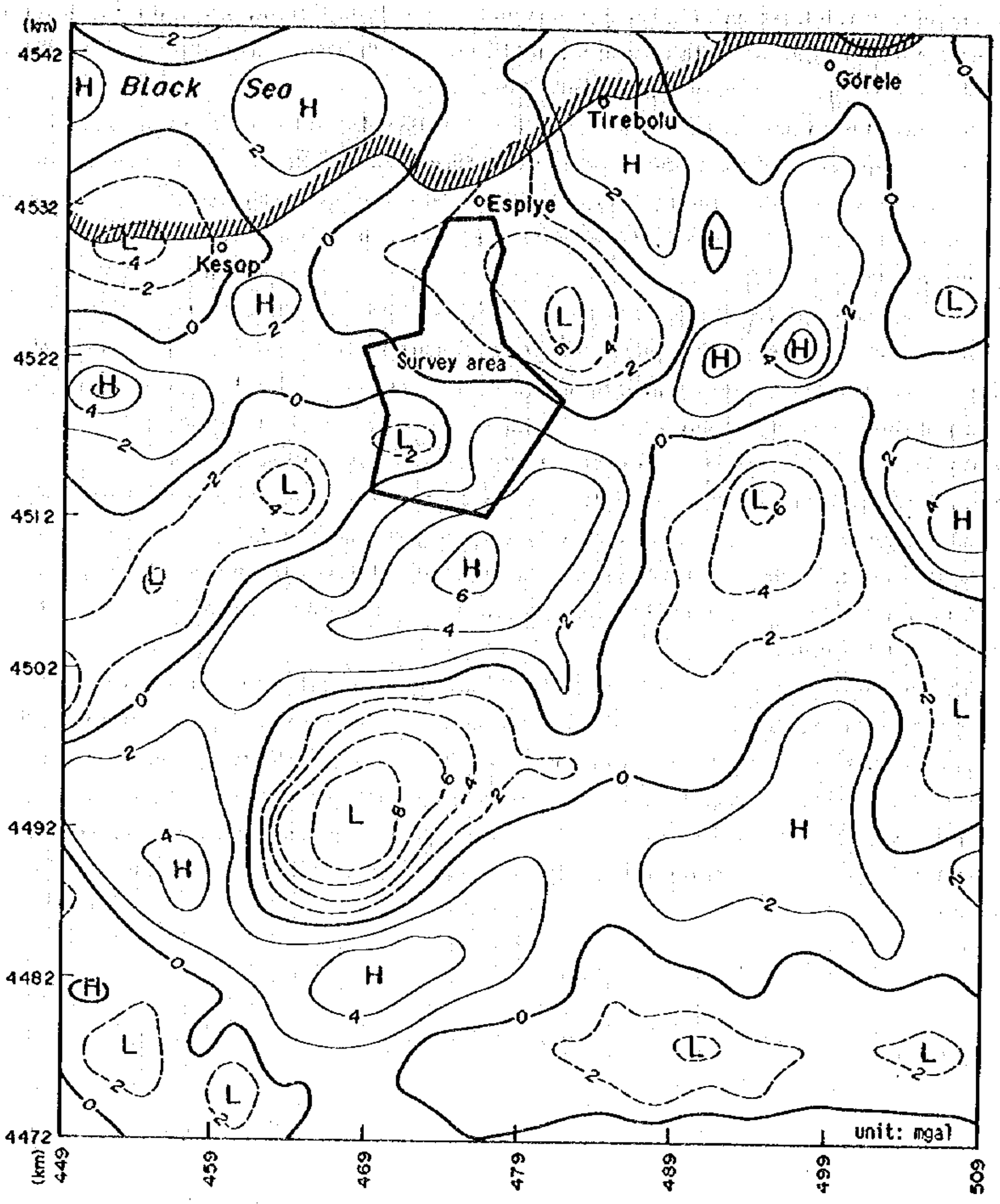

Fig. 5-16 Regional Residual Gravity

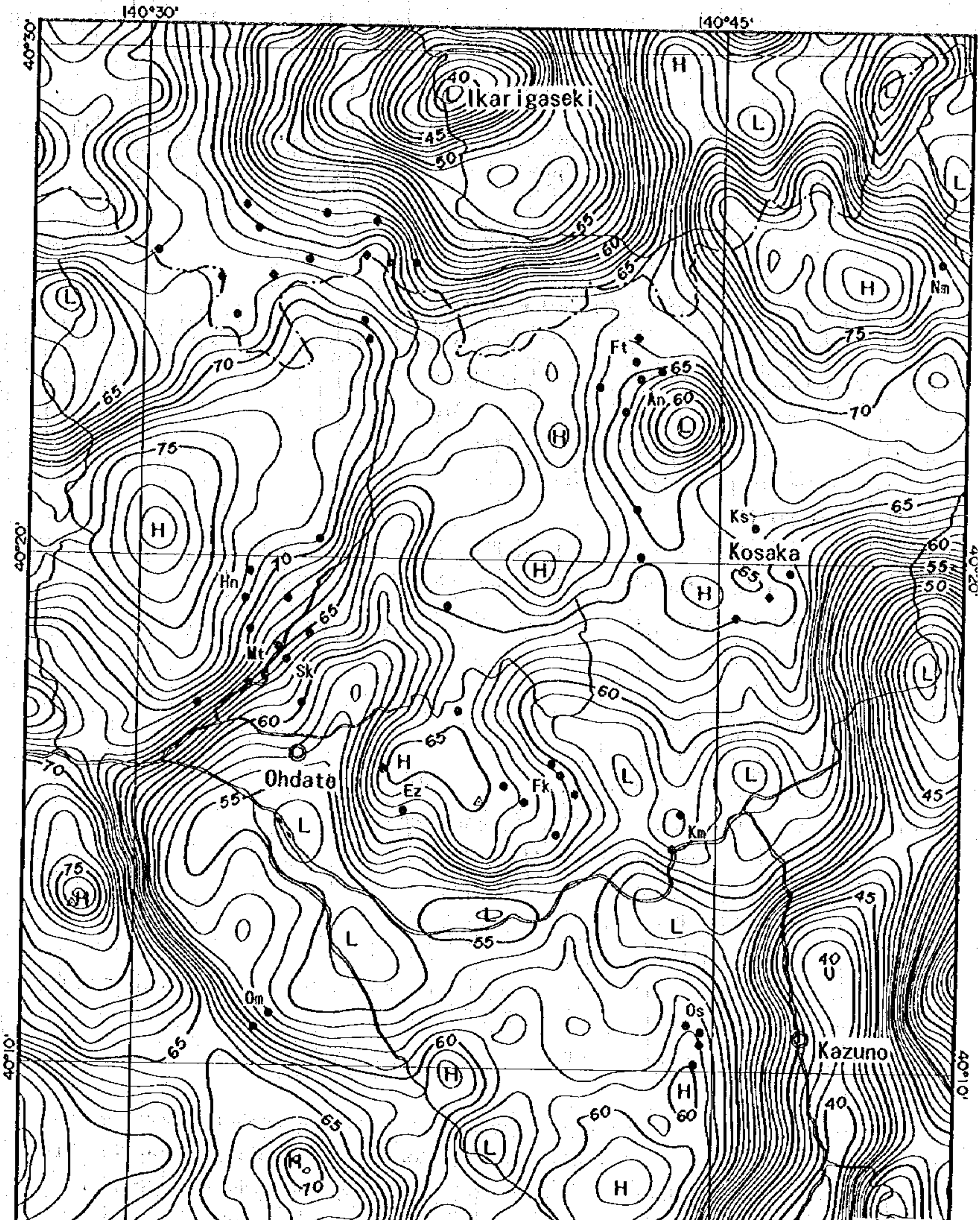

Fig. 5-17 Bouguer Anomalies over the Kuroko Area in Japan (ρ =2. 30g/cm^3)

Chapter 6 IP Survey

6-1 Survey Methoed

6-1-1 Content of the Survey

The survey areas for electric survey(IP survey) were established in the areas concluded to be hopeful by analysis of existing documents and geological survey.

Locations of the areas are shown as Fig. 6-1.

Specification of geophysical survey is shown in Table 6-1.

Table 6-1 Specification of Geophysical Survey

Method	Induced polarization method (IP method)
Detection method	Time domain method
Electrode arrangement	Dipole-Dipole
Separation of electrode arrangement	a=100m
Coefficient of electrodes separation	n=1-5
Number of survey line	8
Total length of survey line	23.3km
Tests of physical property of rocks and ores (laboratory test)	45 specimens for chargeability and resistivity

6-1-2 Operation of the Mesurement

1. Determination of Survey Line and Survey

Survey lines were planned to start from cross points of roads.

Open traverse method was adopted to locate exact survey points.

Locations of each survey lines are shown too in Fig. 6-1.

2. Electric Prospecting (IP method)

1)The Principle of IP Method

When an electric current is sent into the earth, various electric chemical phenomena occur in the medium that composes the ground.

IP method measures two phenomena as follows,

〔Over Voltage Effect〕

By sending an electric current, two multi-layer are produced on surface of sulfide or metallic conductors. And when an electric current is switched off, an electric discharge occurs towards opposite direction. This phenomenon is due to combinated effect of ion with electron conduction. The origin of this phenomenon is minerals showing high electron conductivity, and then these minerals can be detected by IP method.

〔Normal Effect or Background〕

Polarization occurs by sending an electric current in ordinary rocks. The main origin of this phenomenon is membrane polarization caused by a small amount of clay minerals in cavities of rocks. The membrane

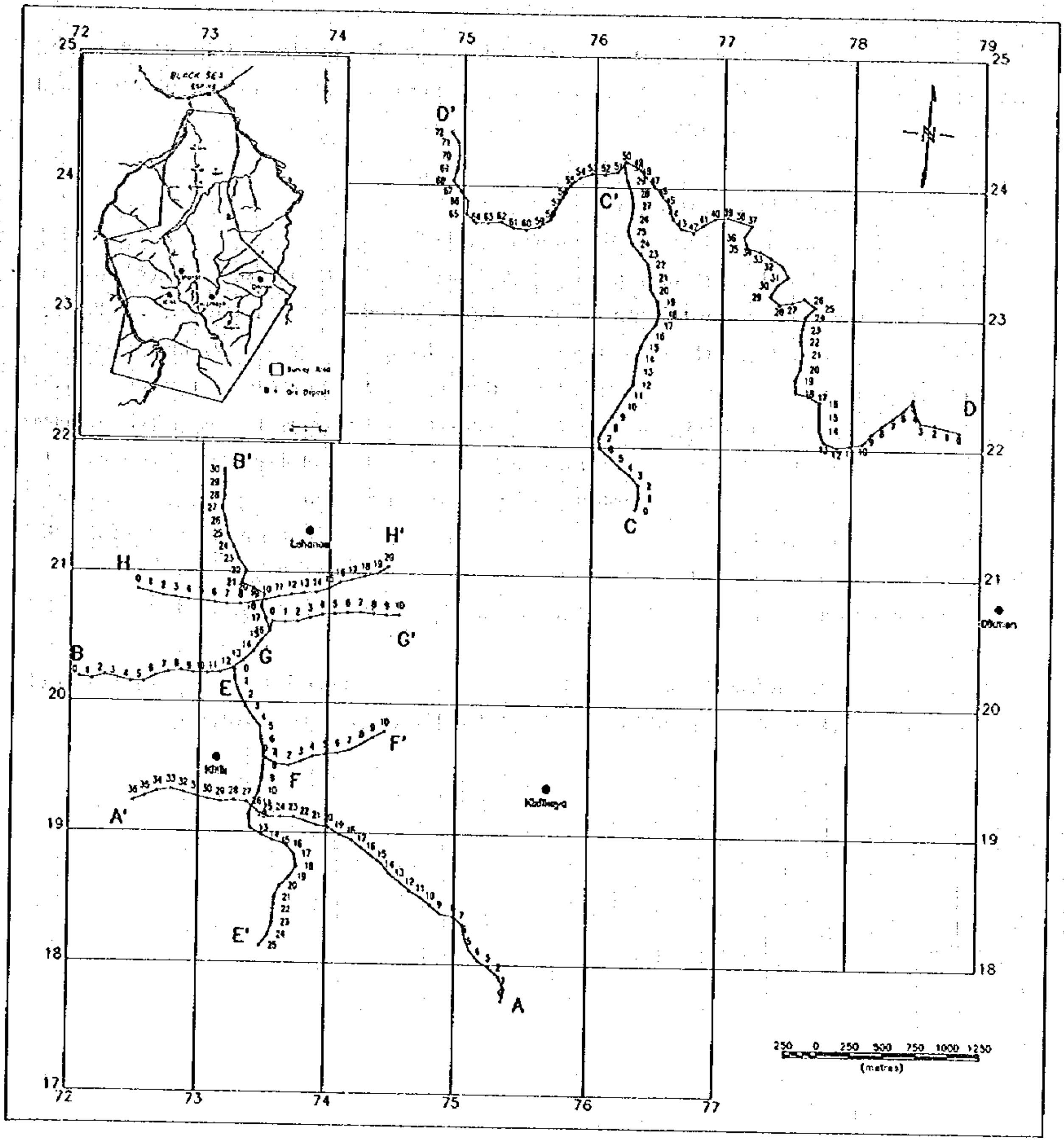

Fig. 6-1 Location of the Geophysical Survey Area

polarization of montmorillonite is the largest among all of clay minerals, and that of kaolinite is small. The membrane polacization shows its maximum value when clay minerals are contained in rocks as around 5% of total volume. However, membrane polarization decrease in the cases when capacity ratio of clay minerals is higher or smaller than 5%.

The membrane polization shows its maximum when montmorillonite are contained around 5% of total volume, and if it is expressed by FE value it is around 2%. But this value is extremely small compared with above mentioned Over Voltage Effect by sulfide minerals.

2)Measuring Method of IP Phenomenon

The outline of measurement is illustrated as shown in Fig. 6-2.

Measurement was carried out by time-domain method(Abb. form;T. D. method)(it is called transient method in another way). In this method at first, direct current is transmitted intermittently(on/off 2. 0sec) into the ground through a couple of current electrodes(that is, C1 & C2), and then two kinds of data can be obtained from a couple of potential electrodes(that is, P1 & P2). One is primary potential difference(Vp) just before switching off an electric current, the other is the secondary potential difference(Vs) during T time(T time is from 60msec to 1, 590msec) after switching off an electric current.

In this survey, Vs during T time after switching off an electric current were measured. The concept of operation is shown in Fig. 6-2, the concept of method of measurement is shown in Fig. 6-3 and the list of sampling time is shown in Table 6-2.

IP effective measurement value by IP method is generally called chargeability and is expressed by Vs/Vp(mV/V).

The data of secondary potential difference in this survey seemed not to be influenced from the effect of electromagnetic coupling. The 935msec data were adopted in this survey as the chargeability of mid-point.

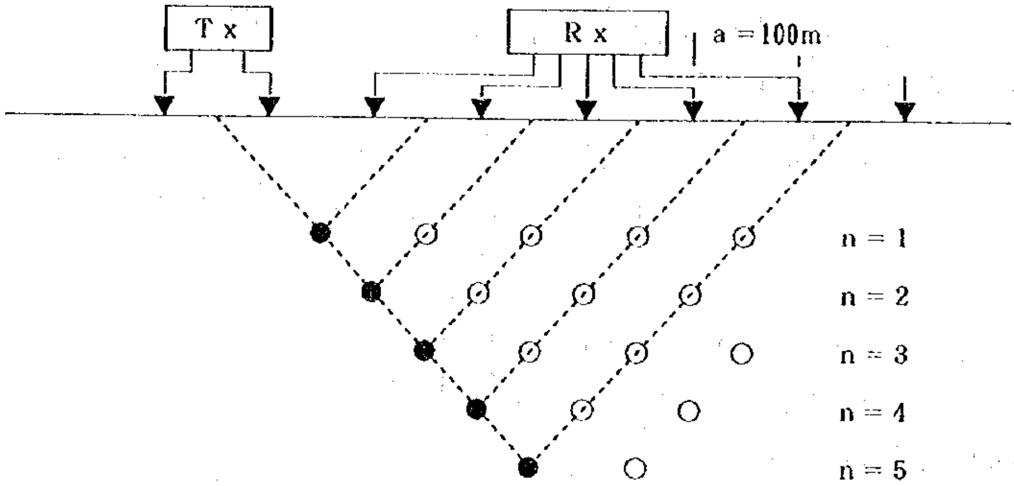

Fig. 6－2 Concept of Operation

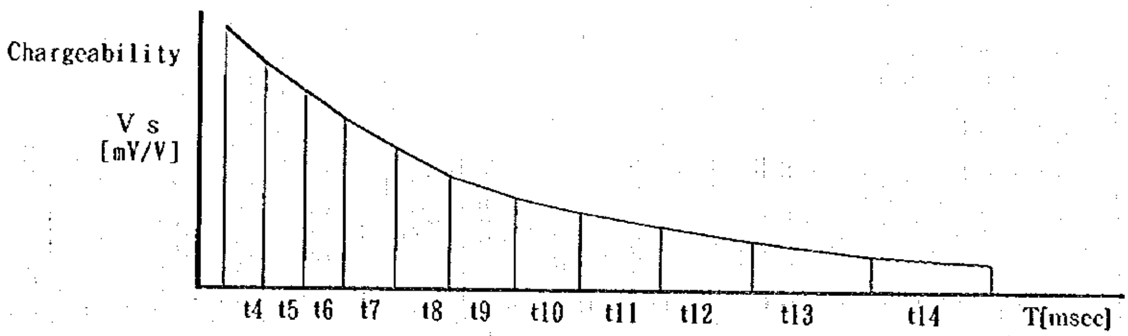

Fig. 6－3 Concept of the Method of Measurement

Table 6－2 List of Sampling Time

Slice #	t4	t5	t6	t7	t8	t9	t10	t11	t12	t13	t14
Midd-Point	60	90	130	190	270	380	520	705	935	1230	1590 msec
Width	20	40	40	80	80	140	140	230	230	360	360 msec

3. Measuring equipments and materials

The measuring equipments and materials are shown in Table 6-3.

Table 6-3 List of Equipments and Materials

Field survey

Equipment	Maker	Type	Specification	Amount
Transmitter	SCINREX	TSQ-3	1500V, 10A max output:3000W	1
Engine Generator	INDUSTRAL COMMERCIAL	10DE	220V 400Hz 8HP single cylinder 2cycle	1
Receiver	SCINTREX	IPR-12	8channel, 14window Input Range:50uV to 14V	1
Electrode		Current	stainless steel	1
		Potential	CuSO4	1
Cable	FUJIKURA		VSF1.25mm²cable	1
Measuring compass	USHIKATA		Pocket compass 100m Esron tape	4
Communication device	KENWOOD	TH-45G	Output:600mAhW Battery:12V	12

Laboratory test

Equipment	Maker	Type	Specification	Amount
Transmitter	IRIS	IP-L	Output:1uA ~ 100mA Max 10V	1
Receiver	SCINTREX	IPR-12	8channel, 14window Input Range:50uV ~ 14V	1
Electrode			Pt	1

6-1-3 Method of Analysis

Simulated Analysis from Pseudo Cross Sections

Electric field originated from point source on surface or underground developes as all energy will be minimized, in both cases of resitivity and IP methods. Electric field is minimized on equation(1) as follows,

$$\Delta \int V \quad f(\phi)\ dv = 0 \qquad (1)$$

In equation(1), $f(\phi)$ means a function of electric potential(ϕ) derived from Maxwell's

$$f(\phi) = \sigma(\Delta\phi)^2 - 2Js \cdot \Delta\phi \qquad (2)$$

electro-magnetic equation, and it is expressed using conductivity(σ) and current density(Js) in case of normal electric field as following equation(2). First equation means integral calculus of whole volumes where currency from point source passes, but in infinite element method it is evaluated approximately after presuming sufficient but limited volume. In this survey analysis was carried out as two dimensional problem, and sufficiently wide sectional areas(horizontally 10km×vertically 3km)were adopted in stead of volume.

Simulation analyses of resistivity and pseudo cross section of IP were carried out using infinite elemental program of 2nd and half dimension by Coggon(1971) and Rijo(1977). After data and modification were input in dialofue style and calculations were repeated several tens times, result was obtained approximately almost same as the presumed model on pseude cross sections.

6-2 Result of Survey

6-2-1 Result of Survey

1. Result of Survey

Apparent resistivity and chargeability acquired in this survey are shown in Figs. 6-4~11 as cross sections, Figs. 6-12~14 show apparent resistivity in plans, and Figs. 6-15~17 show chargeability in plans.

1)Cross Sections of Apparent Resistivity and Chargeability

A-survey line

Dacitic lava and its pyroclatics of Kızılkaya formation and dacitic pyroclastics of Chaglayan formation develop along this line. Intrusive rock also can be seen around Nos. 15 and 30.

Around Nos. 15 and 30 where intrusive bodies of red dacite and nevaditic dacite distribute, high resistivity like as 500Ω・m was shown.

At No. 26 where dacitic pyroclastics of Çağlayan formation develope, around 50Ω・m were shown as resistivity, and in most area where dacite lava occupies resisitivity vary below 200Ω・m.

Chargeability on this line was shown 12mV/V as maximum.

Around Nos. 6~7 and 29, weak IP anomaly like pantaloon shape was recognized and it seems to be derived from superficial ore showings.

B-survey line

Dacite lava and its pyroclastics of Kızılkaya formation and dacitic pyroclastics of Çağlayan formation develope along this line. Intrusive rock exist around Nos. 6, 13 and 16.

Around No. 6, low resistivity like as 20Ω・m were measured due to widely argillized zone on surface.

Resistivity around Nos. 16~22 changed highly because of dacite lava of Çağlayan formation and intrusive rock.

Dacitic pyroclastics of Çağlayan formation around No. 24 showed 40Ω・m.

The maximum chargeability on this line was around 10mV/V.

In the depth of No. 19~20, weak IP anomaly was seen.

C-survey line

Dacitic lava of Kızılkaya formation and dacitic pyroclastics of Çağlayan formation develop along this line.

Low resistivity was usually observed at geological boundary around Nos. 8, 18 and 22, but clear relation between rock facies and resistivity could not be recognized generally.

Chargeability was low on this line as general and its maximum value was 5mV/V.

Any characteristic was not seen in distribution pattern of chargeability on this line.

D-survey line

Dacitic lava of Kızılkaya formation, dacite lava, its pyroclastics and porphyritic dacite lava of Çağlayan formation develop along this line. Around No. 19, red dacite exists.

Relatively low resistivity like as 20～80Ω・m was measured in the whole area where dacite lava of Kızılkaya formation and dacitic pyroclastics of Çağlayan formation distribute. Difference of resistivity between dacite lava and intrusive rock could not be detected clearly.

Relatively low resistivity like as 20～40Ω・m due to argillization on surface was observed commonly.

The maximum chargeability on this line was 17mV/V.

A clear IP anomaly was recognized at the depth of No. 63.

E－survey line

Along this line, dacite lava of Kızılkaya formation, dacite lava and its pyroclastics distribute.

Low resistivity like as 30Ω・m due to argillization was observed around No. 9.

Around Nos. 14 and 19, high resistivity like as about 4,000Ω・m due to intrusive rock was shown.

The maximum chargeability on this line was 15mV/V.

Clear IP anomaly was recognized around Nos. 23～25 where dacite lava of Kızılkaya formation(that is, footwall of massive sulfide ore deposits) was exposed.

High IP anomaly and high resistivity due to shallow intrusive rock was shown around Nos. 14～15 and 19～20.

F－survey line

Dacite lava of Kızılkaya formation and dacitic pyroclastics of Çağlayan formation develop along this line. Around No. 2, red dacite lies.

Clear relation between rock facies and resistivity could not be obtained.

The maximum chargeability on this line was 8mV/V.

The higher chargeability was inclined to be shown in the deeper places.

G－survey line

Dacite lava of Kızılkaya formation and dacitic pyroclastics of Çağlayan formation distribute along this line. Around No. 13, red dacite and andesite exist.

Clear relation between rock facies and resistivity was not obtained.

The maximum chargeability on this line was 18.3mV/V.

High chargeability was observed at the depth of Nos. 3～10.

H－survey line

Dacite lava and its pyroclastics of Kızılkaya formation, and dacite and its pyroclastics develop along this line. Intrusive rock was seen around No. 13.

High resistivity more than 200Ω・m was recognized around No. 13 where intrusive rock lies.

Low resistivity like as 40Ω・m was observed around No. 4 where argillization was seen commonly.

The maximum chargeability on this line was 16mV/V.

High chargeability was generally shown where high resistivity more than 100Ω・m was observed.

2)Plans of Apparent Resistivity and Chargeability

When dipole-dipole array of electrodes and high electrode separation index like as 4 or 5 are adopted in IP survey, pattern of IP anomaly originated from shallow places is characteristically inclined to be enlarged on deeper plans.

In such a case, IP anomaly pattern does not correspond well to actual origin of anomaly. Therefore, description here is based on low electrode separation index like as 1 to 3.

Hereby, the area which includes A, B, E, F, G and H survey lines is defined as Lahanos area, and north-eastern part of the survey area is defined as Çalkaya area.

Plans of Apparent Resistivity

Resistivity less than 200Ω・m prevailed mostly in the survey area and high resistivity areas like as 500 Ω・m were scattered.

High resistivity areas in Lahanos area distribute from No. 13 spot of H-line to No. 13 point of B-line, around Nos. 14 and 19 of E-line, and around No. 21 of A-line. And these high resistivity areas correspond very well to intrusive rocks such as red dacite, andesite and nevaditic dacite. In Çalkaya area, distribution of dolerite body around No. 49 of D-line shows high resistivity like as 4,000Ω・m.

Around Nos. 3 and 8 of B-line where marginal part of nevaditic dacite intrusive body exist, strong argillization could be observed. Low resistivity area less than 50Ω・m which related in argillization seems to prevail southwards along the marginal zone of nevaditic dacite body.

In the area where resistivity less than around 200Ω・m is predominant, it is not clear to detect the relation between resistivity and rock facies because of strong argillization.

Plans of Chargeability

The areas where chargeability more than around 6mV/V predominates are thought to correspond to two cases, one is to high resistivity areas more than 200Ω・m, and the other is to relatively low resistivity areas less than 200Ω・m.

Aound No. 46 of D-line in Çalkaya area and No. 14 of E-line in Lahanos area, high resistivity and high chargeability were observed due to intrusive rocks.

The areas showing relatively low resistivity and around 6mV/V chargeability exist at Nos. 11~20 of H-line, Nos. 6~10 of G-line and Nos. 20~25 of E-line in Lahanos area, and Nos. 9~17 of D-line in Çalkaya area.

The above mentioned facts regarding resistivity and IP patterns are summarized as shown in Table 6-4.

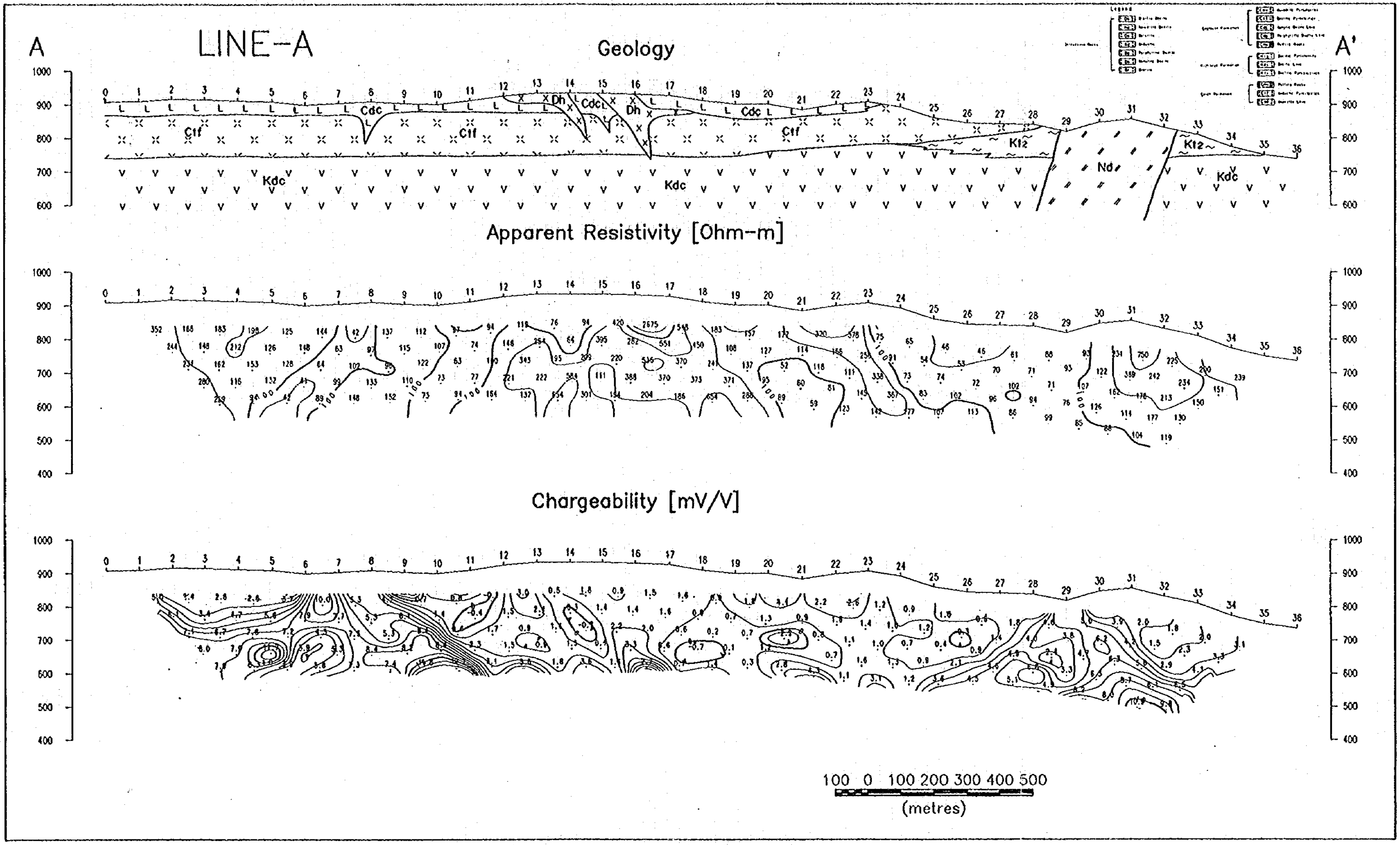

Fig. 6-4 Section of Apparent Resistivity and Chargeability (Line A)

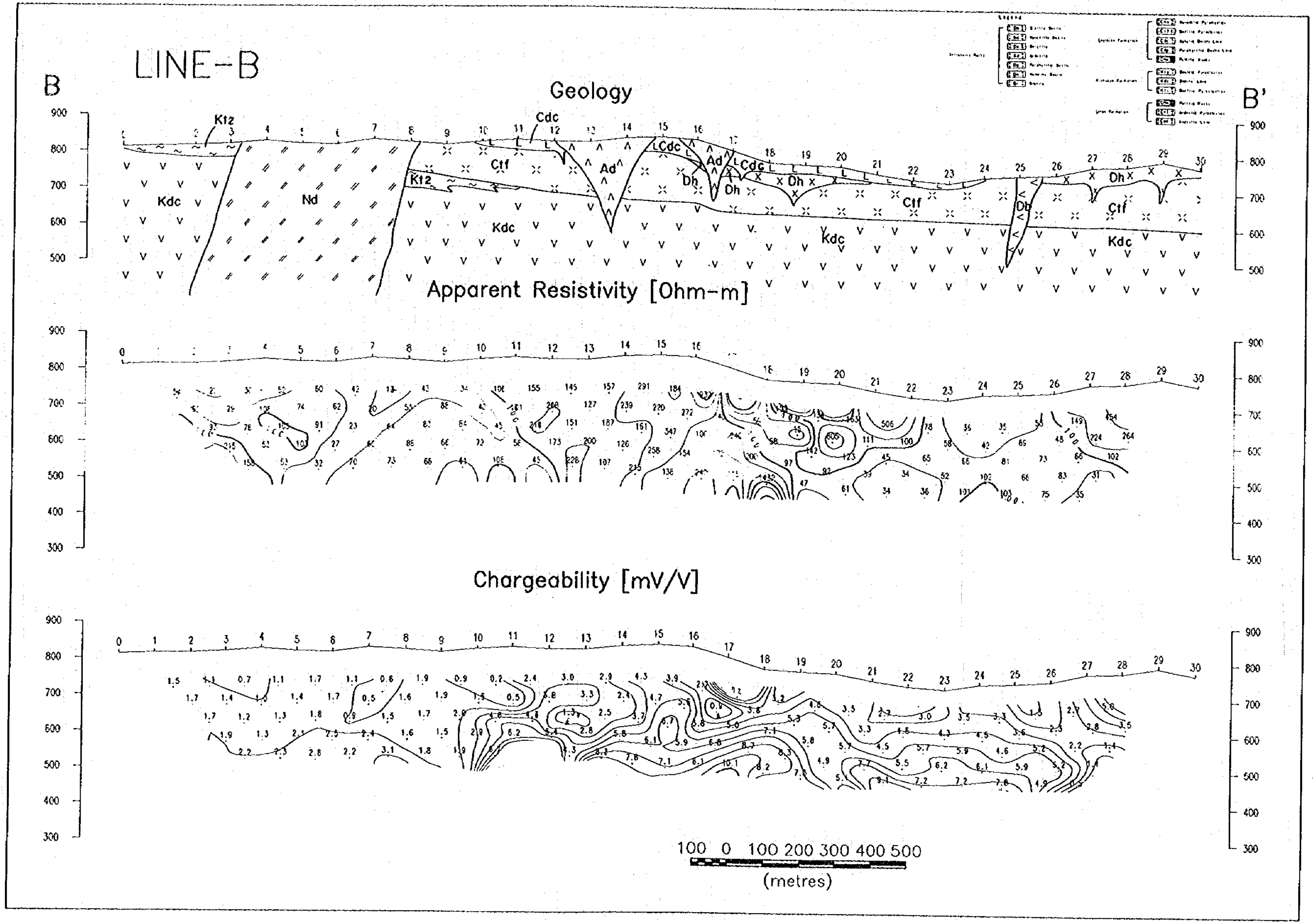

Fig. 6-5 Section of Apparent Resistivity and Chargeability (Line B)

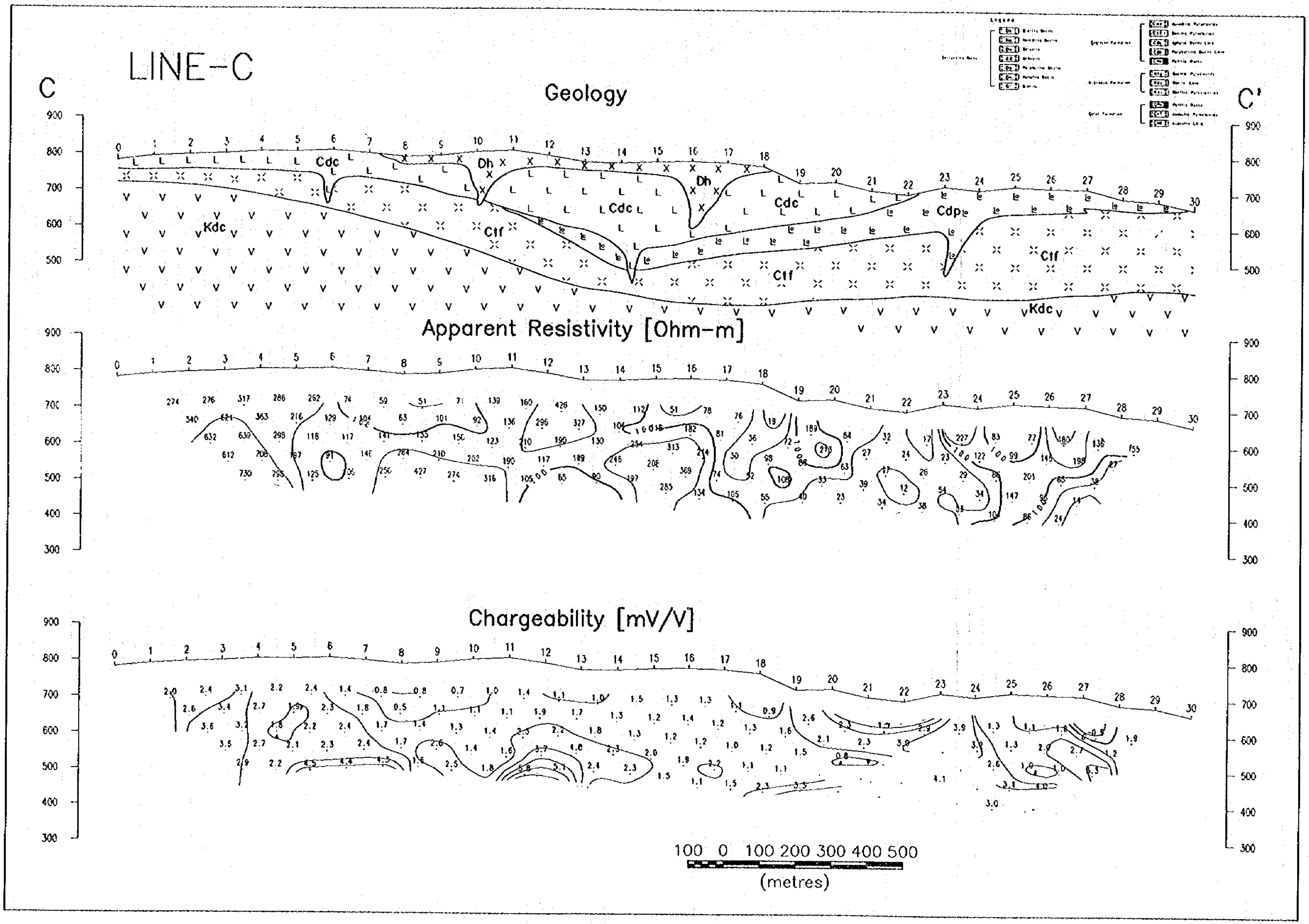

Fig. 6-6 Section of Apparent Resistivity and Chargeability (Line C)

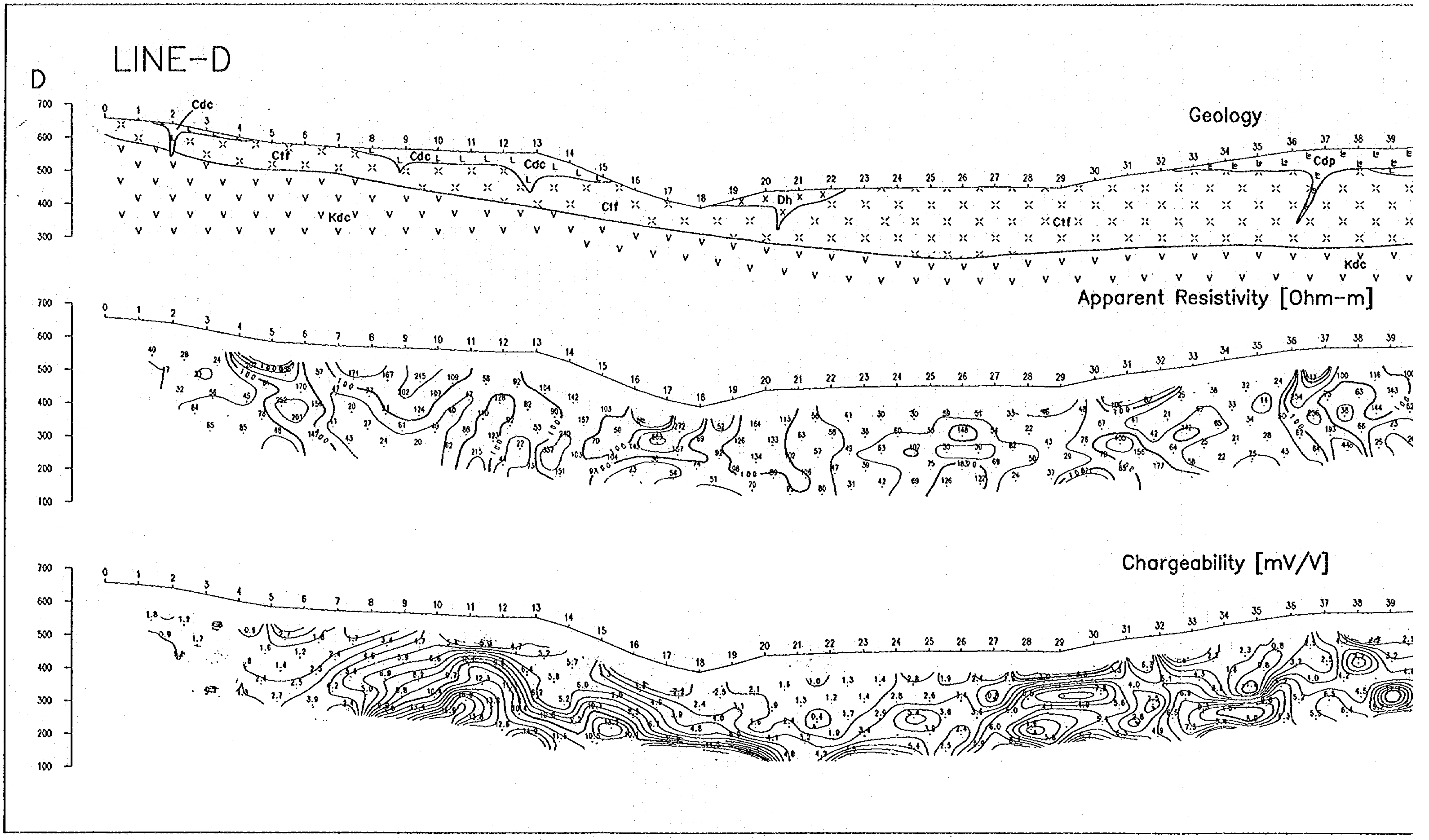

Fig. 6-7 Section of Apparent Resistivity and Chargeal

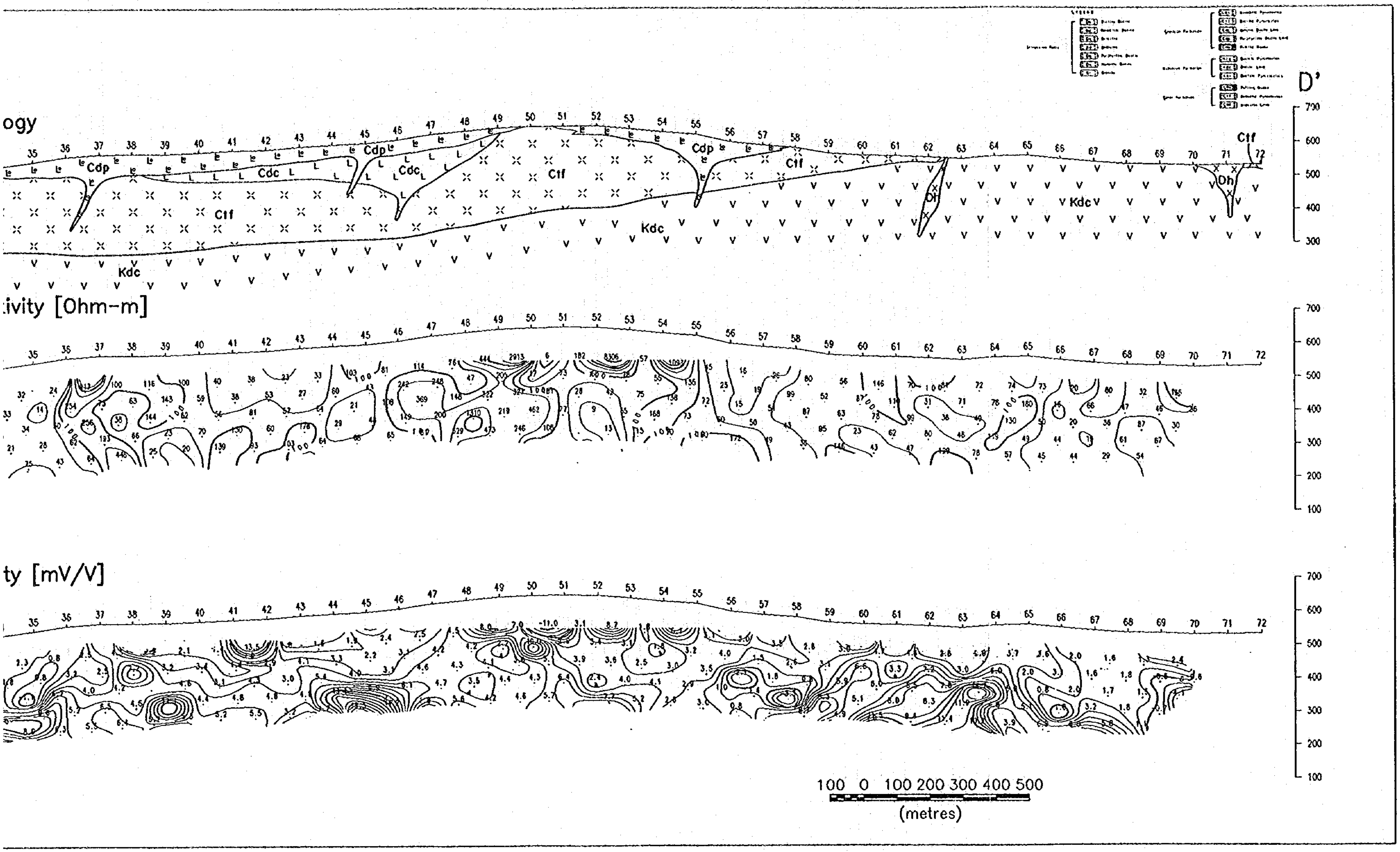

of Apparent Resistivity and Chargeability (Line D)

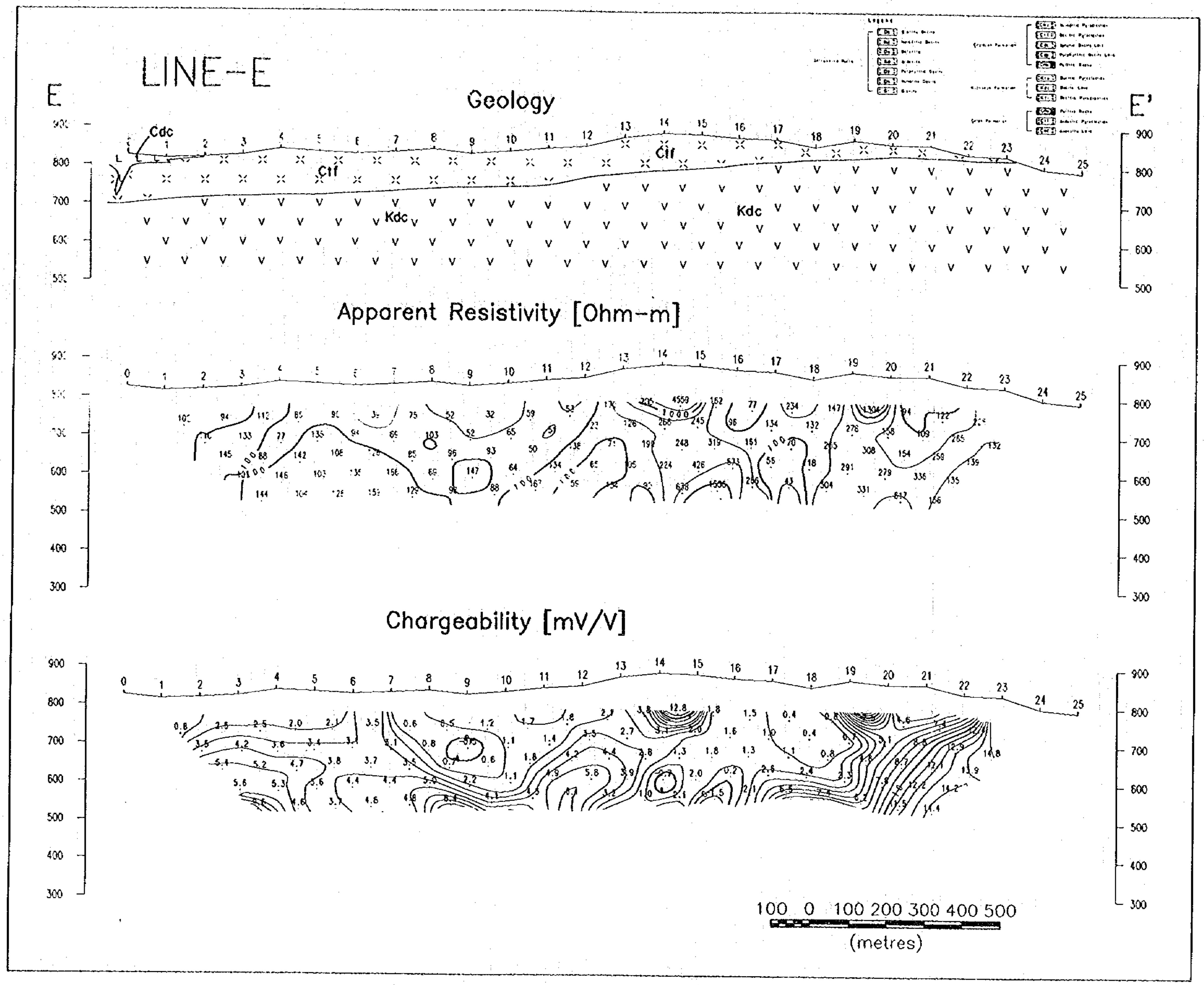

Fig. 6-8 Section of Apparent Resistivity and Chargeability (Line E)

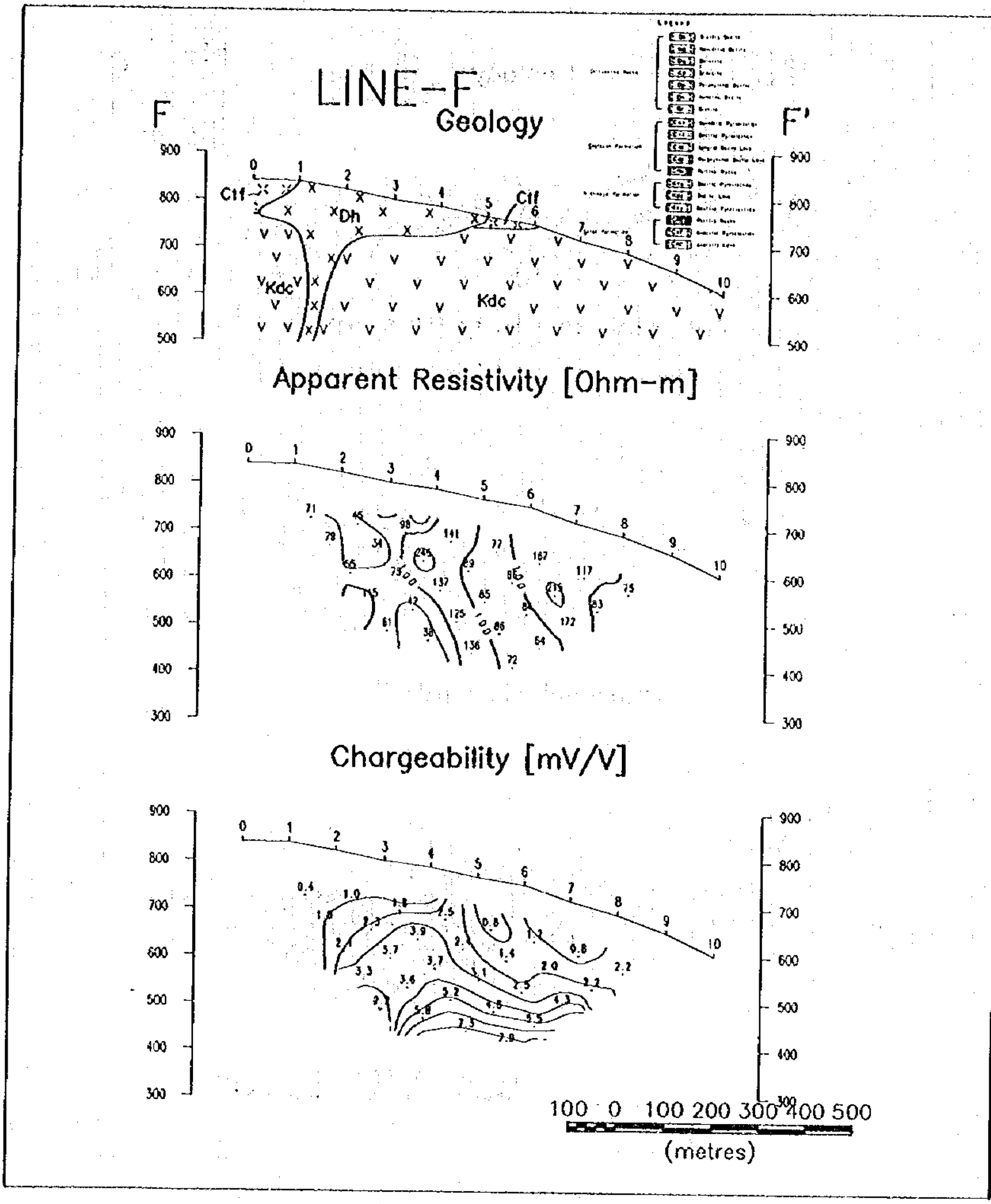

Fig. 6-9 Section of Apparent Resistivity and Chargeability (Line F)

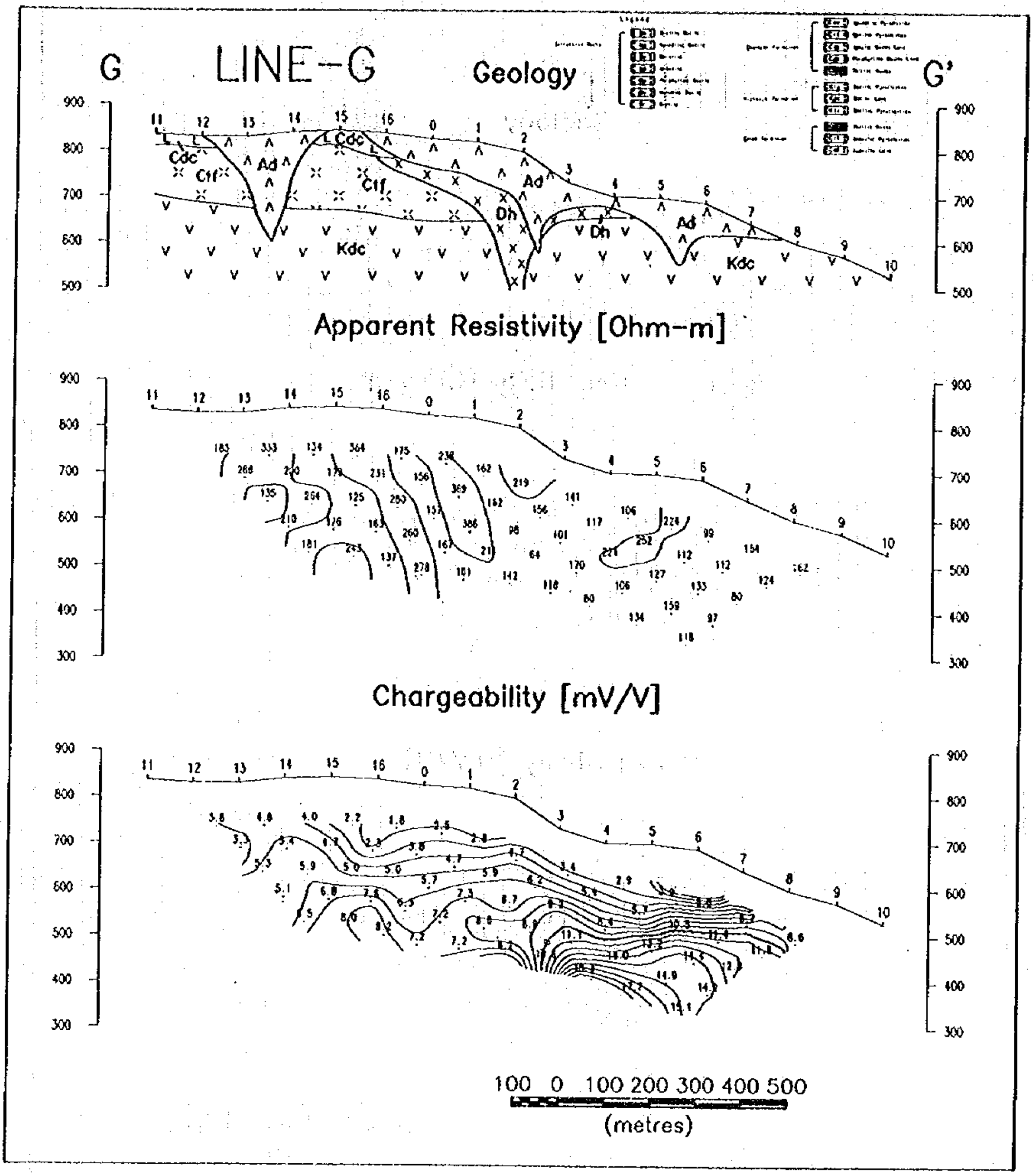

Fig. 6-10 Section of Apparent Resistivity and Chargeability (Line G)

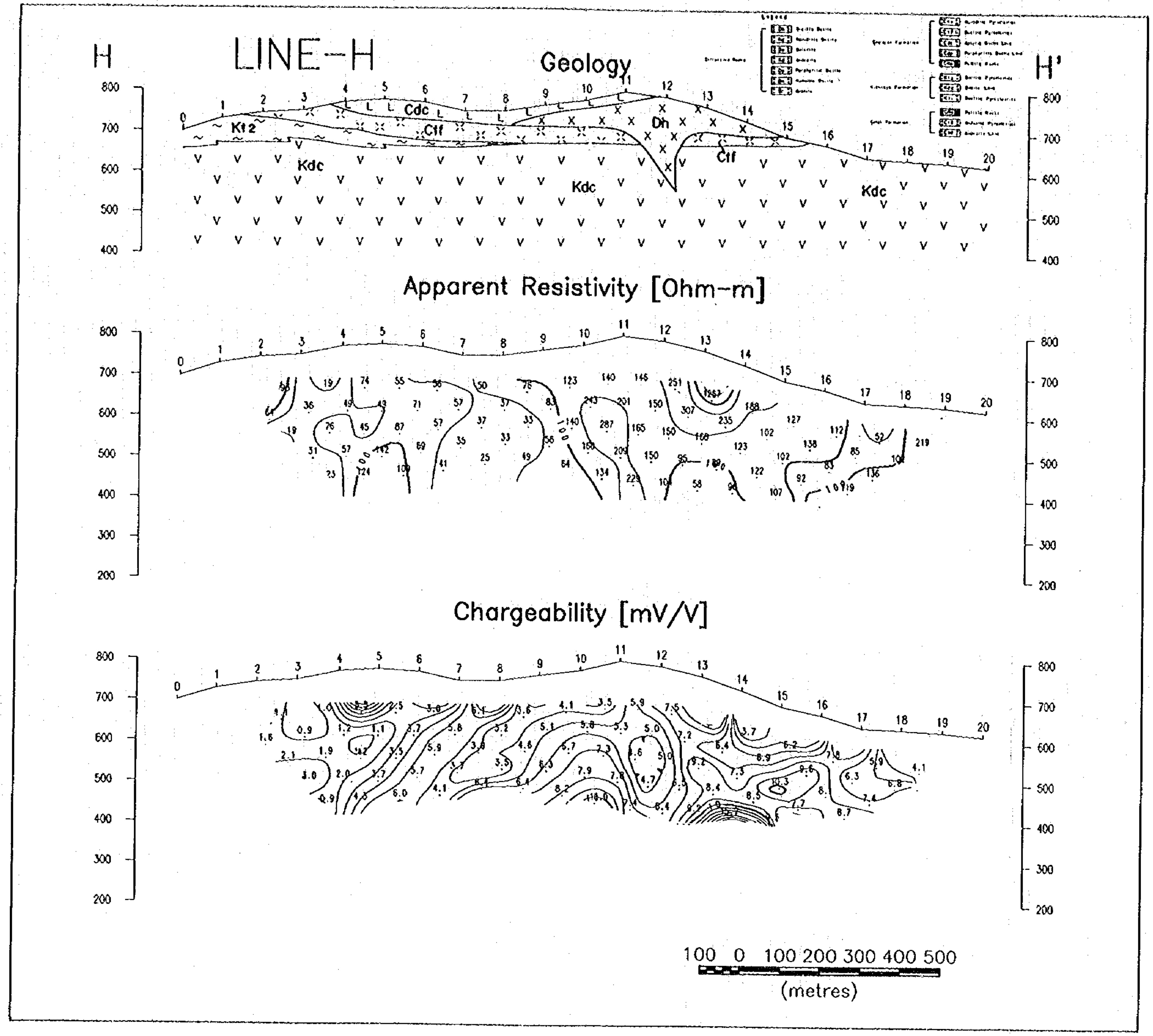

Fig. 6-11 Section of Apparent Resistivity and Chargeability (Line H)

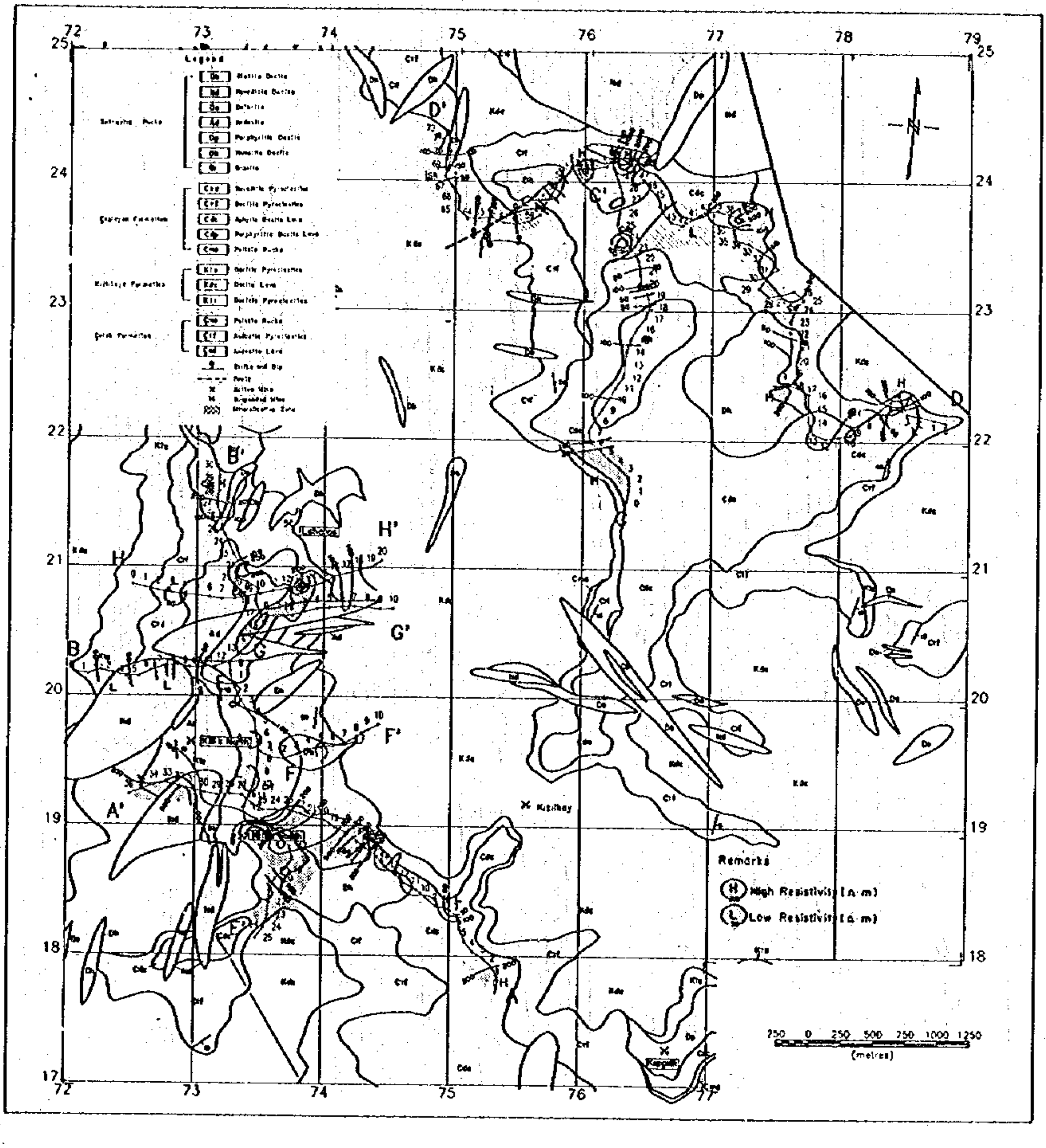

Fig. 6-12 Plane Map of Apparent Resistivity (n=1)

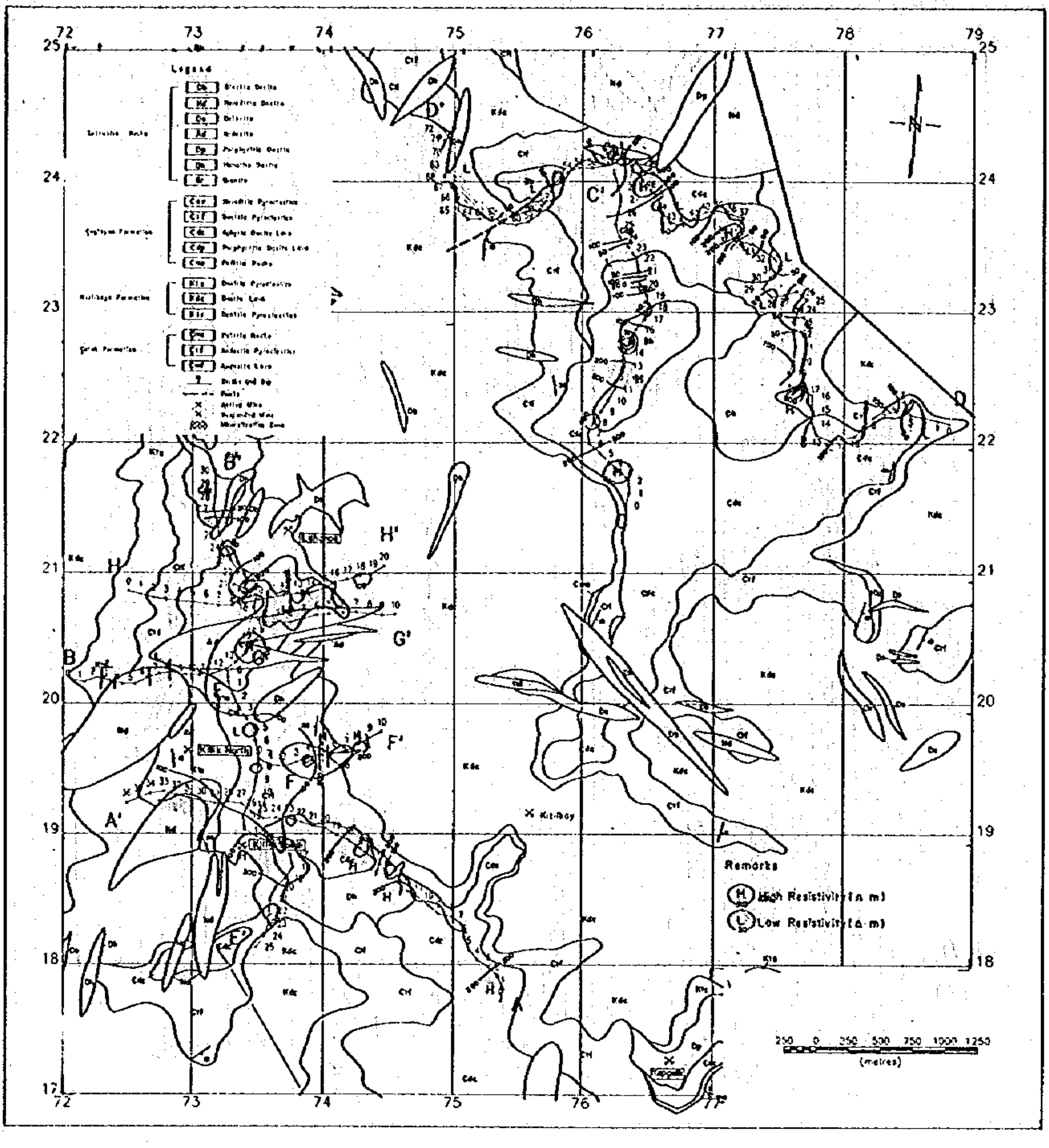

Fig. 6-13 Plane Map of Apparent Resistivity (n=2)

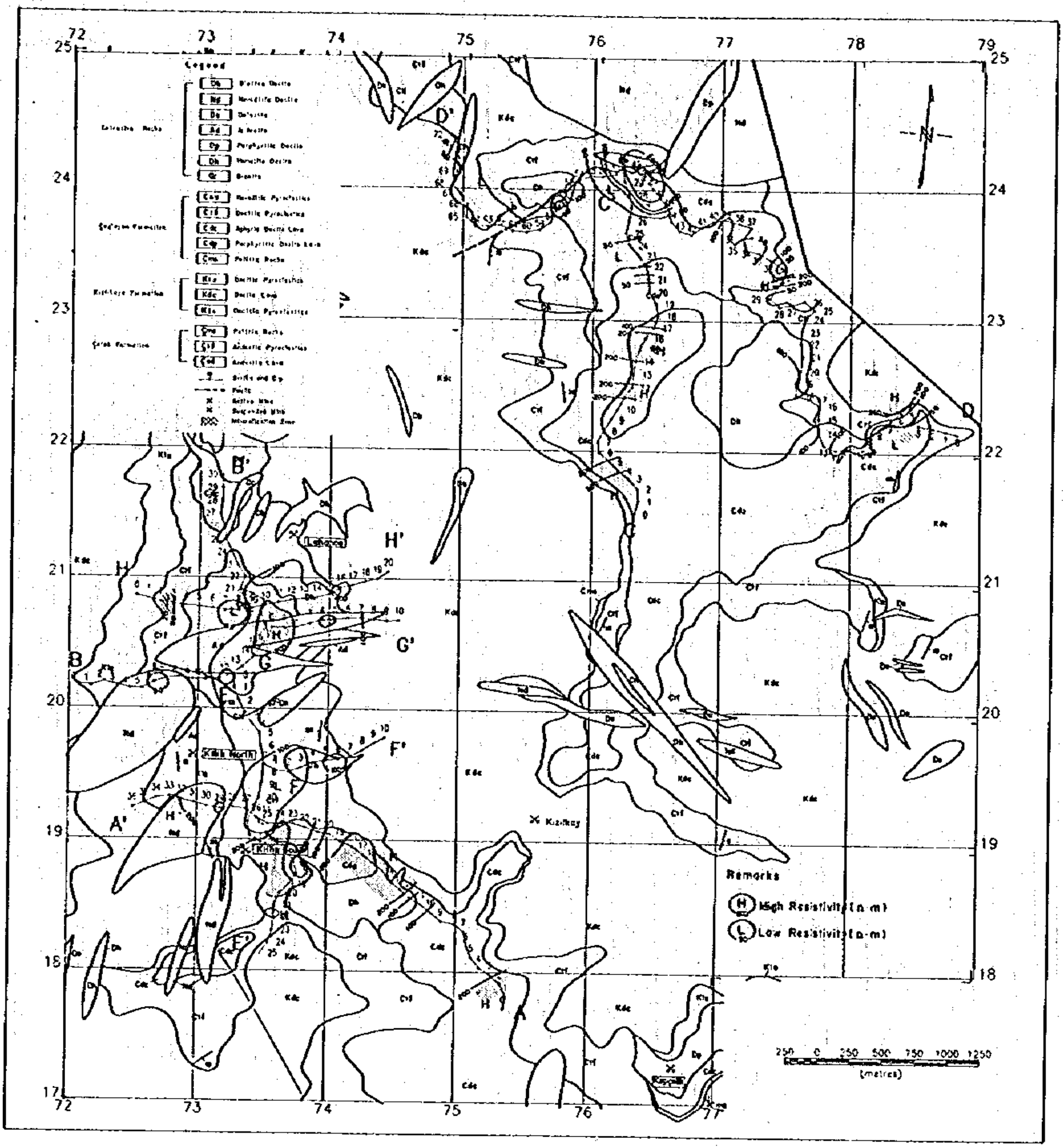

Fig. 6-14 Plane Map of Apparent Resistivity (n=3)

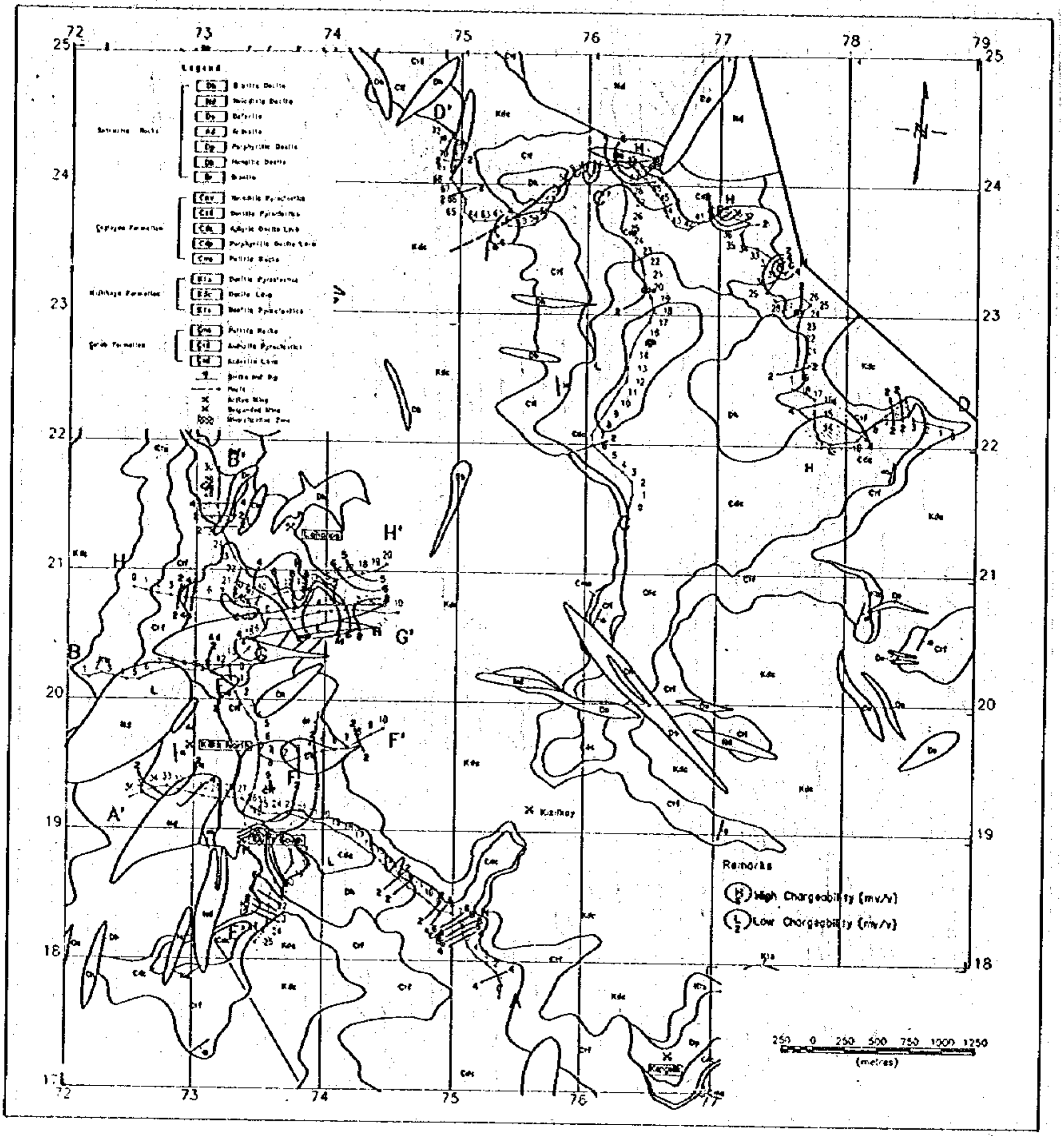

Fig. 6-15 Plane Map of Chargeability (n=1)

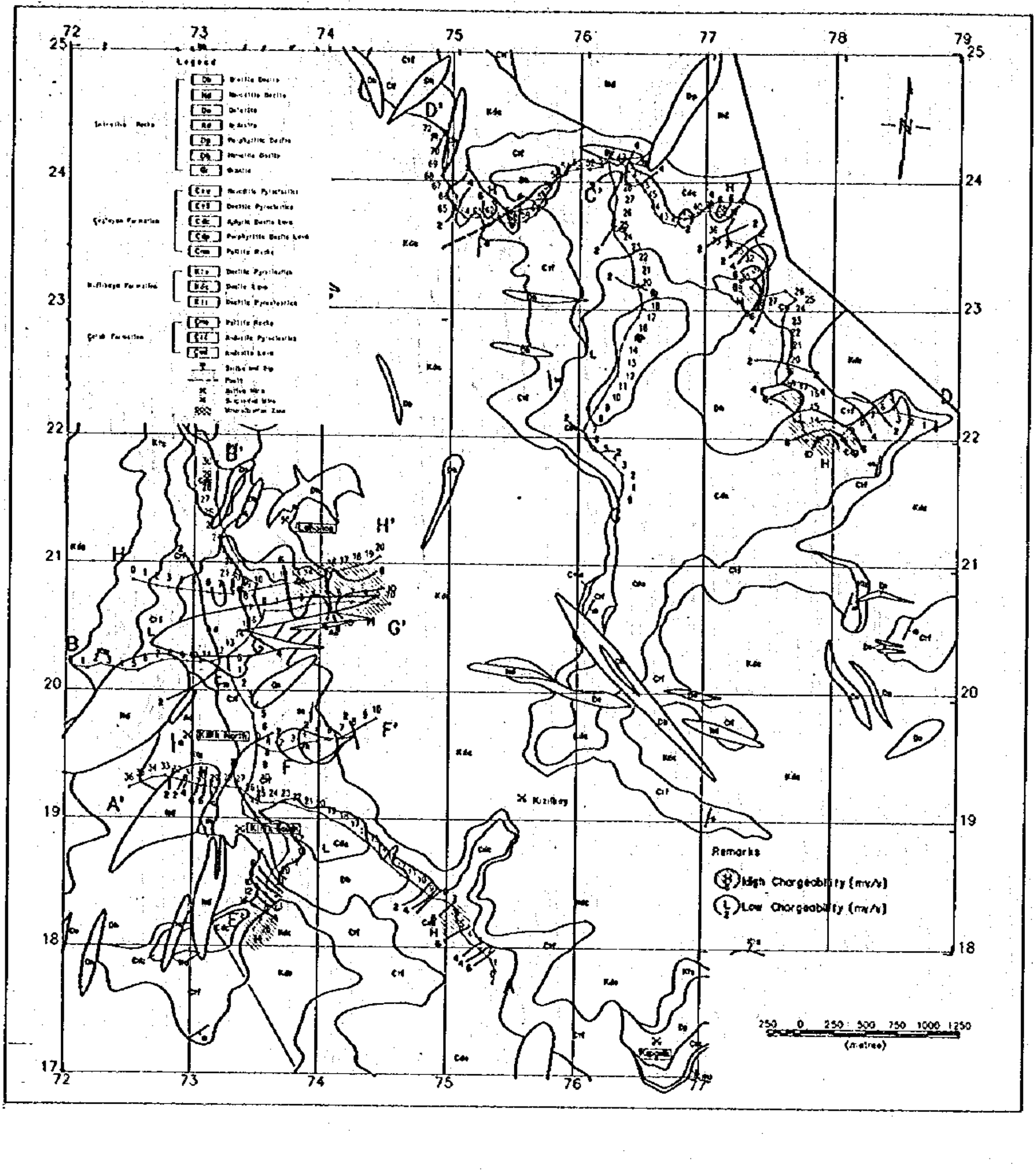

Fig. 6-16 Plane Map of Chargeability (n=2)

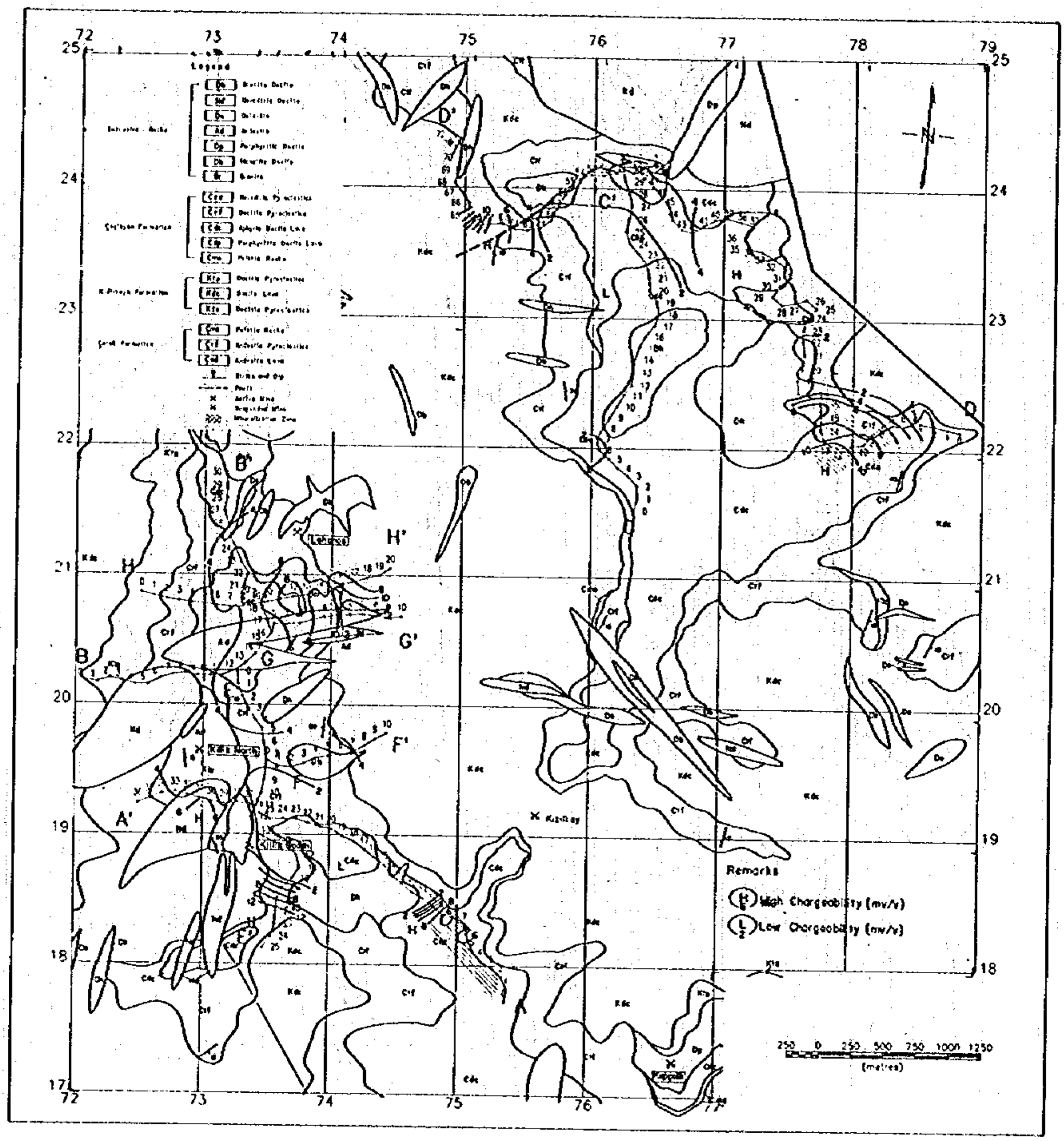

Fig. 6-17 Plane Map of Chargeability (n=3)

Table 6-4 Result of IP Survey

Survey Line	Apparent Resistivity(Ω・m)	Chargeability (mV/V)	Characteristics of IP Distribution Pattern
A	40～2,675	-0.4～12.1	Weak IP anomaly around Nos. 6～7 & 29.
B	7～1,432	0.9～10.1	Weak IP anomaly at depth of Nos. 19～20.
C	14～798	-0.5～5.8	No anomaly.
D	6～8,306	-11.0～18.3	Clear anomaly at depth of No. 11 & weak anomaly around No. 63.
E	43～4,559	-0.7～14.8	Clear IP anomaly around Nos. 23～25 & weak IP anomaly at No. 14.
F	38～246	0.4～7.9	The deeper, the higher IP.
G	80～386	1.8～18.3	Clear IP anomaly around Nos. 3～10
H	19～1,267	0.9～15.7	High chargeability in high resistivity area.

6-2-2 Physical Properties of Rocks and Ores

1. Measuring Method for Physical Properties

In order to have the basic data regarding electrical specialities of rocke and ores in the survey area, typical 45 samples collected in the area were measured their resistivity and chargeability by time-domain method.

2. Employed Equipment

List of employed equipment for this purpose is shown as Table 6-3.

3. Result of Measurement

Result of measurement is listed as shown in Table 6-5.

Relation between apparent resistivity and chargeability in each samples is drawn as shown in Fig. 6-18.

Several Ω・m and 100mV/V were obtained from high grade ores as resistivity and chargeability respectively.

Regarding low grade ores, resistivity highly varies from several Ω・m to 100Ω・m and chargeability also varies from 1mV/V to 14mV/V.

Dacite lava and its pyroclastics of Çağlayan formation was measured their resistivity and chargeability as 20～1,000Ω・m and 1～10mV/V respectively.

Dacite lava of Kızılkaya formation was measured its resistivity and chargeability as several～900Ω・m and 1～14mV/V respectively.

Andesite lava of Çatak formation indicated around 100～300Ω・m and 3mV/V as its resistivity and chargeability respectively.

Intrusive rocks showed 30～600Ω・m and 1～14mV/V as its resistivity and chargeability respectively.

Table 6-5 Results of Physical Property Tests

No.	Sample No.	Location	Rock Type	ρ(ohm-m)	M4	M5	M5	M7	M8	M9	M10	M11	M12 (M12:935msec)	M13	M14
1	TK-1	Lahanos	Yellow Ore	0.77	283.72	252.52	229.71	202.70	177.54	154.61	131.70	116.17	95.14	83.10	71.47
2	TK-11		Yellow Ore	0.64	310.66	283.22	264.15	249.79	226.74	206.08	189.44	167.80	154.55	138.32	122.95
			(anisotropic measurement)	1.13	234.60	208.85	187.87	175.71	151.64	107.41	132.69	120.16	109.05	97.38	81.17
3	TK-18		Pyrite	1.74	739.59	706.45	673.45	632.53	589.72	542.97	495.54	451.99	409.18	366.00	326.39
			(anisotropic measurement)	2.49	730.51	697.81	662.29	615.83	569.84	519.93	473.09	424.39	378.37	334.50	293.29
4	TK-21	Killik	Yellow Ore	0.47	354.99	332.52	308.09	275.11	241.64	212.32	189.99	160.41	140.44	114.88	93.27
			(anisotropic measurement)	1.02	334.95	285.19	257.63	238.13	215.78	188.92	174.95	154.88	135.17	122.50	108.56
5	TK-24		Yellow Ore	0.43	492.55	404.11	372.98	339.05	303.87	276.56	242.23	208.29	174.94	147.67	121.73
			(anisotropic measurement)	0.72	317.04	288.31	270.30	251.98	228.97	204.94	180.85	159.45	136.95	117.89	95.15
6	TK-27		Black Ore	0.98	366.51	343.19	316.64	285.07	256.70	230.95	206.76	179.52	165.82	138.35	118.83
7	TK-29		Siliceous Ore	25.34	113.30	98.53	85.25	72.43	61.08	55.90	42.32	34.79	28.49	23.13	18.67
			(anisotropic measurement)	5.30	111.03	94.36	83.69	70.51	58.84	47.58	38.68	31.90	25.85	20.92	16.75
8	TK-33		Siliceous Ore	7.35	195.93	174.73	154.04	133.38	118.43	97.15	81.91	68.55	57.12	47.29	38.73
			(anisotropic measurement)	11.58	197.57	165.34	144.87	124.73	108.51	90.41	76.32	64.25	54.65	46.15	38.64
9	TK-32	Kizilkaya	Black Ore	6.03	355.01	341.11	314.30	286.65	258.95	231.15	205.83	181.55	155.01	143.52	123.28
			(anisotropic measurement)	7.87	570.39	533.43	495.82	456.27	418.14	378.50	339.15	301.38	259.85	221.38	185.78
10	TK-39	Dikmen	Black Ore	3.33	640.36	603.14	563.92	529.02	493.66	443.99	409.85	371.47	336.15	303.83	269.97
			(anisotropic measurement)	0.43	623.58	595.16	562.95	521.29	475.83	435.34	398.01	369.23	341.75	308.18	285.52
11	TK-42		Siliceous Ore	142.66	23.30	19.72	16.79	13.95	11.52	9.39	7.59	6.14	5.03	4.19	3.65
			(anisotropic measurement)	5.94	36.02	30.57	25.62	21.03	17.03	12.94	9.25	6.89	6.75	6.49	6.67
12	TK-45	Agatlik	Pyrite	2.25	429.02	385.83	342.89	295.75	256.47	218.59	184.77	151.06	137.79	110.70	72.01
			(anisotropic measurement)	1.45	418.71	378.09	342.85	304.27	259.81	238.66	208.22	187.04	155.77	135.45	101.57
13	TK-53	Kartlar	Pyrite	0.84	323.03	231.12	260.65	235.24	209.73	180.13	159.48	140.57	125.19	115.84	95.40
14	TK-53	Caltepe	Pyrite	27.11	119.64	105.90	92.68	79.20	65.72	55.38	45.54	36.99	29.77	23.87	19.07
			(anisotropic measurement)	39.73	134.19	117.69	102.17	85.85	73.37	61.71	51.54	42.25	33.14	27.28	24.45
15	YH-65		Cdc	69.09	11.17	9.21	7.72	6.37	5.23	4.25	3.44	2.77	2.21	1.76	1.38
			(anisotropic measurement)	80.10	23.71	19.59	16.21	13.14	10.54	8.43	6.64	5.20	4.07	3.22	2.57
16	HM-106		Cdc	67.32	13.59	11.71	10.16	8.69	7.31	6.07	4.99	4.06	3.25	2.55	1.95
			(anisotropic measurement)	60.37	13.92	12.11	10.60	9.11	7.74	6.43	5.34	4.44	3.63	2.91	2.38
			(anisotropic measurement)	75.14	20.27	17.07	14.45	12.09	10.02	8.17	6.73	5.35	4.45	3.42	2.69
17	HM-100		Ctf	317.85	19.73	16.77	14.30	11.95	9.87	8.07	6.53	5.24	4.17	3.28	2.57
			(anisotropic measurement)	406.97	18.33	15.62	13.33	11.17	9.24	7.58	6.17	4.92	3.91	3.08	2.40
18	KM-10	Caglayan Formation	Ctf	211.05	20.07	17.41	15.15	12.94	10.93	9.19	7.53	6.13	4.94	3.93	3.09
			(anisotropic measurement)	903.33	11.74	9.89	8.41	7.05	5.85	4.80	3.91	3.15	2.52	2.01	1.59
19	KM-140		Cdc	21.48	15.77	13.50	11.53	9.65	7.95	6.44	4.98	3.69	2.56	1.59	0.72
			(anisotropic measurement)	27.95	24.31	21.80	19.45	17.55	15.70	14.11	12.90	11.17	10.05	8.49	7.84
20	HM-97		Cms	40.80	6.63	5.43	4.43	3.65	2.85	2.13	1.55	1.15	0.84	0.73	0.71
			(anisotropic measurement)	44.70	11.13	9.30	7.84	6.42	5.22	4.24	3.45	2.88	2.30	1.84	1.43
			(anisotropic measurement)	61.10	20.20	17.45	15.14	12.83	10.88	9.04	7.27	5.78	4.43	3.55	2.97
21	KM-58		Cdc	269.81	23.33	19.66	16.83	14.09	11.62	9.45	7.60	6.01	4.66	3.59	2.77
			(anisotropic measurement)	357.19	25.39	22.43	19.14	16.07	13.39	11.03	8.97	7.22	5.75	4.53	3.50
22	HM-13		Cdp	98.15	21.52	18.06	15.25	12.58	10.29	8.45	6.93	5.69	4.64	3.76	3.11
			(anisotropic measurement)	74.74	18.86	15.92	13.51	11.32	9.41	7.75	6.33	5.20	4.13	3.35	2.81
23	HM-352		Kt2	15.82	15.86	14.28	12.14	9.93	8.02	6.41	5.02	3.60	2.71	2.05	1.69
			(anisotropic measurement)	12.72	12.43	10.31	8.58	6.87	5.27	3.83	2.63	1.69	0.82	0.20	-0.06
24	HM-52		Kt1	34.30	19.36	15.77	14.53	12.28	10.22	8.33	6.62	5.08	3.66	2.78	1.67
25	YH-86		Kdc	229.08	24.09	21.20	19.67	16.11	13.81	11.65	9.68	8.05	6.61	5.29	4.33
			(anisotropic measurement)	75.53	19.20	16.21	13.79	11.52	9.49	7.70	6.25	5.10	4.14	3.45	2.65
26	YH-2		Kdc	378.89	17.88	15.48	13.42	11.42	9.58	7.92	6.47	5.22	4.14	3.26	2.52
		Kizilkaya Formation	(anisotropic measurement)	344.13	16.73	14.20	12.18	10.21	8.54	7.05	5.78	4.59	3.83	3.11	2.18
27	HM-299		Kdc	20.71	56.09	48.77	42.17	35.71	29.85	24.69	20.18	16.45	13.36	10.62	8.65
			(anisotropic measurement)	17.55	62.88	54.45	45.73	39.12	32.24	25.06	20.73	16.44	13.00	9.92	7.10
28	HM-289		Kdc	29.76	12.23	10.13	8.40	6.99	5.92	4.41	3.57	2.77	2.32	1.81	1.02
			(anisotropic measurement)	32.82	8.38	6.64	5.23	3.94	2.85	1.98	1.21	0.68	0.52	0.53	0.34
			(anisotropic measurement)	52.73	8.18	5.07	4.64	3.50	2.97	1.74	1.34	0.94	0.75	0.53	0.35
29	YH-71		Kdc	629.99	8.85	7.39	6.25	5.19	4.23	3.38	2.68	2.07	1.60	1.21	0.93
			(anisotropic measurement)	843.50	12.28	10.42	8.90	7.45	6.18	4.96	4.00	3.31	3.53	1.75	1.53
30	HM-275		Dh	8.25	27.64	24.42	21.60	18.85	15.22	13.82	11.83	9.76	8.03	6.31	4.65
			(anisotropic measurement)	19.51	19.85	15.73	14.02	11.05	8.29	5.74	3.97	1.76	0.73	0.14	0.93
31	YH-13		Cms	65.40	9.68	7.91	6.53	5.29	4.23	3.27	2.60	2.09	1.51	1.10	0.83
			(anisotropic measurement)	143.22	10.75	8.78	7.18	5.72	4.55	3.54	2.89	2.22	1.59	1.15	0.99
32	HM-253		Cad	205.34	9.78	6.66	5.95	5.87	4.84	4.05	3.20	2.56	2.01	1.53	1.28
		Catak Formation	(anisotropic measurement)	195.55	11.92	9.53	7.62	5.94	4.53	3.49	2.60	1.81	1.54	0.94	0.44
33	HM-339		Cad	124.32	14.95	12.91	11.16	9.35	7.71	6.35	5.15	4.11	3.29	2.57	2.00
			(anisotropic measurement)	145.42	15.52	13.99	11.95	10.03	8.34	6.88	5.65	4.62	3.75	3.07	2.59
34	YH-62		Cad	125.25	19.23	16.09	13.45	11.04	8.95	7.22	5.77	4.57	3.60	3.01	2.34
			(anisotropic measurement)	127.07	16.47	13.75	11.59	9.58	7.85	6.41	5.15	4.11	3.29	2.56	1.91
35	YH-56		Cms	250.34	7.43	5.95	4.83	4.25	4.00	3.58	2.74	2.28	1.81	1.46	1.29
			(anisotropic measurement)	314.09	7.18	6.72	5.29	4.49	3.77	3.12	2.55	2.04	1.64	1.26	0.95
36	KM-8		Dh	34.63	17.76	14.49	11.88	9.59	7.67	6.05	4.78	3.72	2.83	2.29	1.92
		Intrusive Rock	(anisotropic measurement)	32.25	17.44	14.61	12.04	9.54	7.37	6.30	5.87	5.28	4.23	3.31	1.94
37	KM-54		Dh	318.68	37.52	32.83	28.83	23.61	19.71	15.35	13.34	11.05	9.03	6.82	5.65
			(anisotropic measurement)	415.15	37.45	32.20	27.69	23.38	19.43	16.08	13.19	10.68	8.58	6.89	5.45
38	YH-35		Nd	232.64	19.37	15.38	12.91	10.61	8.61	6.89	5.45	4.19	3.19	2.38	1.69
			(anisotropic measurement)	251.99	14.48	12.09	10.08	8.29	6.68	5.28	4.09	3.11	2.33	1.69	1.20
39	YH-37		Nd	544.08	18.19	15.29	13.72	11.72	9.90	8.24	6.78	5.52	4.45	3.51	2.71
			(anisotropic measurement)	573.15	19.73	17.10	14.88	12.72	10.74	8.95	7.34	6.03	4.81	3.78	2.93
40	HM-212		Nd	415.21	25.64	23.28	20.38	17.54	14.97	12.63	10.56	8.77	7.22	5.88	4.75
			(anisotropic measurement)	452.70	26.97	23.00	20.15	17.28	14.73	12.41	10.38	8.56	7.06	5.73	4.63
41	HM-236		Db	263.23	44.73	39.56	34.89	30.17	25.78	21.70	18.07	14.82	12.04	9.84	7.65
			(anisotropic measurement)	298.78	49.13	43.45	38.43	33.31	29.55	24.15	20.19	15.63	13.56	10.91	8.69
			(anisotropic measurement)	339.74	51.82	45.24	40.37	34.47	27.47	21.83	19.31	15.61	12.22	9.83	7.64
42	YH-14		Ad	45.72	7.13	5.91	5.06	4.23	3.45	2.84	2.31	1.91	1.52	1.16	0.82
43	YH-69		Do	32.70	4.65	3.52	2.83	2.25	1.85	1.50	1.24	1.10	0.93	0.80	0.63
			(anisotropic measurement)	33.47	4.34	3.32	2.70	2.25	1.88	1.57	1.31	1.15	1.03	0.72	0.44
44	YH-57		Gr	203.11	17.15	14.79	12.87	10.88	9.17	7.65	6.39	5.29	4.39	3.75	3.21
45	HM-294		Dh	135.00	9.31	7.36	6.10	5.03	4.00	3.11	2.42	1.85	1.39	0.99	0.67
			(anisotropic measurement)	124.95	10.71	8.83	7.39	8.05	4.93	3.99	3.17	2.53	1.97	1.57	1.27

Intrusive rock
- Db : Biotite Dacite
- Nd : Nevaditic Dacite
- Do : Dolerite
- Ad : Andesite
- Dp : Prophyritic Dacite
- Dh : Hesatite Dacite
- Gr : Granite

Caglayan Formation
- dacitic Pyroclastics
- Aphyric Dacite Lava
- Porphyritic Dacite Lava
- Pelitic Rock

Kizilkay Formation
- Kt2 : Dacitic Pyroclastics
- Kdc : Dacite Lava

Catak Formation
- Cms : Pelitic Rock
- Cad : Andesite Lava

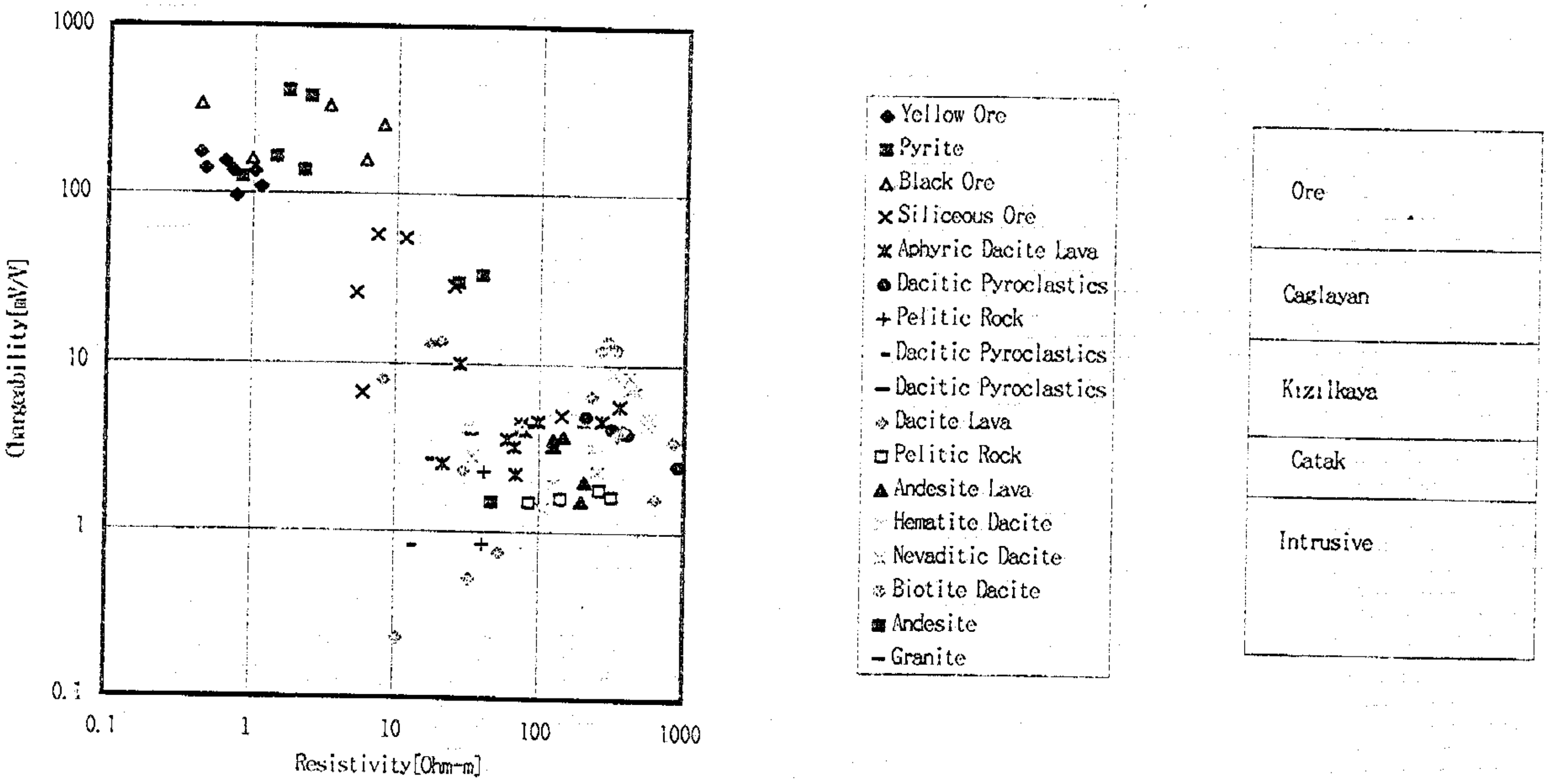

Fig. 6-18 Relation between Apparent Resistivity and Chargeability of Rock and Ore Samples

Result of analysis was summarized as shown in Table 6-6.

Table 6-6 Summarized Table of Electric Survey

Survey Line	Estimated Resistivity & Chargeability of Origin of IP Anomaly	Estimated Distribution Pattern of Origin of IP anomaly
A Lahanos area	120Ω・m & 14mV/V 140Ω・m & 17mV/V	・IP anomaly zone is expected to develop widely in depth. On surface it is thought to be flat. Geologically it distributes over Kızılkaya to Çağlayan formations.
D Çalkaya area	2Ω・m & 42mV/V 35Ω・m & 20mV/V 2Ω・m & 40mV/V	・It is flat at deeper place than 200m. ・It is flat at deeper place than 100m. ・It is flat at depper place than 100m. Geologically it developes in both Kızılkaya and Çağlayan formations.
E Lahanos area	180Ω・m & 10mV/V 30Ω・m & 20mV/V	・It extends from surface to deeper places. ・It developes from surface to depth. Geologically it developes in Kızılkaya formation.
G Lahanos area	200Ω・m & 15mV/V 20Ω・m & 32mV/V	・It exists horizontally at deeper place than 100m. ・It is the same anomaly that just above mentioned, but inclined. Geologically it exists in Kızılkaya formation.

Generally speaking, clear difference of resistivity among each formations could not be recognized, but argillization affected much influence to country rock's resistivity. And mineralized rocks were inclined to show high chargeability.

Intrusive rocks which indicated high resistivity and high chargeability like as around 10mV/V seems to contain magnetite.

6－2－3 Result of Analysis

Referring the result of measured physical properties of collected rocks and ores, simulating analysis were performed on A, D, E and G survey lines that indicated principal IP anomalies.

A－survey line

IP anomaly around No. 6 was simulated and was concluded to be due to IP anomaly from intrusive rock.

The IP anomaly was simulated to have drived from area around 50m below Nos. 7－9 zone that showed around 200Ω・m as resistivity and arround 20mV/V as chargeability.

Weak IP anomalies on surface were analized to be due to mineralized zones and its extension developing between Kızılkaya and Çağlayan formations or due to intrusive rock.

D－survey line

IP anomaly around No. 11 where dacitic pyroclastics develope was analyzed, consequently origin of anomaly was estimated to be around 150～200m below Nos. 11 and 16 where Kızılkaya and Çağlayan formations seem to develop, and to have low resistivity like as 2～35Ω・m and high chargeability like as 20～42mV/V derived from mineralization.

E－survey line

IP anomaly around Nos. 23～25 where dacite lava of Kızılkaya formation distributes was simulated, consequently weak mineralized zone was expected to continue from shallow part below No. 25 to depth of No. 18.

Origin of IP anomaly was analized to have 50～180Ω・m as resistivity and 10～20mV/V as chargeability.

G－survey line

IP anomaly around Nos. 4～6 where dacite lava of Kızılkaya formation was analized, consequently origin of IP anomaly was expected to develop widely in deeper place more than 100m from surface.

Origin of IP anomaly was estimated to have 20Ω・m and 32mV/V as resistivity and chargeability respectively, from mineralized zones in kızılkaya and Çağlayan formations.

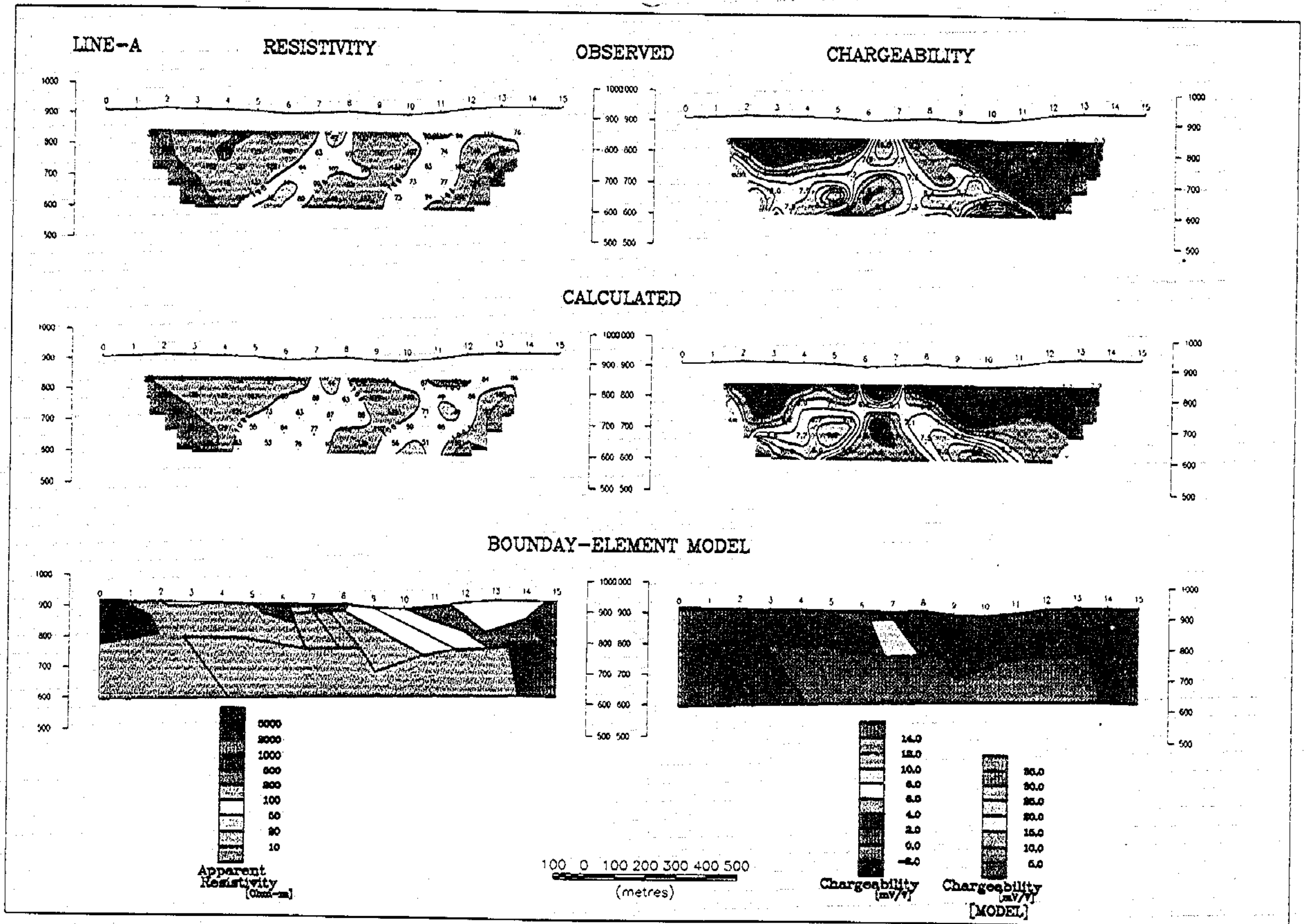

Fig. 6-19 Section of Simulated Result (Line A)

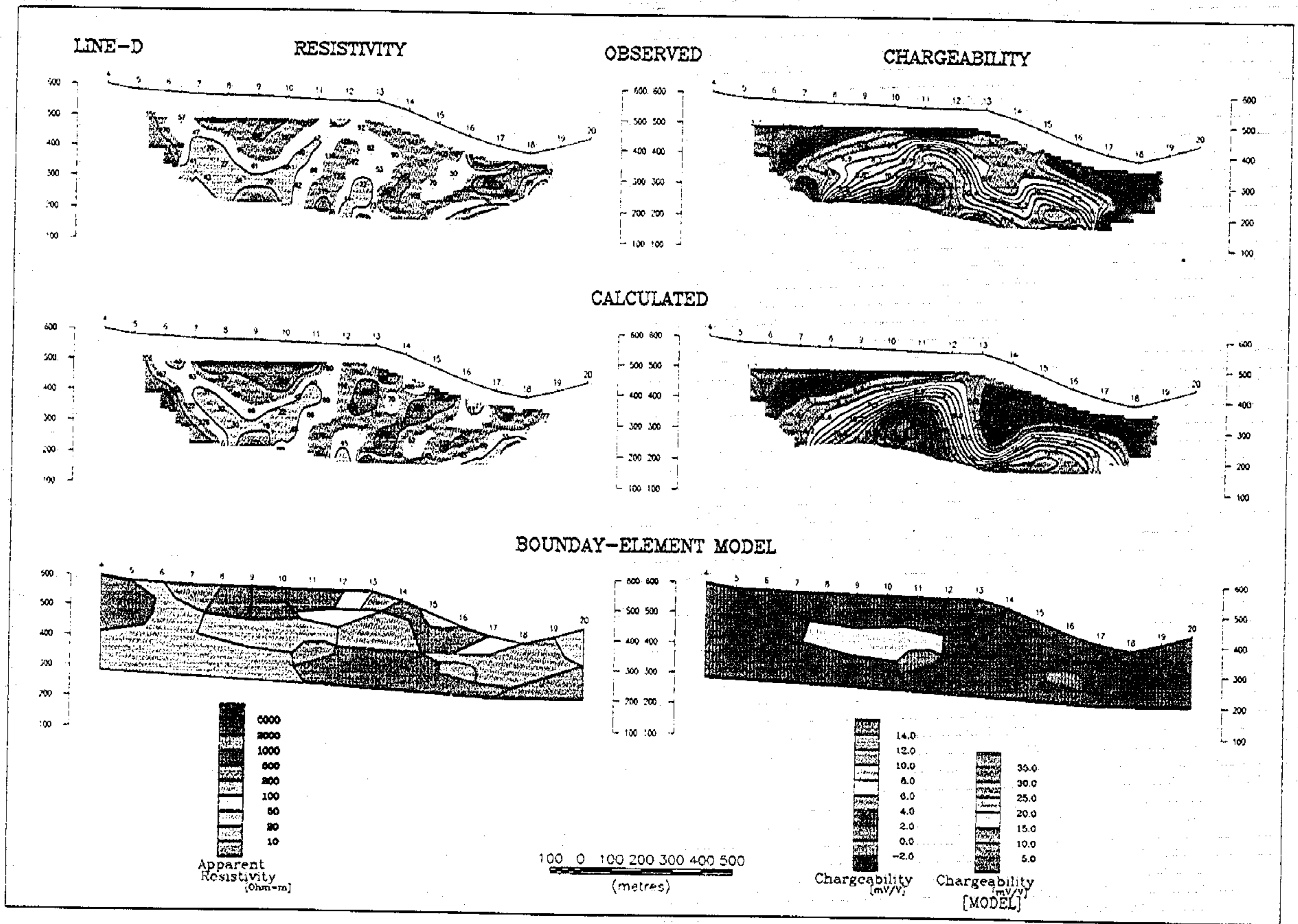

Fig. 6-20 Section of Simulated Result (Line D)

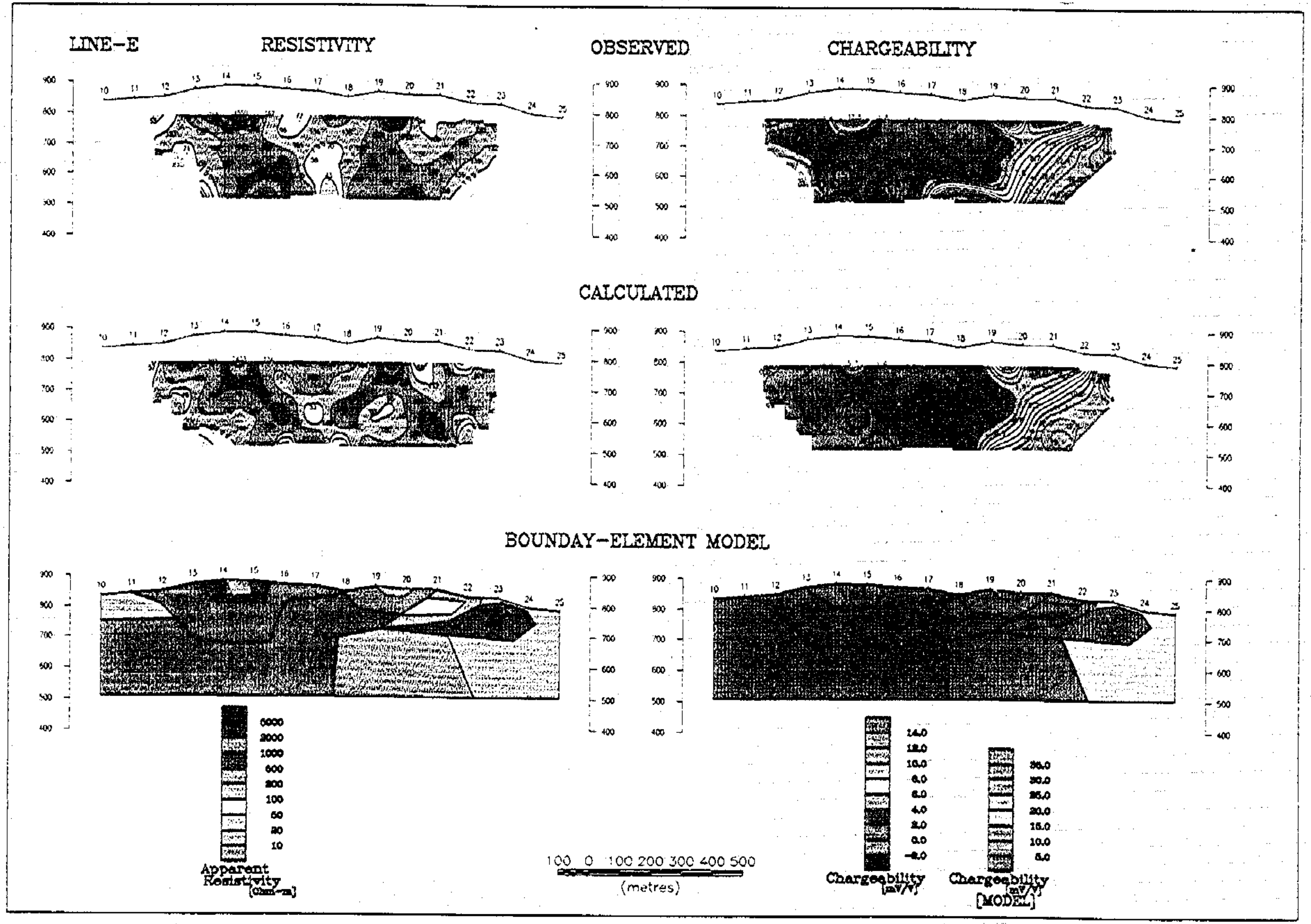

Fig. 6-21 Section of Simulated Result (Line E)

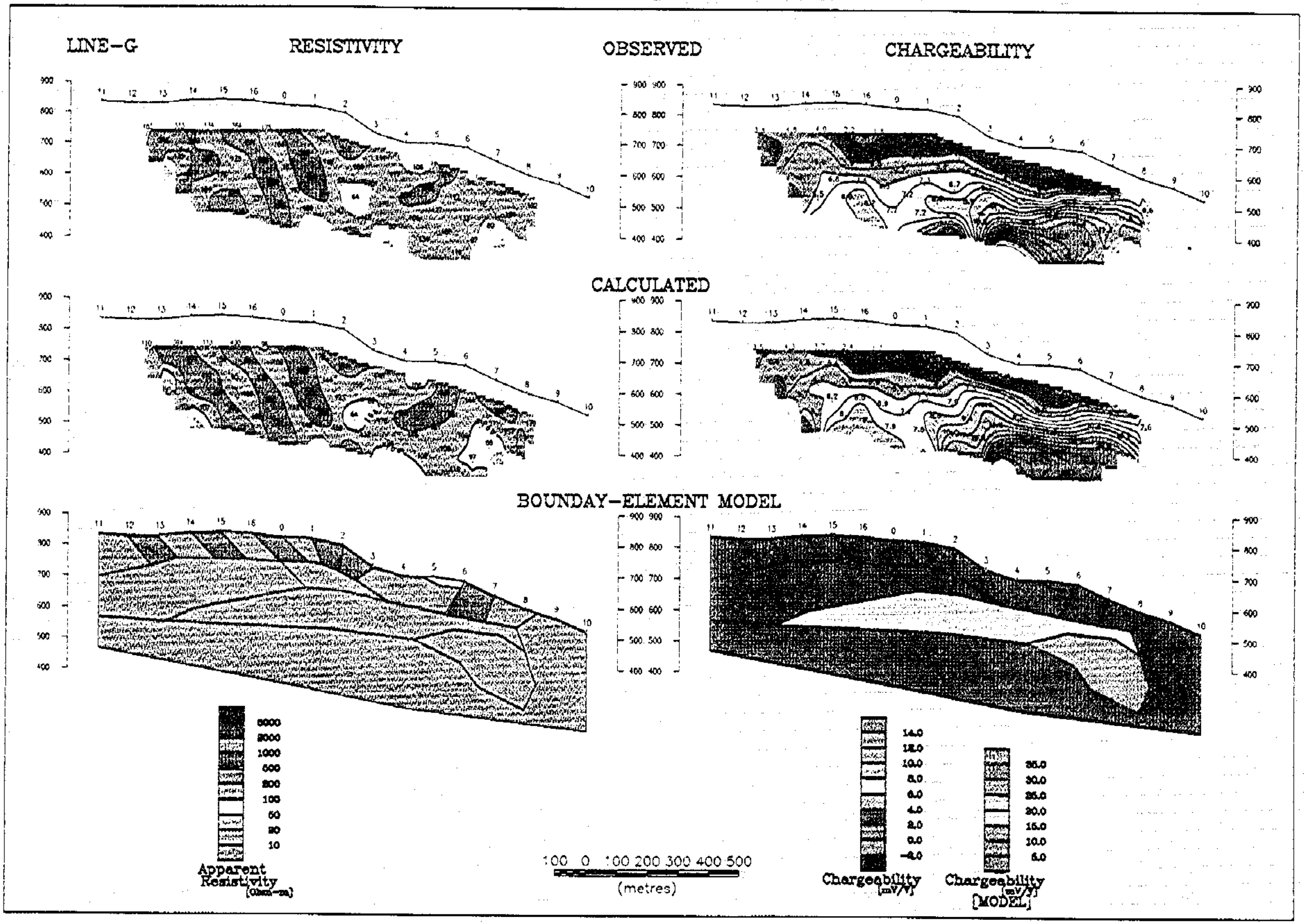

Fig. 6-22 Section of Simulated Result (Line G)

6-3 Consideration

Result of IP survey wa summarized and was shown in Fig. 6-23 as Analytical map of IP survey.

Higher resistivity area than 500 Ω・m was concluded to correspond very well to the distribution area of intrusive rocks. But in the area of around 200 Ω・m resistivity, correspondence of resistivity to rock facies could not be recognized clearly because of argillization and mineralization.

Low resistivity area like as around 50 Ω・m correponded very well to argillization relating with superficial alteration.

Regarding physical properties of samples, high grade ore showed low resistivity and high chargeability, but low grade ore showed low resistivity and variable chargeability.

Higher chargeability than 200 Ω・m in itrusive rock area was due to the existence of magnetite.

Anomalous chargeabilities were observed in A, D, E and G survey lines. In depth of F and H survey lines, weak IP anomalous zones were estimated to exist.

After simulative analysis on A, D, E and G survey lines, shallow IP anomaly in A line was expected to have derived from depth where intrusive rock showed high chargeability or dacitic pyroclastics were slightly mineralized.

IP anomaly in D line was concluded to have shown the effect from deeply existing mineralized zone in Kızılkaya and Çağlayan formations.

IP anomalies in E and G lines were considered to have shown the effect from mineralized zone in dacite lava of Kızılkaya formation.

IP anomalies in D, E and G lines were concluded to have derived from mineralized zones, therefore further detailed surveys are requested to be performed in these areas and to clarify them.

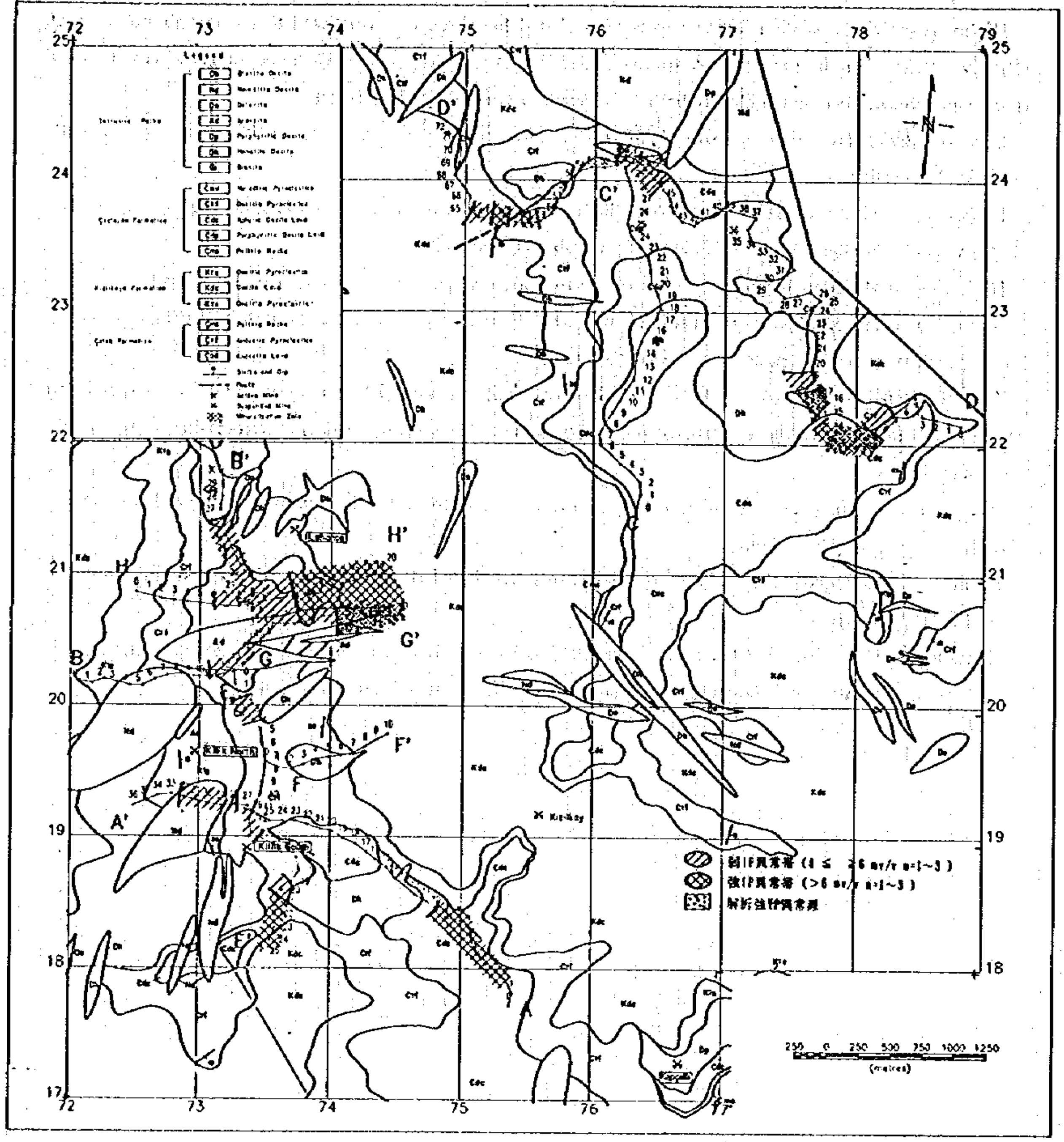

Fig. 6－23 Summarized Map of IP Survey